Optimum Selection of Direct-Coupled Photovoltaic Pumping System in Solar Domestic Hot Water Systems

by

ABDULRAHMAN MOHAMMED AL-IBRAHIM

A dissertation submitted in partial fulfillment

of the requirements for the degree of

DOCTOR OF PHILOSOPHY

(MECHANICAL ENGINEERING)

at the

UNIVERSITY OF WISCONSIN-MADISON

1997

Optimum Selection of Direct-Coupled Photovoltaic Pumping System in Solar Domestic Hot Water Systems

Abdulrahman Mohammed Al-Ibrahim

Under the supervision of Professor William A. Beckman

At the University of Wisconsin-Madison

The performance of photovoltaic powered pumps in direct and indirect solar domestic hot water (PV-SDHW) systems has been studied. The direct PV-SDHW system employs a photovoltaic array, a DC-motor, a centrifugal pump, a thermal collector, and a storage tank. The indirect PV-SDHW system employs similar components to those in the direct PV-SDHW system in addition to a heat exchanger to transfer the energy from the collector-loop fluid to the tank-loop fluid. Both a forced convection heat exchanger and a natural convection heat exchanger were investigated. The primary objective of this thesis is to optimize the design and quantify the performance of PV-SDHW systems.

The search methodology for an optimum PV-SDHW system has been performed in a unique two-phase procedure. In phase one the goal is to find, among the possible PV pumping systems' flow rate profiles, the profile that maximizes the performance of a given SDHW system. In phase two the goal is to select the components of the PV pumping system. Each combination of PV cells, DC-motor and pump exhibits a

unique flow rate profile. Therefore, the problem in this phase is to identify the PV pumping system components that results in the best match to the optimum flow rate profile found in phase one. This decoupling considerably eased the process of optimal search. An analysis of actual flow rate profiles of PV pumping systems showed that the optimum search can be restricted to the family of profiles represented by a function dependent upon three parameters only.

A comparison is made between the performance of the optimum direct PV-SDHW system and a conventional direct SDHW system operating under three control schemes: an ON-OFF flow SDHW system operating at the manufacturer's recommended constant flow rate, an ON-OFF flow SDHW system operating at the optimum constant flow rate and a linear proportional flow SDHW system, with the flow proportional to the solar radiation operating under an optimum proportionality. It was found that the optimum direct PV-SDHW system was superior to the systems with conventional control schemes.

Approved:

William A. Beckman _____

Date _____

Acknowledgments

All praises are due to Allah, Lord of the world, and peace and blessing be upon His Messengers. Without the well and the help of Allah, this work would have never been accomplished. All thanks are due to Him.

I would like to thank my advisors, Professors Bill Beckman and Sandy Klein for their guidance and support during the course of this research. Their encouragement and constructive criticism made the completion of this study possible. Bill you have leadership skills that I admire you for. Thank you Sandy, you would be surprise to know that your random number idea made my program run smoother![1] Special thanks go to Professor John Mitchell. John I liked your "window" idea a lot.[2] I am also thankful to Jim Huggins and Steve Long from the Florida Solar Energy Center (FSEC). Their experimental data were extremely useful for this research.[3]

I would like to thank my parents ..... *Ah....what should I say*? Before sending me to my pre-school, you began calling me Dr. Abdulrahman. This way you made sure that your son continues in his academic career with a one-way ticket. You have taken full care of your son; in house and abroad. My father, I will never forget your ending comment during any phone conversation;.... your study, ... your study. My mother,

[1]If anyone don't believe it, then let him run the PV pumping model without the random number generator subroutines and see by himself.
[2]To know more about the "window" concept, then read chapter 5.
[3]To know how valuable is FSEC's contribution to this research, then count the number of the word "FSEC" that have appeared in this thesis.

you lived my academic life more than me. Both of you were working hard and were waiting for this moment since I was born. Thank you. This work is all yours.

This work would have never been accomplished without the continuos support of my family. Sara, Reem, Ruaa, Tariq, and Mohammad, this thesis is all yours. Sara, you waited so long for this moment. You lived every aspect of this research as if you are the researcher. Reem, I will never forget your common question: Baba, how many tasks are left to go. Ruaa, I will never forget your advise on how to start my oral defense exam. Tariq, I will never forget your smile, and your common comment: Baba, why our car isn't smiling? Mohammad, this young boy, although you are a one year old by now, but I feel that you have struggled as well. You came into our house at the time your father was overwhelmed with his research. All of you lived with me the ups and downs of this research. It is all yours. Thank you.

My brothers and sisters, you all lived my work. Thank you.

My friends in Madison, you made my stay in Madison fruitful and convenient. I may not have been able of accomplishing my tasks without you. Thank you.

Thanks go to the solar lab graduate students. It has been a great environment to live in. Special thanks go to Nate Blair, TRNSYS Engineer. You have been always there when I need you the most.

My parents, Sara, Reem, Ruaa, Tariq, Mohammad, and my brothers and sisters, here I am coming, *in sha' Allah*.

Abdulrahman *ibn* Mohammed Al-Ibrahim
Madison, WI
Sha'ban, 29th, 1417 *H*
January 8th, 1997 *G*

Table of Contents

Nomenclature

English Letter Symbols

A	area	[m^2]
a	thermal voltage	[1/Volt]
a, b, c	parameters of the PV pumping system flow rate profile	
C	DC-motor coefficient	
c_1, c_2	curve-fitting constants of the H-Q pump characteristic curve	
C_e	voltage-torque coefficient, for permanent magnet DC-motors	[N-m/Amp]
C_{stat1}	load-sensitive torque losses constant	[N-m]
C_{stat2}	speed-sensitive torque losses constant, the static term	[N-m]
C_{visc}	speed-sensitive torque losses constant, the viscous term	[N-m/s]
e_1, e_2	curve-fitting constants of the □-Q pump characteristic curve	
$\mathcal{F}$	annual solar fraction	[-]
G	solar radiation	[W/m^2]
g	gravitational acceleration	[m/s^2]
G_t	threshold solar radiation	[W/m^2]
H	pump head	[m]
I	current	[Amp]
I_d	diode current	[Amp]
I_L	light current	[Amp]
I_{mp}	current at the maximum power point	[Amp]

I_o	reverse saturation current	[Amp]
I_{sc}	short circuit current	[Amp]
k_1, k_2	constants of the *H-Q* piping system characteristic curve	
k_f	torque constant, for separately excited DC-motors	[N-m/Amp]
L_a	energy delivered from an auxiliary heater	[J]
L_o	total energy required by the load	[J]
L_s	energy delivered from an SDHW system	[J]
M_{af}	mutual inductance, for series excited DC-motors	[N-m/Amp^2]
N	total number of PV cells	[-]
n	shaft speed	[rps]
N_s	total number of PV cells connected in series	[-]
P	number of parallel PV cells strings	[-]
P	power	[W]
P_{max}	maximum power	[W]
Q	flow rate	[m^3/s]
R	DC-motor resistance	[Ohms]
R_a	armature resistance	[Ohms]
R_{a+f}	sum of the armature resistance and the field resistance	[Ohms]
Re	Reynold's number	[-]
R_s	series resistance	[Ohms]
S	number of PV cells connected in series	[-]
T	shaft torque	[N-m]

T_{amb}	ambient temperature	[K]
T_c	cell temperature	[K]
Type	DC-motor type	[-]
V	voltage	[Volt]
V_{mp}	voltage at the maximum power point	[Volt]
V_{oc}	open circuit voltage	[Volt]

Greek Letter Symbols

	band gap energy	[eVolt]
f	Darcy friction coefficient	[-]
μ_{Isc}	temperature coefficient at the short circuit current	[Amp/K]
μ_{Voc}	temperature coefficient at the open circuit voltage	[Volt/K]
□	pump efficiency	[-]
□	density	[kg/m^3]

Subscripts

amb	ambient
c	cell
dyn	dynamic
losses	losses
max	maximum
ref	reference
stat	static

List of Figures

List of Tables

Chapter 1 Introduction

This chapter discusses important aspects of solar domestic hot water (SDHW) systems and photovoltaic (PV) pumping systems. First, an introductory review of the common characteristics of both systems is given. Emphasis is given to the feasibility and the advantage of integrating a PV pumping system in an SDHW system. This part is followed by an overview of PV pumping systems and SDHW systems, with emphasis on issues related to the current research. Next, the challenges encountered when designing a PV pumping system and integrating it in an SDHW system are presented. Finally, the problem statement and the research objective for this study are presented.

1.1 Prologue

SDHW systems are ranked among the most promising solar energy technologies. However, despite this optimistic view, several technical obstacles remain. Among these obstacles is that SDHW system requires an auxiliary electric source to operate a pump to circulate the fluid through the thermal collector. Also, the collector circulating fluid flows at a constant rate and is commonly controlled by an ON/OFF differential temperature sensing controller. This controller is the weakest component in SDHW hardware (Cromer, 1983; Argonne National Laboratory, 1981 as reported in Winn, 1993), and the device that can produce operational instabilities which make the pump cycle between ON and OFF (Beckman *et al.*, 1994).

As an alternative, PV cells can be used to power the SDHW system's pump(s) and provide a continual adjustment of fluid flow, and possibly improving the system performance. Parker (1975), Merchant (1977), and Czarnecki and Read (1978) experimentally demonstrated the practicability of using PV cells to power the pumps of SDHW systems.

The use of PV cells to power the pumps of SDHW systems is an attractive concept because it serves two purposes. The first is that a PV pumping system can act as a fast-response sensor to solar energy and therefore pumping will only occur at the times when the thermal collector is also receiving solar radiation. Secondly, the use of a PV power source eliminates the demand for an auxiliary power source to operate the pump. Although each motor-pump is small, the pumps of conventional SDHW systems are in operation at the same time and their operating periods include the ON-peak times. Therefore, a reduction in the ON-peak electricity demand as seen by an electric utility with many thousands of PV driven SDHW systems is expected.

1.2 System Overview

1.2.1 Direct-Coupled PV Pumping Systems

A direct-coupled PV pumping system is a group of interactive pieces of equipment designed: (i) to collect and convert the solar radiation into electrical energy (direct current); and (ii) to convert the electrical energy into mechanical energy to provide enough mechanical torque to spin a pump, or a set of pumps, to circulate a fluid.

Direct-coupled PV systems consist of a set of PV cells[4], a DC-motor, a pump and a hydraulic piping system. The direct-coupled PV pumping system has no electric storage device, such as batteries, and no power conditioning units, such as DC-DC converters or DC-AC inverters (i.e., maximum power point trackers). Figure 1.2.1 is a schematic drawing of a direct-coupled PV pumping system.

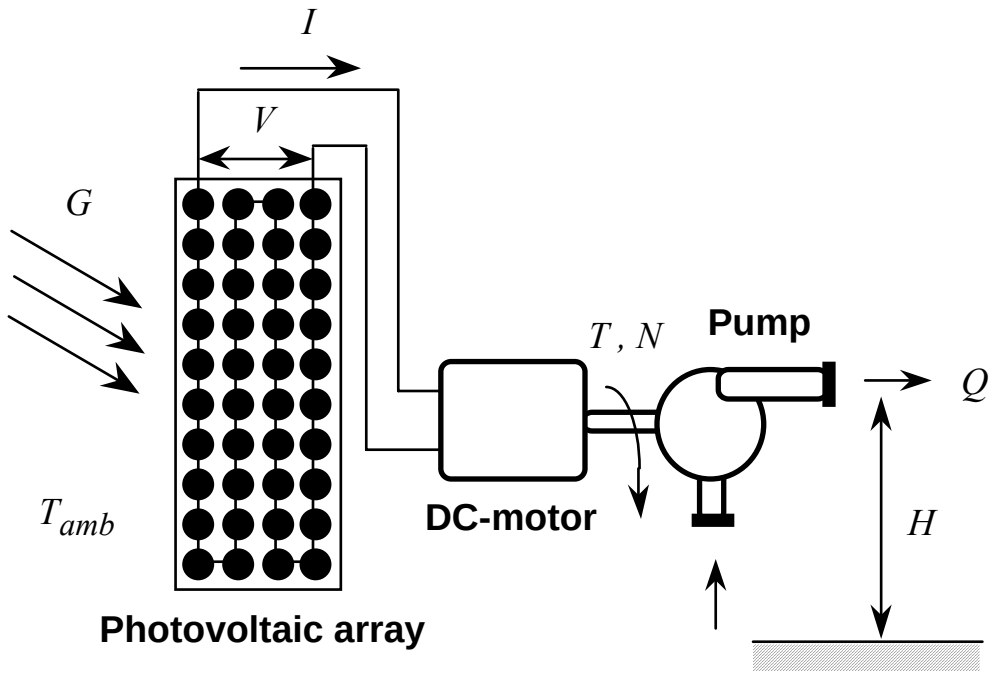

Figure 1.2.1 Schematic drawing of a direct-coupled PV pumping system.

[4]PV cells are grouped in parallel and series to increase the current and the voltage, respectively. Normally, PV cells are grouped in a matrix called modules (or panels), and modules can be grouped in another matrix called arrays. For large applications, arrays are grouped in matrices called fields. Unless otherwise indicated, the terms PV cells, PV modules, PV panels, and PV arrays will be used to describe any group of PV cells connected together.

PV cells are current generators. The PV cells and the attached load (i.e., a DC-motor and a pump installed in a hydraulic piping system) are characterized by their current-voltage relation (*I-V* curve). The power output, *P*, is the product of the current, *I*, and the voltage, *V*. Figure 1.2.2 shows the *I-V* and *P-V* curves of a PV module made of 40 cells connected in series (measured at a solar radiation of 895 W/m^2 and a cell temperature of 50.8 °C) along with the *I-V* curve of a load comprising of a separately excited DC-motor coupled to a centrifugal pump that move water in a hydraulic piping system.

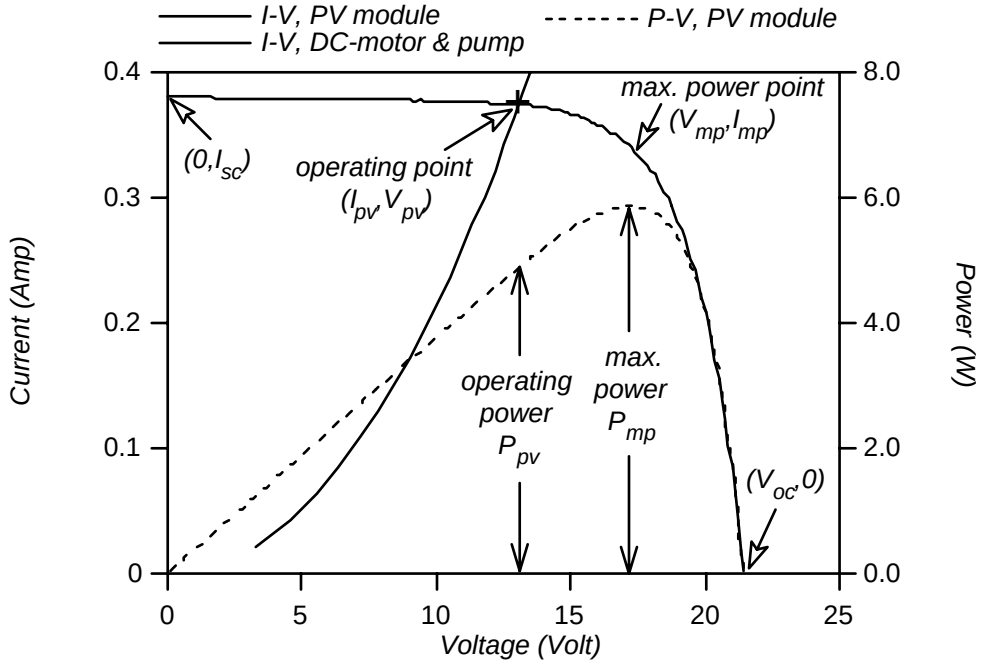

Figure 1.2.2 The *I-V* and *P-V* curves of a PV module and the *I-V* curve of a load comprising of a separately excited DC-motor coupled to a centrifugal pump along with the PV system operating point if the aforementioned components are directly coupled.

The *I-V* curve of the PV cells represents the locus of operating points of the PV system. The operating point of a PV system is the point at which the characteristics of both the PV cells and the attached load match (i.e., *I* and *V* of the PV cells match *I* and *V* of the load). Figure 1.2.2 shows also the expected operating point if the aforementioned PV module and DC-motor and pump are coupled (at a solar radiation of 895 W/m^2 and a cell temperature of 50.8 °C).

PV system operating voltage ranges from the short circuit condition—maximum current, I_{sc}, and zero voltage (where the circuit resistance is zero)—to the open circuit condition—maximum voltage, V_{oc}, and a zero current (where the circuit resistance is infinite). Accordingly, the power output of PV cells varies from zero (at both of the above conditions) to a maximum power level (the maximum power point, P_{max}). A direct-coupled PV system can be designed so that the system operates at the maximum power point of the PV cells at only one radiation level. For the case of Figure 1.2.2, the operating point and the maximum power point would be equal at a much higher radiation level than 895 W/m^2.

The short circuit current I_{sc} of a PV cell is directly proportional to solar radiation and cell temperature. The open circuit voltage V_{oc} of a PV cell increases logarithmically as the incident solar radiation increases, and drops linearly as the cell temperature increases. Accordingly, the *I-V* curve changes as changes occur in the solar radiation level and the cell temperature. Figure 1.2.3 depicts several *I-V* curve measurements of the above PV module obtained at different levels of solar radiation and cell temperature. Figure 1.2.3 depicts also the system operating points if the PV module was directly coupled to the separately excited DC-motor and the centrifugal pump

mentioned above. The system operating points fall along the *I-V* curve of the DC-motor and pump.

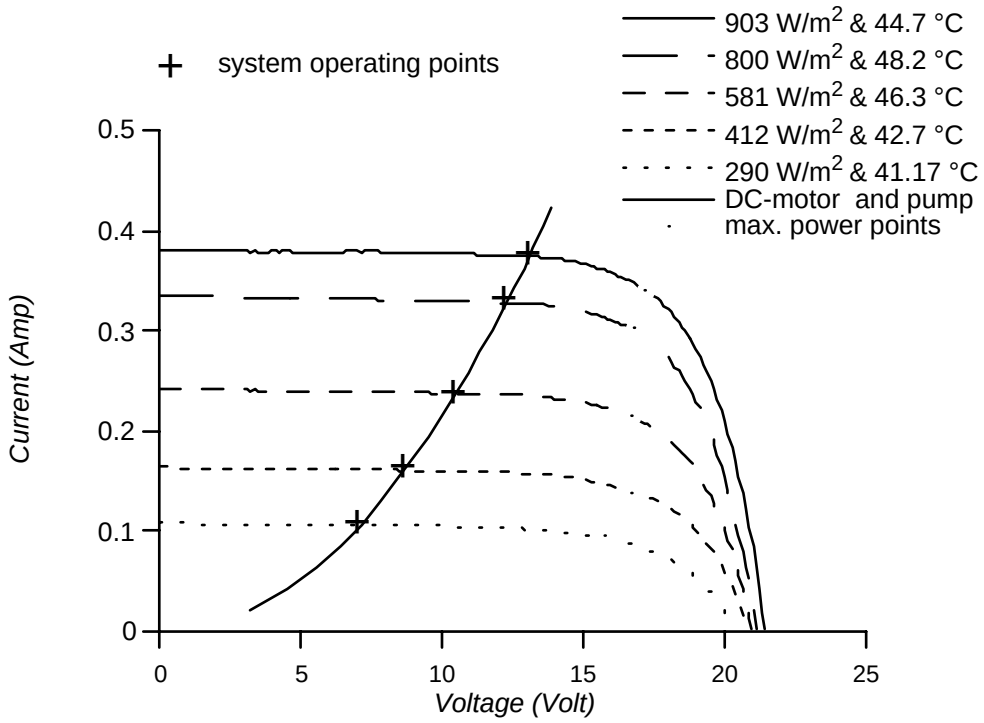

Figure 1.2.3 The effect of solar radiation intensity and cell temperature on PV *I-V* curves and PV system operating points.

As shown in Figure 1.2.3, the operating point of a PV system varies with changes in solar radiation and temperature; consequently, the output power varies. As a result, the pump flow rate varies during the course of the day. This power characteristic highlights the major distinction between PV power generators and conventional fossil fuel power generators. Fossil fuel generators are constant power sources, whereas PV generators are variable power sources.

The performance of a PV system depends upon the performance of its individual components (e.g., PV cells, DC-motor, pump ...etc.) and their relative sizes. The system performs satisfactorily only if its components are matched properly. The system may not function at all if the components are not matched.

Despite the extensive research devoted to enhance the PV cell conversion efficiency (nominal range of 8-12%, with the highest laboratory record of 32.6% (Green and Emery, 1993))[5], the wide adoption of PV systems has faced a crucial obstacle; that is a low system efficiency. The system efficiencies of PV systems are generally much less than the efficiencies of PV cells alone (Balasubramanian, 1992). Hori *et al.* (1985), Balasubramanian (1992), Chaurey *et al.* (1992), Koner *et al.* (1992) and others have attributed the low PV system conversion efficiencies to mismatches among subsystems that constitute the PV system. These mismatches were mainly attributed to the improper sizing of the subsystem components.

The task of properly selecting and sizing the subsystem components of any integrated system is a challenging task of the overall system design. Moreover, in the case of designing a direct-coupled PV system, the difficulties are magnified because PV cells are neither a constant current nor a constant voltage source.

---

[5]PV cell efficiency hereafter is reported at the standard test condition; solar radiation of 1000 W/m^2 and an ambient temperature of 25 °C unless otherwise indicated.

1.2.1.1 Flow Rate Profile of Direct-Coupled PV Pumping Systems

PV pumping systems are characterized by the flow rate, Q, as a function of solar radiation, G, and ambient temperature, T_{amb}. (hereafter, the flow versus solar radiation curve will be called the flow rate profile). Figure 1.2.4 shows typical flow rate profiles of a direct-couple PV pumping system at two ambient temperatures. Different sizes and types of the system components will result in different flow rate profiles; however, the trend of the profile remains the same.

PV pumping systems require a threshold radiation level just to start the pump. Afterward, the flow rate increases as the solar radiation increases. Hydraulic static head (e.g., elevation) increases the pumping threshold radiation level and consequently delays the pump starting. Hydraulic dynamic head decreases the flow rate. Therefore, increasing pipe length, adding more fittings, and/or decreasing pipe diameter decreases the flow rate.

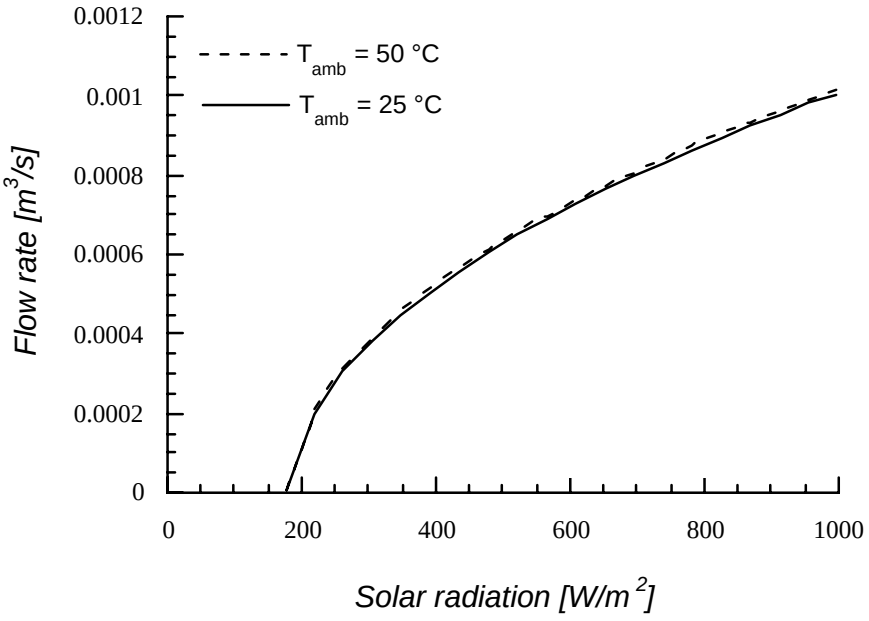

Figure 1.2.4 Typical flow rate profiles of a direct-coupled PV pumping system.

1.2.2 SDHW Systems

SDHW systems are classified as one-tank or two-tank systems. In a direct SDHW system, the thermal collector absorbs solar radiation energy and transfers this energy to a circulating fluid. The circulating fluid transfers the collected energy to a storage device or, in some cases, to the load directly. In an indirect SDHW system, there exists two separate fluid loops: collector loop and tank loop. Energy is transferred from the collector loop to the tank loop through a heat exchanger. Various kinds of heat exchangers can be placed inside or outside the storage tank.

The elements of an SDHW system can be arranged in several configurations. Duffie and Beckman (1991) outline the common configurations as: (a) One-tank system; (b) System with antifreeze loop and internal heat exchanger; (c) System with antifreeze

loop and external heat exchanger. Figure 1.2.5 shows these common configurations. Auxiliary energy is shown added in three different ways; in a line heater, in the solar storage tank, or in a second tank. Any of these auxiliary methods can be used with any of the collector-tank arrangement.

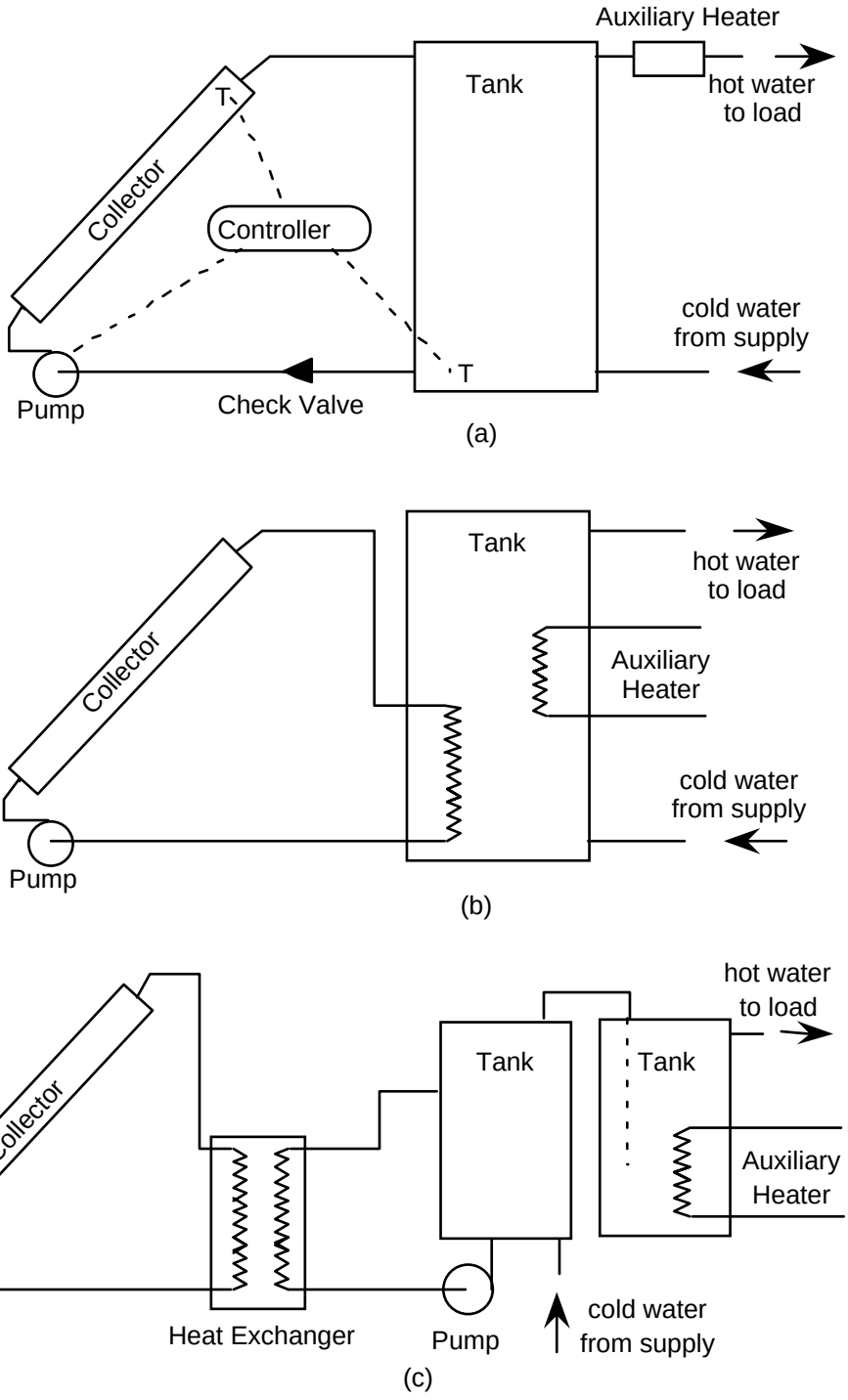

Figure 1.2.5 Schematic drawings of common configurations of active SDHW systems. Adapted from Duffie and Beckman (1991).

1.2.2.1 Effect of Flow Rate on SDHW System Performance

The thermal performance of an SDHW system is influenced by the rate at which the heat transfer fluid within the system is circulated. Similarly its components (e.g., thermal collector, storage tank, ...etc.). However, the thermal performance of some components increase with increased flow rates while others decrease. The following is a summary of the effect of flow rate on the main components of SDHW systems:

Thermal collector: Its performance is characterized through a heat removal factor F_R. The higher the collector flow rate, the higher the efficiency of the collector. From the thermal collector view point, it is preferred that the flow rate be at its maximum level. However, at very high flow rates the temperature rise though the collector approaches zero.

Storage tank: The degree of thermal stratification in the storage tank is a measure of its performance. High tank performance is achieved when stratification is maintained. Increasing flow rate through the collector results in greater mixing in the storage tank, and consequently reduces the degree of thermal stratification in the tank. From the tank view point, it is preferred that the flow rate in the collector loop and the load loop be at their minimum level.

Heat exchanger: Its performance depends on its heat transfer coefficient area product UA which is directly proportional to the fluid flow rate in both sides of the heat exchanger. From the heat exchanger view point, it is preferred that the flow rate in both sides of the heat exchanger be at their maximum level.

Circulation pump: Auxiliary power required to circulate the fluid is a quadratic function of flow rate. From the pump view point, it is preferred that the flow rate be at its minimum level.

1.3 Problem Statement

Although the idea of implementing direct-coupled PV pumping systems in SDHW systems is attractive; however, it is not a viable concept unless further efforts are made to overcome several challenges. Among these challenges are:

(i) There are numerous configurations of direct-coupled PV systems and SDHW systems to choose from. Due to the highly non-linear nature of direct-coupled PV pumping systems, the selected PV pumping system may not function satisfactorily—or may not function at all—if the components are not matched.

(ii) It is necessary to identify the optimum flow rate required by an SDHW system that maximizes the system's performance and to design a PV pumping system accordingly.

(iii) SDHW systems are designed to operate under a wide ranges of operating conditions. Therefore, the advantages of integrating a self-adjusting flow device in an SDHW system provides another challenge; that is the optimization analysis be based on a time-integral quantity rather than a one reference condition.

To overcome these challenges, it is essential to establish a robust design procedure for an optimal configuration of a PV pumping system in SDHW systems.

1.4 Research Objective

The primary objective of this research is to optimize the design and quantify the performance of photovoltaic powered direct and indirect solar domestic hot water (PV-SDHW) systems. Different PV pumping system configurations and SDHW system configurations will be investigated to determine an optimal PV-SDHW system. A direct search optimization method will be used to search for an optimal PV-SDHW configurations.

A secondary objective of this research is to conduct a comparative analysis between the long-term performance of the proposed optimal PV-SDHW system and a conventional SDHW system operating under three control schemes. The three schemes are: an ON-OFF flow controlled SDHW system operating at the manufacturer recommended flow; an ON-OFF flow controlled SDHW system operating at the optimum constant flow rate; and, a linear proportional flow controlled SDHW, with the flow proportional to the solar radiation operating under an optimum proportionality. Emphasis will be placed on quantifying the expected gain in system performance and the expected reduction in electric demand during the utilities' ON-peak hours.

The overall investigation will be based upon mathematical models of the PV-SDHW system components. Experimental measurements will be used to examine the validity of these models. The proposed models of the system components will be integrated into the transient system simulation program TRNSYS.

Chapter 2 Literature Review

The following chapter summaries previous investigations related to the goals of the present research. This chapter is divided into four main sections. The first section reviews literature investigating the modeling and the operational performance of PV-SDHW systems. Only seven references were found that discussed limited issues related to the design and the operation of PV-SDHW systems. Therefore, a review of direct-coupled PV pumping systems and conventional SDHW systems was essential. The second section is devoted to summarizing the modeling and the performance investigations of PV pumping systems. The third section is devoted to summarizing the performance investigations of SDHW systems. Finally, the last section highlights the main conclusions obtained from the literature reviewed.

2.1 PV-SDHW Systems

2.1.1 System Simulation Techniques

Chandra and Litka (1979) simulated a PV-SDHW system by developing a correlation to monitor the performance of a direct-coupled PV pumping system integrated in an SDHW system. The performance data were obtained experimentally and then used to develop a TRNSYS subroutine to model the performance of the PV pumping system. No information was provided on the performance indicator nor the experimental setup.

Miller and Hittle (1993) simulated a direct-coupled PV pumping system by generating a linear correlation of flow rate profile versus solar radiation. The correlation was generated from mathematical evaluations of the flow rate at five different solar radiation levels. In the Miller and Hittle analysis, the voltage of PV array was assumed to be independent of solar radiation, and temperature effects on the PV current was ignored. The linear flow profile correlation was used to develop a PV pumping subroutine to perform an annual simulation of the PV-SDHW system.

2.1.2 Comparative Analysis of PV-SDHW Versus Conventional SDHW

Chandra and Litka (1979) numerically investigated the possibility of replacing the conventional AC pump and controller of a direct one-tank SDHW system with a PV module directly coupled to a DC-motor and a circulating pump. As indicated earlier, Chandra and Litka obtained the performance data of a PV pumping system experimentally. During their experiment, the flow rate was adjusted such that a maximum flow rate equal to the value of nominal flow rates in conventional SDHW systems was achieved. Based on the simulation of a one sunny day with intermittent cloud cover, Chandra and Litka observed a slight improvement in the performance the PV-SDHW system over the conventional SDHW system.

Mertes and Carpenter (1985) numerically compared the performance of a PV powered indirect two-tank SDHW system with an internal heat exchanger to the performance of a thermosyphon and a conventional SDHW system. Mertes and Carpenter found that the PV-SDHW system produced 5% more energy than the conventional SDHW system and 5% less energy than the thermosyphon SDHW system. Comparisons were made

by evaluating energy savings as a function of average flows. No information was given on the method of computing the average flows of the thermosyphon and the PV-SDHW systems, nor did they furnish information related to the configurations of the referenced thermosyphon and SDHW systems.

Miller and Hittle (1993) investigated the integration of a PV powered pump to drive the fluid through an SDHW system employing a wrap-around heat exchanger and an immersed auxiliary energy source. Results were compared to a base system that has an identical collector configuration, storage tank and pump. However, a collector-tank heat exchanger was not considered. Instead, a fully-stratified variable-inlet water storage tank was assumed to replace the wrap-around heat exchanger and tank system. The base system was found to perform slightly better than the proposed system. However, Miller and Hittle stated that their model for the wrap-around heat exchanger tank and PV powered pump lacked experimental validity.

2.1.3 Pump Starting

Cromer (1983) indicated that conventional direct-coupled PV pumping systems are commonly designed such that PV panels are oversized just to produce high current to start the motor-pump. Cromer proposed the use of a pump starter to start the pump-motor because the cost of the pump starter is significantly lower than the cost of the additional PV panels. On the other hand, Mertes and Carpenter (1985) proposed the use of a solar cell-based controller to delay the starting of the pump such that no pumping occur below critical radiation levels.

2.2 PV Pumping Systems

2.2.1 System Simulation Techniques

Kiatsiriroat *et al.* (1993) developed a modified concept of the utilizability function[6] to estimate the long-term performance of a direct-coupled PV pumping system. Kiatsiriroat *et al.*'s modified utilizability function defines the critical threshold solar radiation level as the radiation intensity during which pumping starts. They mathematically represented the power output of the direct-coupled PV pumping system as a function of the area of the PV module, the monthly-averaged hourly global radiation, and a lumped parameter to represents the overall efficiency of the direct-coupled PV pumping system.

Loxsom and Durongkaveroj (1994) used a modified utilizability function similar to the one proposed by Kiatsiriroat *et al.* (1993) to estimate the performance of a direct-coupled PV pumping system. However, Loxsom and Durongkaveroj used a measured flow rate versus solar radiation to estimate the flow rate profile, and consequently the performance of the system. The continuous non-linear flow rate profile (shown in Figure 1.2.4) was modeled using two linear segments. Loxsom and Durongkaveroj compared the performance of the proposed system to a similar system that uses hourly TMY data and a third order polynomial fit of the flow rate profile. Results of this comparison revealed that the utilizability model predicts the monthly pump output within a maximum uncertainty of up to 13% on a seasonal basis and up to

[6]Solar radiation utilizability is defined as the fraction of total radiation incident on a surface that exceeds a specified intensity level.

140% on a monthly basis. Loxsom and Durongkaveroj attributed the observed large uncertainties to the inaccuracy of the solar radiation correlation.

None of the preceding analysis have considered the effect of ambient temperature on the flow rate profile.

2.3 SDHW Systems

The performance and modeling of SDHW systems has been well studied and documented. There exists a large body of literature investigating the different factors that influence the performance of the SDHW system.

Wuestling (1983), Hirsch (1985), Hollands and Lightstone (1989), Parent *et al.* (1990), Hollands and Brunger (1992) and others investigated the effect of several factors on the performance of SDHW systems.

2.3.1 Effect of Flow Rate on SDHW Systems Performance

The thermal performance of a SDHW system is influenced by the rate at which the heat transfer fluid within the system is circulated. Different SDHW control schemes have been implemented to control the flow rates. Early analyses of SDHW systems recommended the use of the maximum possible flow rate to enhance the system efficiency. In these analyses, however, two major assumptions are employed (as seen in TRNSYS (1994) and F-CHART (1985)): (1) The storage tank is fully mixed; i.e., a lumped temperature value is to be used to represent the fluid temperature contained in

the storage tank and therefore, the effect of stratification is eliminated; and, (2) Pumping power is ignored. Therefore, the rule of thumb conclusion is that: it is preferable to increase the flow rate to its maximum. However, if either or both of the above assumptions is/are not assumed, different conclusions will be obtained. The following two sections summaries the investigations that have not assumed either or both of the above assumptions. Because of the role of the collector flow rate on the tank thermal stratification, distinction is given to direct and indirect SDHW systems.

2.3.1.1 Direct SDHW Systems

Lavan (1977), Sharp (1978), Cole and Bellinger (1982), Wuestling *et al.* (1985) and others indicated that there exists a collector flow rate that maximizes the SDHW system efficiency. This optimum flow rate is generally lower than the flow rates recommended by the collector manufacturer.

Wuestling *et al.* (1985) showed that the increase in collector efficiency due to lower inlet temperature often outweighs the decrease in efficiency due to the reduction in the collector efficiency factor F_R and that an optimum flow rate exists.

Collares-Pereira *et al.* (1984) analytically compared the implementation of two control strategies in SDHW systems with no storage tank. The first strategy was a constant collector flow rate identical to the load flow rate. The second control strategy is to vary the collector flow rate such that a pre-set constant collector outlet temperature is achieved. Collares-Pereira *et al.* concluded that the system with the

constant flow rate strategy will deliver more yearly useful energy than the variable flow rate strategy.

Wuestling *et al.* (1985) performed annual simulations to monitor the thermal performance of direct SDHW systems operated under several control strategies. Among these strategies were reduced constant collector flow rates and variable collector fluid flow rates. Wuestling *et al.* concluded that an improvement in the thermal performance of the system occurs at reduced constant flow rate (on the order of 20% of conventional flow rates). Slightly smaller improvements were observed if the flow rate was varied to obtain a specified collector outlet temperature or if the flow rate was varied to achieve a constant temperature rise across the collector. Wuestling *et al.* also found that if the collector flow rate was varied proportionately to the utilizable radiation; the difference between the radiation incident on the collector and the critical threshold level, the system performance was found to be nearly equal to the optimum reduced fixed flow performance. Wuestling *et al.* commented that this later strategy requires advance knowledge of future radiation levels and ambient temperatures and therefore could not be implemented in practice.

Wuestling *et al.*'s analysis of the proportional flow rate strategy was based upon the following assumptions: (a) the fluid flow rate was computed based upon the assumption that the inlet temperature to the collector is constant regardless of the tank outlet temperature, (b) the flow rate was assumed to be linearly dependent on the utilizable energy, (c) to avoid re-circulation, the size of the storage tank was set to be equal to the integral collector flow during one full day of operation. Therefore, advance knowledge of future radiation levels and ambient temperatures was essential for Wuestling *et al.*'s case.

Figure 2.3.1 depicts a re-computation of the flow rate profile in Wuestling *et al.*'s system operated under the strategy of varying the flow rate proportional to the utilizable energy. The relation is almost linear at nominal radiation levels. Significant similarities can be observed between the flow profile of the direct-coupled PV pumping system (as shown in Figure 1.2.4) and the flow profile of the strategy of varying the flow proportionally to the utilizable radiation.

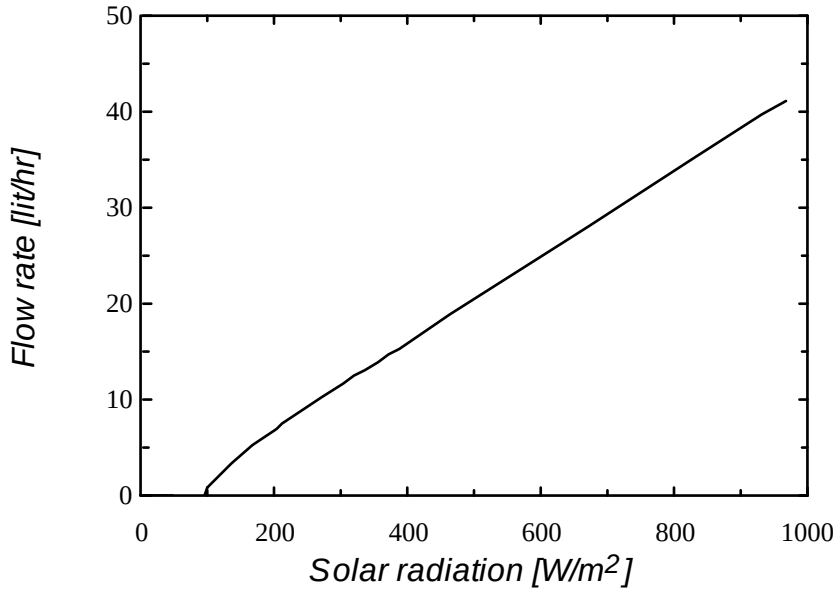

Figure 2.3.1 Flow rate profile of the strategy of varying the flow proportionally to the utilizable radiation in Wuestling *et al.*'s SDHW system.

Fanney and Klein (1988) performed side-by-side experimental investigations to evaluate the influence of the flow rate on the thermal performance of two direct SDHW systems. The first system was a direct SDHW system utilizing a conventional return tube to the storage tank. The return tube discharges the hot fluid at the top of

the storage tank. The second system was a direct SDHW system in which the tank was fitted with a stratification-enhancing return tube designed to reduced internal tank fluid mixing. All experiments were subjected to the same environmental conditions and were subjected to the same load profile. Results of the first system employing conventional return tubes show improvements in the overall system performance as a result of lowering the collector fluid flow rate. For the second system, where the return tube was replaced with stratification-enhancing returned tubes, results show insignificant difference in overall performance for conventional and reduced flow rates. Fanney and Klein reported, that the results of the second system proves the conclusion of Karaki *et al.* (1985) that when effective stratification devices are used within storage tank, little difference in daily energy collected is observed for identical systems utilizing low and moderately high flow rates.

2.3.1.2 Indirect SDHW Systems

Hirsch (1985) extended Wuestling *et al.*'s mathematical investigation to study the impact of various control strategies on the performance of SDHW systems with heat exchangers. Hirsch's results show a reduction of system performance when the flow rate was reduced from standard values on either side of the heat exchanger. Hirsch concluded that the penalty of reduced heat transfer coefficient at lower flow rate generally outweighs the advantage of a stratified storage tank so that performance improvements for systems with collector-storage heat exchangers at reduced flow rates are not likely.

As another control strategy, Hirsch restricted cycling during periods of low radiation level (start-up, cloud cover, shut down). Simulation results of this strategy showed a reduction in the systems efficiency when compared to systems operating at constant high flow rate. However, insignificant difference was found if compared to systems operating at constant low flow rates. Simulation with a combined proportional controller and an ON/OFF controller resulted in an increased solar fraction of 2 and 0.5% for the single and double tank systems, respectively. The proportional controller was set to adjust the flow rate such that the collector outlet temperature did not exceed the supply set temperature.

Fanney and Klein (1988) performed side-by-side experimental investigations to evaluate the influence of the flow rate on the thermal performance of an indirect SDHW system employing an external counter-flow heat exchanger to transfer heat from the solar collector to the potable water. The results of their investigation showed that the system exhibited no optimum flow rates at either side: the higher the flow rate, the better the performance.

Hollands and Brunger (1992) perform a theoretical investigation to determine the optimum collector flow rate in SDHW systems having an external counter flow heat exchanger. Their analysis was based upon the assumption that the overall exchanger conductance *UA* can be held fixed while the flow rates are varied in the search of an optimum. This assumption requires the design (or in other words, the heat transfer area) of the heat exchanger to vary with flow rate. Based on analytical investigation, they showed that optimum flow rates exist on both sides of the heat exchanger. Hollands and Brunger concluded that the optimum value of the collector flow rate is

independent of the amount of solar radiation, the tank-side heat exchanger inlet temperature and the ambient temperature.

2.3.2 Effect of Load Profile on SDHW systems

The performance of an SDHW system depends upon the amount and the frequency of the input energy as well as the amount and the frequency of the discharged energy. Furthermore, the tank performance depends upon the thermal stratification. Therefore, flow rate and frequency, in both the collector and the load, affect the performance of the overall SDHW system. Tabarra and Bowman (1985) performed experimental investigations to investigate the effect of the size and the pattern of domestic loads on systems using stratified storage. Tabarra and Bowman found that changing the daily load pattern from evening peak to noon peak caused a 17% rise in solar fraction; changing to a morning peak produced a 30% drop in solar fraction; and, increasing the volume of daily load from 175 liters at 60 °C to 231 liters at 45 °C could increase the solar fraction by 45%. Tabarra and Bowman concluded that SDHW systems with stratified storage tank are best suited to the daily loads displaying noon peaks and lower delivery temperatures.

Wuestling *et al.* (1985) numerically investigated the effect of the variation in the daily and the weekly load profiles on the optimum reduced flow rate discussed earlier. Wuestling *et al.*'s results show that the optimum value of the ratio of monthly averaged daily total collector flow rate to daily total load flow ($\overline{M}_c/M_L$) was found to be independent of the load profile. However, for various tank sizes it was found that $\overline{M}_c/M_L$ decreases slightly as the total daily draw increases. The magnitude of the

solar fraction was found to be dependent upon the load profiles and the total daily draw.

2.4 Literature Review Summary

The performance and the modeling of photovoltaic powered direct and indirect solar domestic hot water (PV-SDHW) systems has not been the subject of an in-depth study. In specific:

- No design procedure has been proposed to optimally select the components of a PV-SDHW system.
- A very limited number of configurations have been examined.
- The potential gains in the systems' performance have not been quantified.
- Comparative analysis of PV-SDHW systems to conventional SDHW systems operating under different control strategies is not complete.
- Among the possible configurations of SDHW system, no one design has been clearly advanced as a candidate for the optimal configuration.

On the other hand, the literature review showed that the flow rate profile (the flow rate Q as a function of the solar radiation G) to be the most significant factor in the efficiency of PV pumping and PV-SDHW systems. Therefore, more emphases should be given to the rule of flow rate profiles on PV pumping and PV-SDHW systems performance. Moreover, the large errors observed in the results of Kiatsiriroat *et al.*'s (1993), Miller and Hittle (1993) and Loxsom and Durongkaveroj's (1994) indicated

that if the flow rate profile needs to be curve-fitted, then non-linear curve fitting techniques should be used instead of linearizing this non-linear curve.

Chapter 3 Mathematical Modeling of PV-SDHW System Components

The following chapter summaries the mathematical modeling of the major components of PV-SDHW systems. The first section presents the governing equations of the PV pumping system components. The second section presents the available and validated models of the SDHW system components. The third section reviews literature related to the system simulation time step. Finally, the last section validates the proposed PV pumping system model against experimental measurements. The PV pumping system model will be coupled with the SDHW system model to constitute the PV-SDHW system model.

3.1 Mathematical Modeling of PV Pumping System Components

3.1.1 PV Cells

Rauschenbach (1980) and Townsend (1989) showed that PV cells can be modeled by a simplified equivalent electrical circuit that contains parameters having physical meaning related to physical phenomena in the cell.

Rauschenbach (1980), Macomber *et al.* (1981), Green (1982) and Townsend (1989) reviewed several equivalent circuits and recommended the use of the single-diode four-parameter equivalent circuits. Roger *et al.* (1984), Hori *et al.* (1985), Appelbaum (1987), Eckstein *et al.* (1990), Duffie and Beckman (1991),

Alghuwainem (1992) and others have used the single-diode four-parameter model to predict the performance of PV cells. The following is a summary of the model as reported by Duffie and Beckman (1991):

$$I = I_L - I_o \left\{ \exp\left[\frac{V + I R_s}{a} \right] - 1 \right\} \qquad 3.1.1$$

where

$$I_{L,ref} = I_{sc,ref} \qquad 3.1.2$$

$$I_{o,ref} = \frac{I_{L,ref}}{\exp(V_{oc,ref}/a_{ref}) - 1} \qquad 3.1.3$$

$$R_{s,ref} = \frac{a_{ref} \ln(1 - I_{mp,ref}/I_{L,ref}) - V_{mp,ref} + V_{oc,ref}}{I_{mp,ref}} \qquad 3.1.4$$

$$a_{ref} = \frac{\mu_{Voc} T_{c,ref} - V_{oc,ref} + \varepsilon N_s}{\frac{T_{c,ref} \mu_{Isc}}{I_{L,ref}} - 3} \qquad 3.1.5$$

$$\frac{a}{a_{ref}} = \frac{T_c}{T_{c,ref}} \qquad 3.1.6$$

$$I_L = \frac{G}{G_{ref}} \left[I_{L,ref} + \mu_{Isc} \left(T_c - T_{c,ref} \right) \right] \qquad 3.1.7$$

$$\frac{I_o}{I_{o,ref}} = \left(\frac{T_c}{T_{c,ref}} \right)^3 \exp\left[\frac{\varepsilon N_s}{a_{ref}} \left(1 - \frac{T_{c,ref}}{T_c} \right) \right] \qquad 3.1.8$$

$$R_s = R_{s,ref} \qquad 3.1.9$$

$$T_c = T_{amb} + \frac{G \tau\alpha}{U_L} \left(1 - \frac{\eta_c}{\tau\alpha} \right) \qquad 3.1.10$$

Here □is the cell material band gap; 1.155 eV for silicon (Green, 1982), I_L is the light generated current, I_o is the reverse saturation current, a is the thermal voltage, R_s is the series resistance, N_s is the number of cells in series times the number of modules in series, G is the solar radiation, T_c is the cell temperature, $\tau\alpha$ is the trasmittance-absorbtance product; (assumed to be 0.9 (Duffie and Beckman, 1991)), U_L is the overall heat transfer coefficient, η_c is the PV cell efficiency and the subscript *ref* denotes the value of the corresponding variable at a reference condition. U_L can be assigned a fixed value throughout the simulation period or it can be related to the ambient temperature and the wind velocity using published heat transfer correlations (Duffie and Beckman, 1991).

The form of Equation 3.1.10 is implicit with respect to I, V, and η_c; η_c is a function of T_c. One way of solving for η_c and T_c is by using a technique, such as the successive-substitution method. However, this method is cumbersome as it adds to the complexity of the overall PV pumping model. This is further complicated by the fact that the PV cells model will be directly-coupled to other nonlinear models. An easier way is to assume that the PV cells efficiency at the reference condition, $\eta_{c,ref}$, is representative of η_c. This is a reasonable assumption as $\eta_{c,ref}$ is generally low (5~12%) and η_c rarely exceeds $\eta_{c,ref}$. Additionally, the term $\frac{\eta_c}{\tau\alpha}$ is small compared to unity (Duffie and Beckman, 1991).

Figure 3.1.1 depicts a simulated *I-V* curve of a PV array compared to a measured *I-V* curve of the same PV array obtained at a reference condition of 1080 W/m^2 and 35.5°C. A close match is observed. Table 3.1.1 lists the error between the simulated

and the measured *I-V* curves of five PV modules supplied by different manufacturers. The error indicator is the normalized sum of square of error, *nsse*[7].

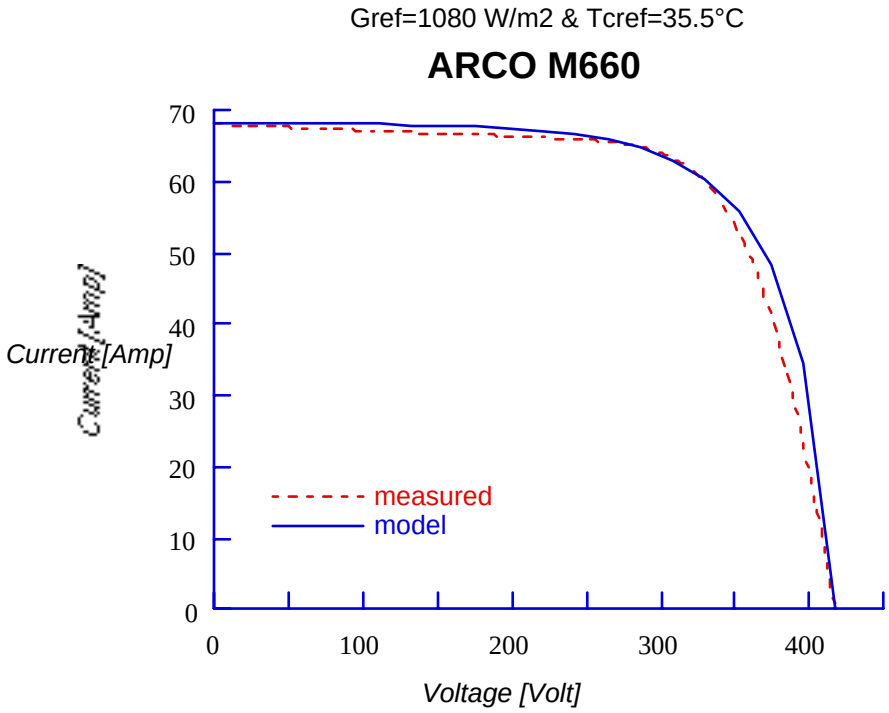

Figure 3.1.1 Measured and calculated *I-V* curve of a PV module at a reference condition of 1080 W/m^2 and 35.5 °C.

[7] *nsse* is defined as $nsse = \sum_{i=1}^{n} \left[I_{meas,i} - I_{cal,i}\right]^2 / \left(n\, I_{meas,sc}\right)$ where *n* is the total number of data points.

Table 3.1.1 Normalized sum of square of error between the measured and the simulated *I-V* curves of five PV modules supplied by different manufacturers.

PV module	***nsse***
AEG (PQ 10/40/01) Indoor test; 1 module	0.00288
AEG (PQ 10/40/01) Outdoor test; 1 module	0.00098
ARCO M660; 20 X 20 modules	0.00016
Kyocera LA36/J45V; 1 module	0.00049
Sharp NT-11-H; 1 module	0.00253

3.1.2 DC-Motors

DC-motors are electro-mechanical devices which convert electrical energy into mechanical energy. The inputs to DC-motors are *I* and *V* and the outputs are torque, *T*, and speed, *n*. The *T-n* relation is a characteristic relation that enables the system designer to predict the performance of DC-motors.

DC-motors are classified (Singer and Appelbaum, 1993) as either: (i) permanent magnet; (ii) series excited; (iii) shunt excited; or, (iv) separately excited.

The mathematical modeling of DC-motors has been addressed by Roger (1979), Slemon and Straughen (1980), Hsiao and Blevins (1984), Appelbaum (1986), Eckstein *et al.* (1991), Khater (1991), Alghuwainem (1992), Singer and Appelbaum (1993) and others. The available models govern both the steady state and transient operation of DC-motors.

Of related interest to solar radiation application are fluctuations in the solar radiation and the demand load. If the fluctuations period of the solar radiation are smaller than the time constant of any of the system components, then dynamic effects should be included. Otherwise, steady-state operation could be reasonably assumed. Fam and Balachander (1988) theoretically studied the dynamic performance of a shunt DC-motor directly coupled to a PV array driving a constant torque load. They showed that the transient interval of their studied system under consideration was less than 3 seconds. Anis and Metwally (1994) experimentally studied the dynamic performance of a permanent magnet DC-motor directly coupled to a PV array that derives a centrifugal pump. Anis and Metwally observed that the system variables (e.g., *I*, *V*, and *n*) vary considerably when a sudden change in clouds takes place. However, the system parameters reach steady state operation in less than 3 seconds. Due to the small time interval of the system transient condition and the rare occurrence of the power or load interruption within this small time interval, the dynamic effects of the DC-motors will be ignored.

Townsend (1989) investigated the direct-coupling of different DC-motors, and showed that shunt DC-motors demand the highest starting torque among the four DC-motor types. Furthermore, because of the possibility that multiple operating points exist, Townsend indicated that PV pumping system employing a shunt DC-motor might suffer from unstable operating conditions. Therefore, shunt DC-motors will not be considered in this investigation of the optimum PV-SDHW system.

The following is a summary of the steady-state *T-n* relations for the series excited, the permanent magnet and the separately excited DC-motors as it appears in the literature sited above.

Series Excited DC-Motor

$$n = \frac{1}{2\pi M_{\text{af}} I}\left[V - R_{a+\text{f}} I\right] \qquad 3.1.11$$

$$T = M_{\text{af}} I^2 \qquad 3.1.12$$

where M_{af} is the mutual inductance and $R_{a+\text{f}}$ is the sum of the armature resistance, R_a, and the field resistance, R_f.

Permanent Magnet DC-Motor

$$n = \frac{1}{2\pi C_e}\left[V - R_a I\right] \qquad 3.1.13$$

$$T = C_e I \qquad 3.1.14$$

where C_e is the torque coefficient and R_a is the armature resistance.

Separately Excited DC-Motor

$$n = \frac{1}{2\pi k_{\text{f}}}\left[V - R_a I\right] \qquad 3.1.15$$

$$T = k_{\text{f}} I \qquad 3.1.16$$

where k_f is the torque coefficient.

Townsend (1989) and Koner *et al.* (1992b) recommended the use of separately excited DC-motors in PV pumping systems as the *I-V* curve of the DC-motor-pump-load follows closely the maximum power point locus of the PV cells. However, their criterion was the maximum flow rate. Whereas, in the case of the present investigation of the optimum PV-SDHW system, the criterion of the PV-SDHW performance is to maximize the annual solar fraction, which could occur at a flow rate other than the maximum. Therefore, all of the forgoing three DC-motors will be considered in the present investigation.

The DC-motors' model constants (i.e., R_a, R_{a+f}, k_f, ...etc.) are not usually supplied by the DC-motors manufacturers. If this is the case, the constants are to be evaluated using a non-linear regression analysis provided that a characteristic curve such as the *T-n* curve is available.

3.1.2.1 Torque Losses in DC-Motors

Of related importance to the modeling of PV pumping systems is the modeling of the torque losses in DC-motors. In several PV pumping applications, it was found that DC-motors never start until a very high current is generated from the PV cells. These current values are often higher than the values required to pump the fluid. In some applications, these starting currents are higher than the maximum currents that can be generated at the maximum solar radiation levels, preventing the DC-motor from ever starting. Figure 3.1.2 shows two examples of PV pumping systems that exhibit a delay in starting. While both PV pumping systems share identical PV cells and a hydraulic load, each system employs different DC-motors; MARCH 12V DC-motor and

MARCH 24V DC-motor. The system employing the MARCH 12V DC-motor does not start until the solar radiation level exceeds 875 W/m^2 and the system employing the MARCH 24V DC-motor does not start until the solar radiation level exceeds 350 W/m^2.

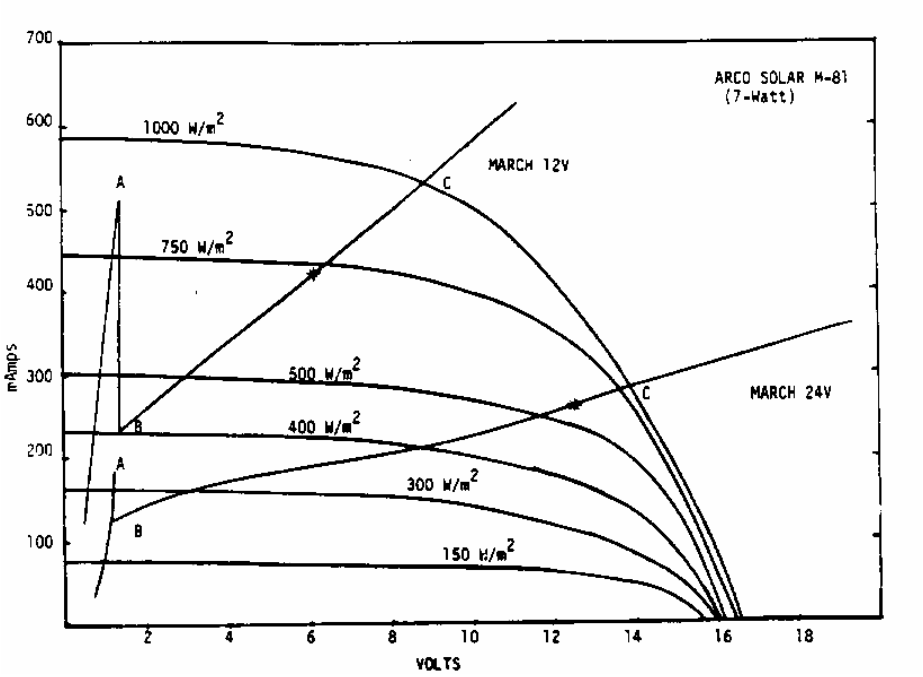

Figure 3.1.2 I-V curves of a PV cells and two different DC-motor-pump loads. From Cromer (1984).

The origins of the losses can be categorized into two groups (Electro-Craft Corporation, 1978); the load sensitive losses group which is dependent upon the generated torque, and the speed sensitive losses group which is dependent upon the rotational speed. The load sensitive losses are caused by winding losses. The speed sensitive losses are caused by brush contact losses, eddy current losses, hysteresis effect, winding and friction and short circuit currents. When added together, the

overall torque loss profile as a function of the shaft rotation speed follows a general profile similar to the profile depicted in Figure 3.1.3 (Electro-Craft Corporation, 1978; Novotny, 1996).

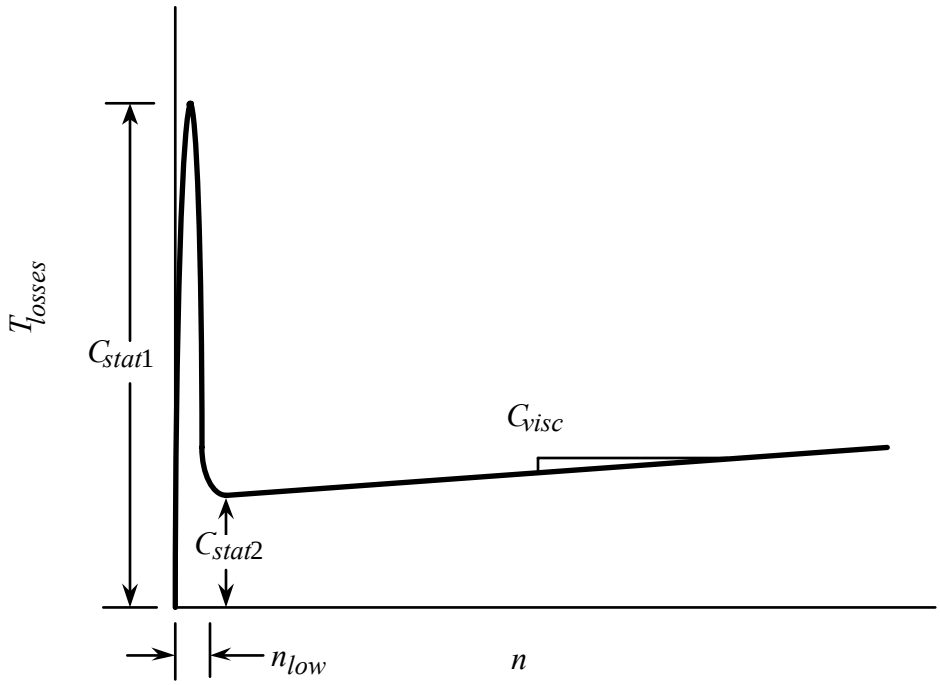

Figure 3.1.3 The general torque losses profile as a function of the shaft speed. Drawing is not to-scale.

The general torque losses profile in Figure 3.1.3 can be modeled using the following equations:

$$T_{losses} = \begin{cases} C_{stat1} & \text{for } n \le n_{low} \\ C_{stat2} + 2\,\pi\, n\, C_{visc} & \text{for } n > n_{low} \end{cases} \qquad 3.1.17$$

where C_{stat1} is the load sensitive losses constant, C_{stat2} and C_{visc} are the speed sensitive losses constants. n_{low} can be chosen to be as low as 1 rpm. Novotny (1996) indicated that for small DC-motors (< 2~3 hp) the effect of the second term of the speed sensitive losses, C_{visc}, is very small compared to the other terms. Also C_{stat2} can be approximated as 5~10% of the rated torque of the DC-motor.

3.1.3 Pumps

Pumps are mechanical devices that add mechanical energy to liquids. Karassik *et al.* (1976) and White (1994) classified pumps as either positive displacement pumps or dynamic pumps.

White (1994) indicated that positive displacement pumps periodically add energy to the fluid, thereby, delivering pulsating or periodic flows. Such pumps are suitable for fluids of any viscosity, in applications that are characterized as: (i) demanding a constant discharge speed; and, (ii) operating at high heads and low flow rates. In contrast, dynamic pumps add energy continuously to increase fluid flows. Dynamic pumps are suitable for fluid with moderate viscosity in applications that are characterized as: (i) demanding continuous operations at different discharge speeds; and, (ii) operating at high flow rates and moderate heads.

Solar systems, containing no storage subsystems, are characterized by their high dependence to the incident solar radiation which varies considerably during the operating period. As a result, significant variations are expected in the system outputs (flow rate for the case of the PV pumping systems). Consequently, positive

displacement pumps are seldom used in PV pumping applications; and therefore, mathematical modeling of this class of pumps will not be considered.

Karassik *et al.* (1976) and White (1994) indicated that dynamic pumps are classified as either rotary pumps or a special effect pumps. The special effect pumps are designed to operate in non-solar application such as: to eject fluids in main stream; induce liquid metals; or, to act as gas-lifts. Therefore, attention in the current investigation will be given to rotary pumps only.

Rotary pumps can be further classified as either: centrifugal (or radial) exit flows; axial exit flows; or, mixed (between radial and axial) flows. Streeter and Wylie (1985) indicated that: centrifugal flow pumps are best adapted for application with relatively high heads; axial flow pumps are best for application operated under large discharge and at small heads; and, mixed flow pumps are best adapted for applications demanding medium heads and medium discharge.

Nearly all of the literature addressing the issue of PV pumping have considered the use of centrifugal pumps: Roger *et al.* (1977); Braunstein and Kornfeld (1982); Hori *et al.* (1985); Koner *et al.* (1991); Fam and Goswami (1992); and, Anis and Metwally (1994), are examples. Roger *et al.* (1977) recommended the use of centrifugal pumps in PV pumping systems. Their recommendation was based upon the fact that centrifugal pumps required less torque to start, and produce more head than other pumps. Balasubramanian (1992) indicated that centrifugal pumps are commonly considered owing to their advantages of simplicity, low cost, low maintenance, and availability of large selection of designs for wide range of flow rates and heads.

At a given speed, *n*, the head-flow, *H-Q*, and the efficiency-flow, □-*Q*, of a pump are characteristic relations that describe the pump performance. Elementary pump theory can be used to generate a theoretical *H-Q* and □-*Q* correlations. However, due to complex phenomena during operation, such theoretical curves can never reflect reality (Streeter and Wylie, 1985). Circulatory flow, friction and turbulence are examples of these complex phenomena. Therefore, the *H-Q* and □-*Q* curves must be obtained through experimental measurements. Figures 3.1.4 (a), (b) and (c) depict the *H-Q* and the □-*Q* curves at a reference rotation speed n_{ref} for centrifugal pumps, axial pumps and mixed pumps, respectively.

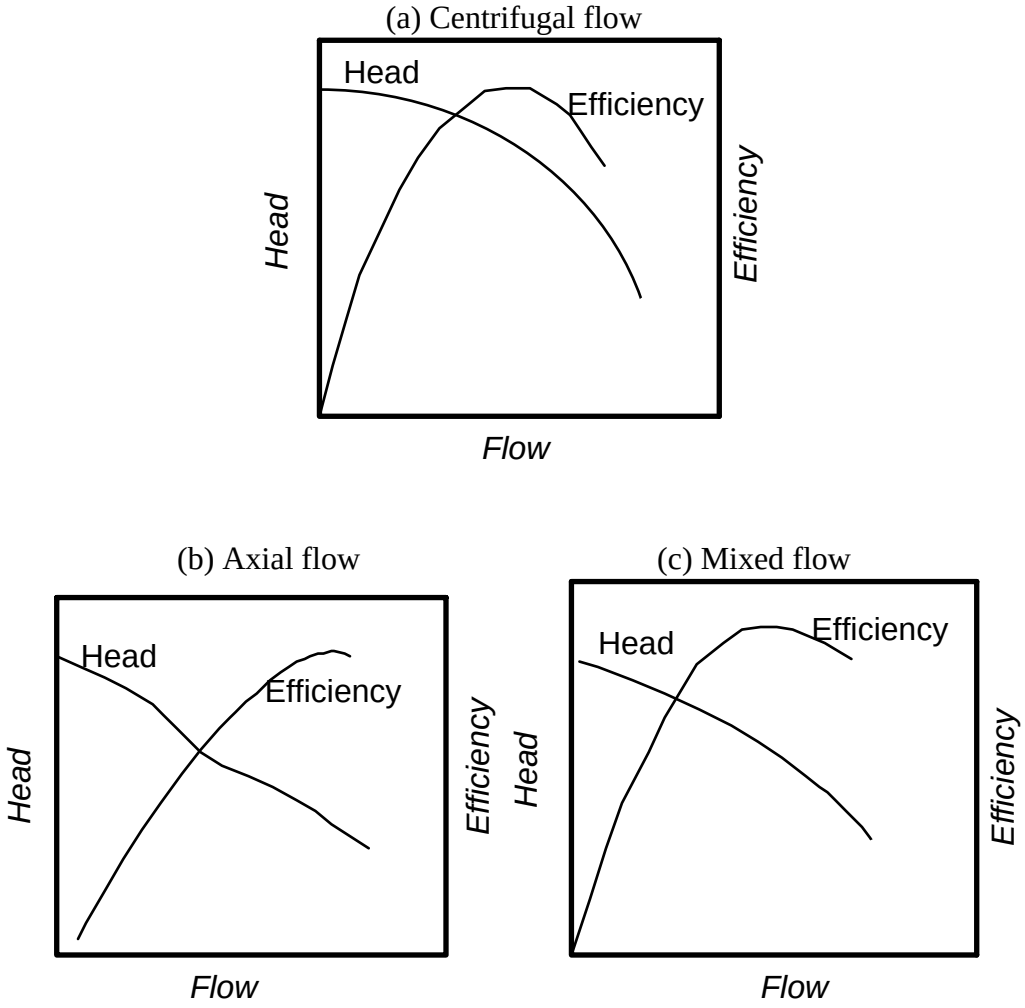

Figure 3.1.4 The *H-Q* and □-*Q* curves for the rotary type pumps: (a) centrifugal flow; (b) axial flow; and, (c) mixed flow.

Given measurements of *H-Q* and □-*Q* at a reference speed, a polynomial function can be used to generate the correlations for any rotary type pumps.

To generate the *H-Q* function; Streeter and Wylie (1985) used a third order polynomial; Hodge (1985), Weiner and Levinson (1990) and Fam and Goswami

(1992) used a second order polynomial; Eckstein *et al.* (1991) used a second order polynomial with the elimination of the linear term.

White (1994) indicated that the pump *H-Q* curve at zero flow rate has a zero or a negative slope. In rare occasions the pump *H-Q* curve may exhibit a positive slope but this condition causes unstable operation of the pump. Therefore, considering normal steady state operation reduces the third and the second polynomial function to the function used by Eckstein *et al.* (1991) with no penalty in the accuracy. Hence the *H-Q* correlation at the reference speed is:

$$H_{ref} = c_1 + c_2 Q_{ref}^2 \qquad 3.1.18$$

where c_1 and c_2 are curve-fitting constants.

To generate the □-*Q* curve, Hodge (1985), Cummings (1989) and Eckstein *et al.* (1991) used a third order polynomial. The function is:

$$\square_{ref} = e_o + e_1 Q_{ref} + e_2 Q_{ref}^2 + e_3 Q_{ref}^3 \qquad 3.1.19$$

where e_o, e_1 , e_2 and e_3 are curve-fitting constants. The pump efficiency is defined as:

$$\eta = \frac{\rho g Q H}{2 \pi n T} \qquad 3.1.20$$

where □ is the fluid density and g is the gravitational acceleration.

The process of determining these four constants requires measurements of the pump efficiency at a minimum of four flow rates. However, knowing that the pump efficiency at no flow condition is zero, means that e_o is zero. Additionally, the use of a second degree polynomial instead of a third-order polynomial reduces the amount of data requires to determine these constants without a significant penalty in the modeling accuracy. Therefore, Equation 3.1.19 can be reduced to two terms only as follows

$$\square_{ref} = e_1 Q_{ref} + e_2 Q_{ref}^2 \qquad 3.1.21$$

Figure 3.1.5 presents an actual measurement of a pump efficiency as a function of flow rate The measurement were curve-fitted using both the four-parameter equation (Equation 3.1.19) and the two-parameter equation (Equation 3.1.21). Both equations provided adequate fit to the measurements.

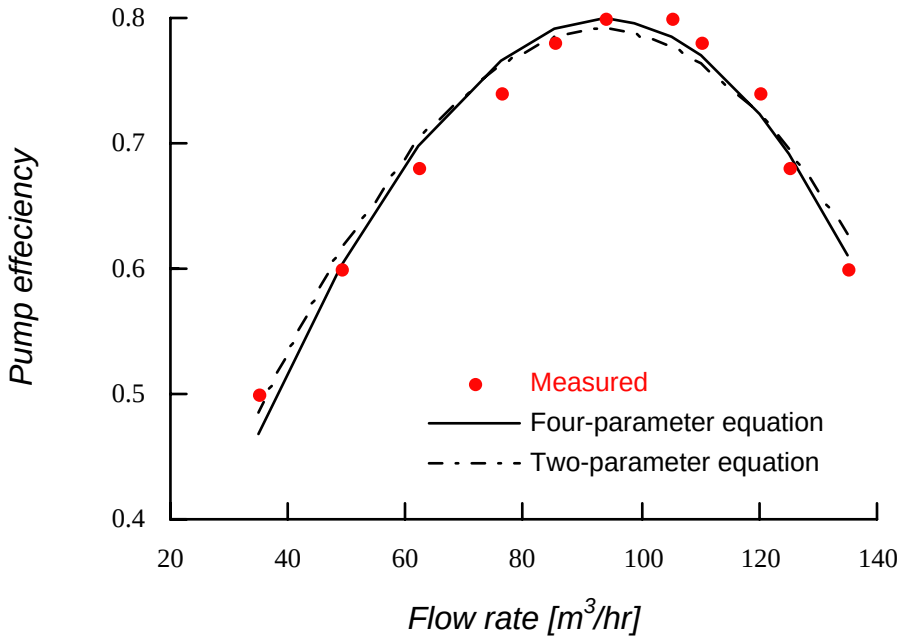

Figure 3.1.5 Curve fitting a measured pump efficiency as a function of flow rate using the four-parameter model and the two-parameter model. Data adapted from ASHRAE (1983).

At other operating speeds, similarity rules (affinity laws) can be used to extrapolate the *H*-*Q* and the □-*Q* curves (Karassik *et al.*, 1976; Cummings, 1989; Eckstein *et al.*, 1991; White 1994) as follows:

$$\frac{Q}{Q_{ref}} = \frac{n}{n_{ref}} \qquad 3.1.22$$

$$\frac{H}{H_{ref}} = \left(\frac{n}{n_{ref}}\right)^2 \qquad 3.1.23$$

$$\frac{P}{P_{ref}} = \left(\frac{n}{n_{ref}}\right)^3 \qquad 3.1.24$$

However, Cummings (1989) indicated that these affinity laws are valid only for heads larger than the static head.

3.1.4 Piping System

A piping system is the sum of pipes, fittings, valves and other restrictions which impose a pressure drop that has to be counter forced by the pump. Pressure drop, or head, is composed of two parts; static head and dynamic head, as follows:

$$H = H_{stat} + H_{dyn} \qquad 3.1.25$$

where H_{stat} is the static head component and H_{dyn} is the dynamic head component. H_{stat} is representative of the pressure drop due to vertical elevation and H_{dyn} is representative of all flow-associated pressure drop. Therefore, for a given SDHW system H_{stat} is a constant and H_{dyn} is a function of flow condition.

White (1994) and others showed that H_{dyn} could be related to the flow rate and the piping system configuration as follows:

$$H_{dyn} = \mathrm{f}\ (L/D)_{eq}\ \frac{Q^2}{2\,g\,A^2} \qquad 3.1.26$$

where f is the Darcy friction coefficient, $(L/D)_{eq}$ is the equivalent length to diameter ratio of the piping components, Q is the fluid flow rate, and A is the pipe cross sectional area.

The Darcy friction factor f for smooth pipes is a function of Reynold's number and is given by Duffie and Beckman (1991) as:

$$\mathrm{f} = \begin{cases} 64/Re_D & \text{for laminar flow} \\ (0.79\ \ln Re_D - 1.64)^{-2} & \text{for turbulent flow} \end{cases} \qquad 3.1.27$$

The equivalent length to diameter ratio $(L/D)_{eq}$ is a lumped parameter which accounts for the effects of the different geometrical shapes facing the fluid flow. $(L/D)_{eq}$ has no systematic relation to Q. Instead the values of $(L/D)_{eq}$ for different objects (e.g., elbows, valves, etc.) are normally obtained from tabulated data.

The difficulty associated with using the forgoing model lies in obtaining a correct estimate for $(L/D)_{eq}$. An estimate of $(L/D)_{eq}$ demands a great deal of knowledge of the piping system which includes the quantities and types of elbows, fittings, valves,

bends and other hidden flow restrictions built in the piping and in the components of the SDHW systems including the thermal collector, the heat exchanger, ...etc.

However, in SDHW systems, the manufacturers of the system components normally provide a value of a pressure drop at a reference flow rate. Therefore, the complete piping system's pressure drop at a reference flow could be obtained. As a result, the above model could be back-solved to find the appropriate value of $(L/D)_{eq}$.

Other simplified hydraulic system models exist. Eckstein *et al.* (1991) used the following equation:

$$H = H_{stat} + k_2 Q^2 \qquad 3.1.28$$

where k_2 is constant. The difficulties associated with Eckstein *et al.*'s model is finding an appropriate value of k_2. However, from the analysis provided by Halle *et al.* (1988) and Kistler and Chenoweth (1988) an auxiliary equation for k_2 can be written as:

$$k_2 = \frac{H_{ref} - H_{stat}}{Q_{ref}^2} \qquad 3.1.29$$

Therefore, Eckstein *et al.*'s model can be rewritten as

$$H = H_{stat} + \left(\frac{H_{ref} - H_{stat}}{Q_{ref}^2} \right) Q^2 \qquad 3.1.30$$

Comparing the detailed $(L/D)_{eq}$ model and the modified Eckstein *et al.*'s model to a set of experimental data obtained from the Florida Solar Energy Center (FSEC) revealed that both models are able of reproducing the data with good accuracy. Figure 3.1.6 shows the measured data and the simulated *H-Q* curves.

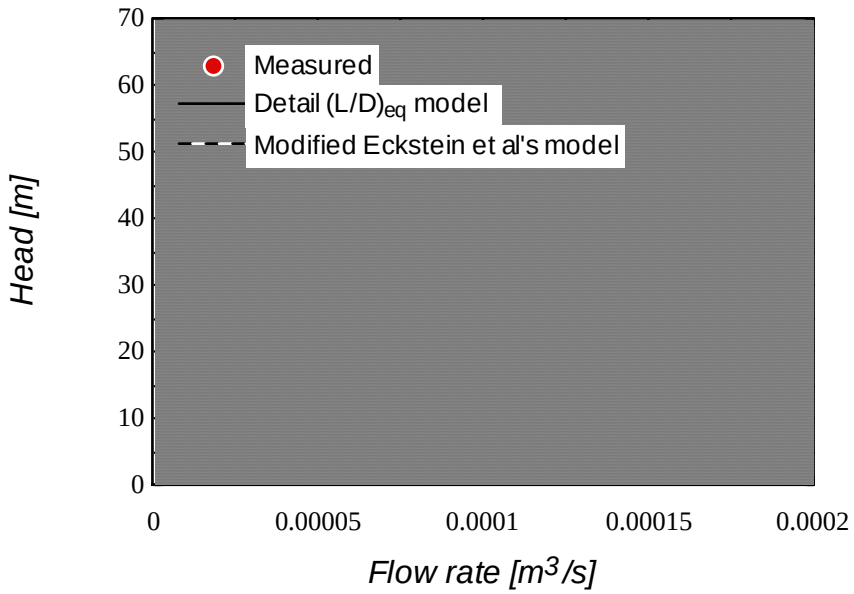

Figure 3.1.6 Measured and simulated hydraulic system *H-Q* curves of an SDHW system. Data were reported by the Florida Solar Energy Center (FSEC).

Although the modified Eckstein *et al.*'s model is simpler than the detailed $(L/D)_{eq}$ model; however, the earlier model does not take into account the effect of fluid temperature on pumping power. As the fluid temperature increases, the viscosity of the fluid increases, and hence the required pumping power decreases. On the other hand, the detail $(L/D)_{eq}$ model takes into account the effect of fluid temperature. The measured *H-Q* data presented in Figure 3.1.6 were reported for water at 25 °C. As the collector fluid temperature increases from 10 °C to 100 °C, the pumping power decreases by 15%. Figure 3.1.7 shows the *H-Q* curves for water at 10 °C, 25 °C and 100 °C compared to the measured *H-Q* data at 25 °C. If water was replaced by propylene glycol mixture, then as the fluid temperature increases from 10 °C to 100 °C, the pumping power decreases by 30%. Figure 3.1.8 shows the *H-Q* for propylene glycol mixture at 10 °C and 100 °C compared to the measured *H-Q* data for water at 25 °C. Therefore, when the modified Eckstein *et al.*'s model is used to quantify the required pumping power, then the reference values of *H* and *Q* have to be reported at low fluid temperatures, otherwise the required pumping power will be underestimated. On the other hand, if more accurate results are desired, then the detail $(L/D)_{eq}$ model should be the choice.

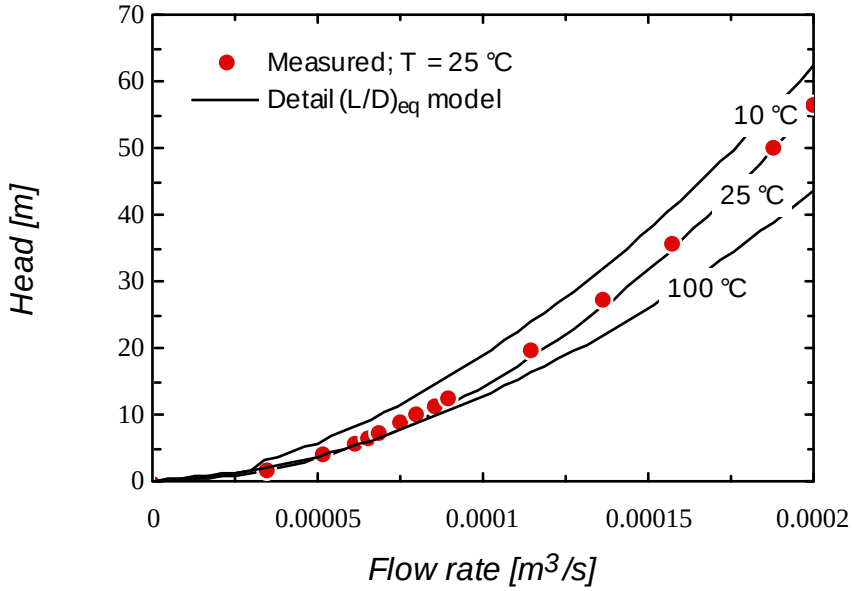

Figure 3.1.7 Simulated *H-Q* curves of an SDHW system at three collector fluid temperatures compared to the measure *H-Q* data. The collector fluid is water.

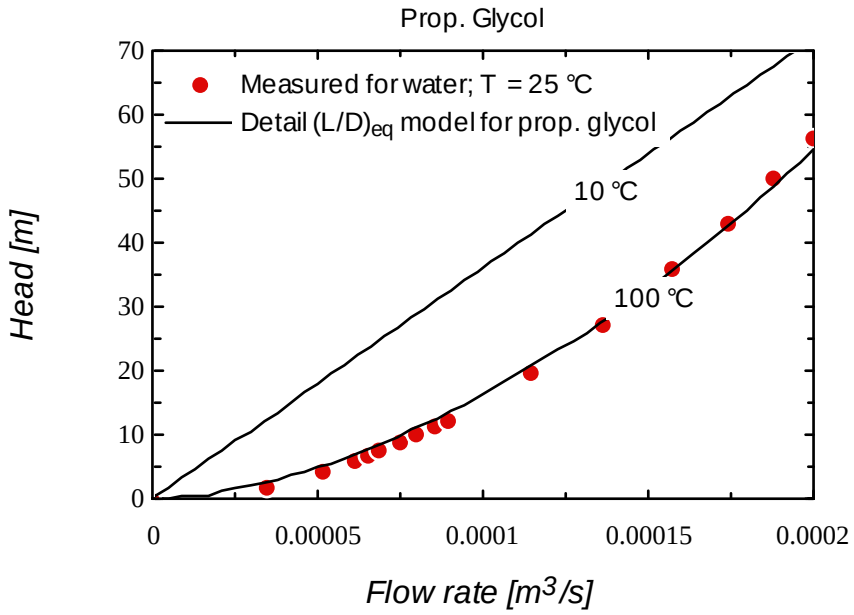

Figure 3.1.8 Simulated *H-Q* curves of an SDHW system at two collector fluid temperatures compared to the measure *H-Q* data for water. The collector fluid is propylene glycol mixture.

3.2 Mathematical Modeling of SDHW System Components

Mathematical models of SDHW system components are well developed and documented (Duffie and Beckman, 1991). The TRNSYS library consists of a variety of individual subroutines that represent SDHW components. The mathematical models are updated continuously by their users. Liu *et al.* (1978), Carlson *et al.* (1991) and others performed experimental validation of TRNSYS for SDHW systems. The following sub-sections briefly list TRNSYS TYPE subroutines that model the components of SDHW systems along with additional discussion, if necessary.

3.2.1 Thermal Collectors

The thermal performance of variety of flat-plate thermal collectors are modeled through TRNSYS TYPE 1. In this subroutine, the thermal performance of a flat-plate thermal collector is calculated using either: (i) theoretical analysis based on the Hottel-Whillier steady-state model (Duffie and Beckman, 1991), or (ii) interpolating the performance from the standard characteristics curve of a flat-plate collector measured at a standard flow rate. Detailed mathematical modeling of the thermal collectors is given in TRNSYS manual (TRNSYS, 1996) and in Duffie and Beckman (1991).

3.2.2 Storage Tanks

The thermal performance of a fluid filled sensible energy storage tank, subject to thermal stratification, is modeled through TRNSYS TYPE 4 and TYPE 60; the stratified fluid storage tank which models the tank by assuming that the tank consists of N fully-mixed equal-volume segments. The degree of stratification is determined by the value of N. If N is equal to 1, the storage is modeled as a fully-stratified tank. Detailed mathematical modeling of storage tanks is given in TRNSYS manual (TRNSYS, 1996), Duffie and Beckman (1991) and Newton (1995).

3.2.3 Heat Exchangers Heat exchangers are static devices that allow heat to transfer from a hot fluid stream to a cold fluid streams. In SDHW systems, heat exchangers are used to transfer the energy absorbed by the collector fluid, to the

tank/load fluid, and therefore, allowing the use of non-potable, anti-freeze and/or anti-corrosion solutions in the collector circuit(s).

Heat exchangers are classified according to variety of criteria; flow arrangement and type of construction, for example. Another classifying criterion, of importance to SDHW systems, is the nature of the force that is inducing the tank/load fluid stream. If the tank/load fluid stream is mechanically induced (e.g., by means of a pump), then the heat exchanger is called a forced convection heat exchanger (FCHE). However, if the same stream is naturally induced by a buoyancy force[8], then the heat exchanger is called a natural convection heat exchanger (NCHE). The following two sections review the modeling of forced and natural convection heat exchangers.

3.2.3.1 Forced Convection Heat Exchangers The thermal performance of parallel, counter, or cross flow sensible FCHE is modeled through TRNSYS TYPE 5. The model uses the *effectiveness-NTU* method (Incropera and De Witt, 1985). The model assumes: (i) that the heat exchanger has a zero thermal mass; and, (ii) that the overall heat transfer coefficient *UA* is independent of flow rates. The first assumption is reasonable because heat exchangers are normally designed such that they have low thermal mass (Incropera and De Witt, 1985). However, *UA* is dependent on the flow rates on the two sides of the heat exchanger (Incropera and De Witt, 1985; Fanney and Klein, 1988). In PV-SDHW systems, variations in the flow rates of both side of the heat exchanger are always expected. Recently, TRNSYS TYPE 5 has been enhanced to account for the effect of the variation in the flow rates of both the cold

[8]A buoyancy force is the net effect of a body of force acting on a fluid in which there are density gradients (Incropera and De Witt; 1985).

and the hot fluid streams and to account for the effect of the fluid temperature on the fluid transport properties (Rabehl, 1997). The modified FCHE subroutine is named TRNSYS TYPE 80. TYPE 80 will be used to simulate FCHEs in indirect SDHW systems.

3.2.3.2 Natural Convection Heat Exchangers

Natural convection heat exchangers are classified as either internal or external heat exchangers. External NCHEs classification are identical to those of FCHEs. Internal NCHEs are mostly custom designed and therefore, are available in various designs. Baur (1992) indicated that in general internal NCHEs are at a disadvantage compared to external NCHEs in that they require custom-made storage tanks, and therefore entail high initial costs. In addition, external NCHEs can be connected to commercially available storage tanks, and therefore low initial costs. As a result, the current investigation will concentrate on the modeling of external NCHEs.

Most recently, the modeling of external NCHE has been addressed by several investigators. Among them are Parent *et al.* (1990), Fraser (1992), Bergelt *et al.* (1993), Allen and Ajele (1994), Avina (1994), Dahl and Davidson (1996) and others. Development of a model is an on-going research effort, and crucial factors are being debated among the NCHE modeling investigators. Due to the importance of these crucial modeling issues to the accuracy of the NCHE models, an in-depth literature review of the modeling of NCHEs was undertaken. The work of Fraser (1992) and Dahl and Davidson (1996) primarily covers the major aspects of the modeling of NCHEs. The following is a review of their work.

Dahl and Davidson (1996) indicated that the modeling of NCHEs requires either extensive experimental measurements, detailed 3-dimensional (3-D) models, or 1-dimensional (1-D) models for which heat transfer coefficients and dynamic pressure drops must be known. While the first two options are prohibitive and costly, the third option is the only practical alternative for modeling NCHEs.

Fraser (1992) developed and validated experimentally a 1-D model for a shell and coil heat exchanger. Avina (1994) integrated Fraser's model in TRNSYS (TYPE 67). Fraser's model requires two sets of experimental data: (i) a data set relating the heat exchanger's dynamic pressure drop to the water flow rates, and (ii) a data set relating the effectiveness of the NCHE as a function of the pumped fluid inlet temperatures and flow rates. To eliminate the need for these experimental data, Avina (1994) enhanced Fraser's model to include published forced convection heat transfer correlations to evaluate the necessary auxiliary data. Fraser's model and Avina's model compare favorably. However, when compared to experimental results, Fraser's model and Avina's model was found to over predict the water flow rate by approximately 13.5% and under predict the water outlet temperature by 8%. These percentage errors diminish when the heat transfer rates are computed. Figure 3.2.1 presents a comparison between the heat transfer rates computed by Avina's model (represented by TRNSYS TYPE 67) and those computed from Fraser's experimental results.

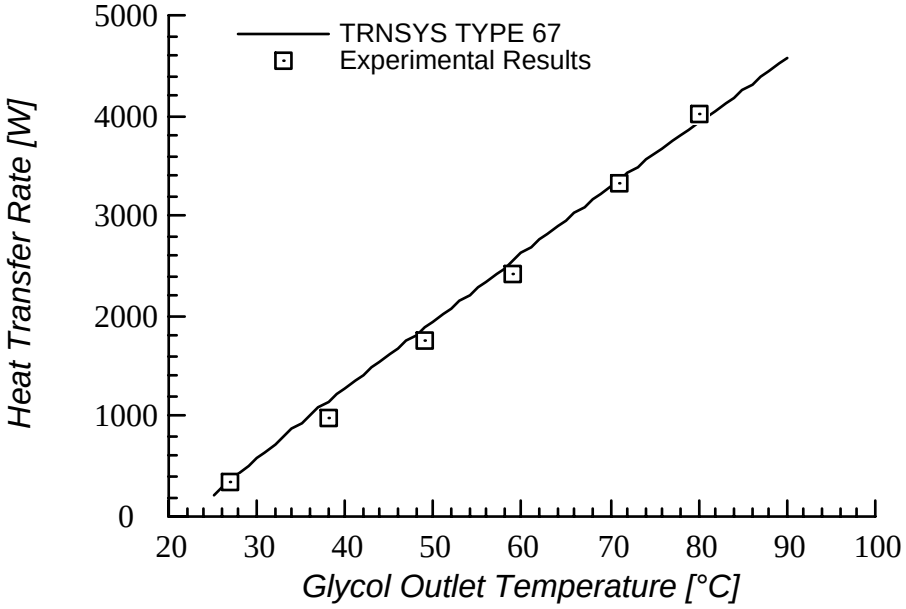

Figure 3.2.1 Comparison of TRNSYS TYPE 67 results to Fraser's experimental results. From Avina (1994).

Causes of Fraser's model errors

In Fraser's model, the static pressure across the heat exchanger was computed using an integral of the local water densities at several heights of the heat exchanger. Each local density is computed using a temperature-height correlation. However, while validating her model with experiments, Fraser found that at low flow rates the model results in negative flow rates, indicating that the flow is reversing direction towards the tank. Fraser pointed out that this is impossible and concluded that the average density values chosen for the heat exchanger is of importance and needs be corrected.

As a result, Fraser introduced a density correction factor to avoid this negative flow rate. Avina found that, while the value of the water density plays a noticeable effect on the prediction of the water flow rates, the introduction of Fraser's density correction factor has very little effect on the prediction of the heat transfer rates.

Dahl and Davidson (1996) performed a detailed performance measurement of a NCHE similar to the one investigated by Fraser. Dahl and Davidson conformed experimentally, using dye added to the water, that the flow never reverses direction. Dahl and Davidson attributed the aforementioned inaccuracy of Fraser's model to the use of a lumped density value rather than the actual density profile.

Dahl and Davidson used their measurement to compute the overall heat transfer-area product, *UA*, (a measure of the heat exchanger effectiveness) and found that *UA* is not a unique function of the glycol flow rates and inlet temperatures; it was found that the water temperature profile in the tank has a measurable effect on *UA* as well. Different *UA* values were found for the case of an isothermal tank than the values found for the case of a stratified tank. The reason for this additional factor, Dahl and Davidson concluded, is that the ratio of Grashof number to Reynolds number (Gr/Re) (which provide a measure of the influence of natural convection in comparison to forced convection) is found to be between 300 to 8000 and therefore the flow is in the operating regime of mixed convection. As a result, Fraser's and Avina's assumption that the flow on the cold side of the heat exchanger can be modeled as forced convection is incorrect. Dahl and Davidson concluded that the modeling of NCHEs should rely on the glycol collector outlet temperature and flow rate as well as: (i) the temperature profiles in the heat exchanger and the storage tank, and (ii) a correlation of Gr, Re and Pr numbers of the cold stream fluid. An attempt was made by Dahl and

Davidson to generate a correlation between Gr, Re and Pr, and *UA*. However, discrepancies can be observed between the proposed correlation and the measurements. Moreover, no information was provided on how to predict the temperature profiles in the heat exchanger and the storage tank.

In summary, the work of Dahl and Davidson provided strong evidence that Fraser's model and Avina's model may not be adequate to predict the *variables* of NCHEs. However, when the *heat transfer rates* are desired, the observed discrepancy diminishes. The current investigation is aimed towards accurately quantifying the annual integral of heat transfer rates of SDHW systems and not the detail modeling of the different components of the SDHW systems. Therefore, the use of Fraser's model (TRNSYS TYPE 67) to model the performance of NCHEs in Indirect SDHW system is adequate for the current investigation.

3.3 Hourly Averaged Simulation Versus Minute-by-Minute Simulation

Most of the available solar radiation data are based on hourly measurements but a few minute-based measurements are available. Duffie and Beckman (1991) pointed out that the performance process is generally not linear with solar radiation, and therefore, the use of averages may lead to serious errors if non-linearities are not taken into account.

Hollands *et al.* (1989) examined the assumption of ignoring the random fluctuations in ambient air temperature during the simulation of SDHW systems. They concluded

that ignoring random fluctuation in ambient air temperature produces acceptably low errors (~1%) when simulating different thermal systems.

Gansler (1993) investigated the use of hourly averaged and minute-by-minute solar radiation data. Gansler's results showed that: (i) for SDHW systems, both data sources resulted in identical performance. Even though the minute-by-minute radiation varied considerably during the hour, it did not affect the SDHW system on an hourly basis. (ii) for predicting the performance of direct-coupled PV resistive system, it was found that hourly simulations can give erroneous results when there is non-uniformity in the distribution of minutes within a given hour. No studies were found to investigate the effect of the hourly averaged radiation data on the performance prediction of PV pumping systems. However, similarities exist between direct-coupled PV resistive systems and direct-coupled PV pumping systems.

Chapman (1990) and Hutchinson *et al.* (1991) proposed methods to synthesize solar radiation data for the use in PV applications. However, their methods are only applicable for PV systems which have storage components that reduces the non-linearity of the system. Suehrcke (1988), as reported in Gansler (1993), has proposed a model to generate a minute-by-minute radiation data. However, Gansler (1993) pointed out that Suehrcke's model is location dependent.

3.4 PV Pumping System Validation

The following section validates the proposed PV pumping system model. Validation data were obtained from a series of test conducted at the Florida Solar Energy Center (FSEC), Cape Canaveral, FL. The data were reported for four non-consecutive days: August 23rd, September 3rd,

September 5th and September 7th all of 1987. Dunlop (1988) used these data and other data to identify an optimum PV pumping system among three PV pumping systems. Eckstein *et al.* (1990) used August 23rd data to validate their proposed model. At the end of this section, a comparison will be made between the proposed PV pumping system model and Eckstein *et al.*'s model.

3.4.1 Experimental Setup The experimental test facility (FSEC system) consists of an array of six PV modules. The PV array is configured in two parallel strings. Each string contains three PV modules connected in series. The PV array is mounted on a single-axis passive sun tracking mechanism. The PV array is directly-coupled to a permanent magnet DC-motor which drives a surface mounted centrifugal pump. The fluid medium is water which circulates through a closed piping circuit.

The reported measured data include solar radiation, G; flow rate, Q; head, H; voltage, V; and current, I. Except for Q and I, all the reported data were hourly averaged. Q was reported cumulative value during each hour, and I was reported instantaneously. No information was provided regarding the original measurement sampling frequency. While G, Q, H and V were reported in a tabulated form, I was reported in the form of a scatter plot of I as a function of V (the DC-motor-pump I-V plot). Therefore, for each tabulated value of V, a corresponding value of I was manually extracted from the I-V plot. Neither the ambient temperature nor the PV cell temperature were reported.

3.4.2 Components' Parameters Estimation The proposed PV pumping system model requires a set of parameters describing the system components. Most of these parameters were either explicitly reported by the manufacturers of the components, or determined from the manufacturers' characteristic curves. The following is a brief summary of the technical specification of the FSEC system components and the parameters extraction process.

3.4.2.1 PV Cells The PV cells employed in FSEC system are Solarex Georgetown PV modules. The manufacturer provided all the necessary parameters except for the short circuit and open circuit temperature coefficients, μ_{Isc} and μ_{Voc}, respectively. However, an independent test for the same PV module was provided by FSEC which reports a pair of I and V at an operating condition other than the manufacturer reference test condition. Therefore, the task was, given the manufacturer information along with V, G, T_C at the independent test condition, find a pair of μ_{Isc} and μ_{Voc} such that the difference between the measured I and the calculated I is minimized. Table 3.4.1 lists the parameters of the Solarex Georgetown PV module.

Table 3.4.1 FSEC system's PV module parameters

PV module parameter	Value	Source
G_{ref}	1000 W/m2	manufacturer data
$T_{c,ref}$	323 K	manufacturer data
$I_{sc,ref}$	4.87 Amp	manufacturer data
$I_{mp,ref}$	4.32 Amp	manufacturer data
$V_{mp,ref}$	13.56 Volt	manufacturer data
$V_{oc,ref}$	18.0 Volt	manufacturer data
N_s	36 cells	manufacturer data
μ_{Isc}	0.003 Amp/K	manufacturer data and an independent FSEC test
μ_{Voc}	-0.074 Amp/K	manufacturer data and an independent FSEC test

3.4.2.2 DC-Motor The characteristic equations of the permanent magnet DC-motor (Equations 3.1.13-14 and 3.1.17) require five parameters be known: C_e, R_a, $C_{stat}1$, $C_{stat}2$ and C_{visc}. Very limited information was provided by the DC-motor manufacturer, and no independent tests were provided. Therefore, the use of part of the validation measurement was found essential.

Visual inspection of the measured *I-V* plot revealed two parameters; R_a and $C_{stat}1$. R_a was obtained by computing the slope of the linear *I-V* plot at n=0.[9] $C_{stat}1$ was

[9]@ n=0, Equation 3.1.13 reduces to $V = I R_a$. For a given V and I, R_a is unique.

found by identifying the starting current I_{start} and relating it to the parameter C_e using Equation 3.1.12.[10] Additionally, as per the recommendation of Novotny (1996), C_{visc} was assumed to be zero. Therefore, the number of the unknown DC-motor parameters have been reduced to two parameters: C_e and I_{start}.

To obtain good estimates of C_e and I_{start}, one pair of measurements of Q and V from the validation measurement was used (August 23rd @ time 14:00). The task was, given Q and V, back solve for C_e and I_{start}. Table 3.4.2 lists the parameters of the permanent magnet DC-motor employed in FSEC system.

Table 3.4.2 FSEC system's permanent magnet DC-motor parameters

DC-motor parameter	**Value**	**Source**
C_e	0.1983 N-m/Amp	FSEC system (August 27 @ Time 14:00)
R_a	0.4300	visual inspection of *I-V* plot
$C_{stat}1$	0.9500 N-m	visual inspection of *I-V* plot
$C_{stat}2$	0.3542 N-m	FSEC system (August 27 @ Time 14:00)
C_{visc}	0.0000 N-m/s	assumed

[10]An attempt was made to apply the same procedure to identify $C_{stat}1$. However, limited information was available at shut-off condition and prevented an accurate identification of $I_{shut\text{-}off}$.

3.4.2.3 Centrifugal Pump The centrifugal pump model demands a set of data relating the pumps' head, H, and efficiency, □, as a function of flow rate, Q. Both sets of data should be reported at a common reference speed, n_{ref}. H-Q data and □-Q at a reference speed were not reported. However, Eckstein (1990) reported a set of tabulated values of H and □ as a function of Q obtained from the pump manufacturer characteristic curves. Eckstein's H-Q and □-Q data were curve-fitted to obtain the pump's constants; c_1, c_2, e_1 and e_2. Table 3.4.3 lists the parameters of the centrifugal pump employed in FSEC system.

Table 3.4.3 FSEC system's centrifugal pump parameters

Pump parameter	Value	Source
c_1	19.238 m	curve-fitting Eckstein's data
c_2	-6.27e6 m^5/s^2	curve-fitting Eckstein's data
e_1	1078.7 s/m^3	curve-fitting Eckstein's data
e_2	-6.6833e6 s^2/m^6	curve-fitting Eckstein 's data
n_{ref}	1500 rpm	Eckstein's data

3.4.2.4 Piping System The simplified model of the pressure drop across a piping system requires three constants; the static head, H_{stat}, and a reference head, H_{ref}, at a reference flow rate, Q_{ref}. These three constants are system dependent. In the FSEC

system, the water was just circulating through a closed piping circuit, and therefore, H_{stat} is zero. Since the measurement at time 14:00 was used to identify the best estimate of the DC-motor's constants, therefore the same data point will be used to represent H_{ref} and Q_{ref}. Table 3.4.4 lists the parameters of the piping subsystem of FSEC system.

Table 3.4.4 FSEC system's piping system parameters

Piping system parameter	Value	Source
H_{stat}	0.00 m	FSEC system
H_{ref}	5.23 m	FSEC system (August 27th @ Time 14:00)
Q_{ref}	1.025e-3 m^3/s	FSEC system (August 27th @ Time 14:00)

3.4.3 Validation Results The PV pumping model requires as inputs, the solar radiation and the ambient temperature (or the PV cell temperature). However, as mentioned earlier, neither of the ambient temperatures nor the PV cell temperatures were reported. Therefore, values for either of the PV cell temperatures or the ambient temperatures have to be assumed. Throughout the test, the PV cell temperature was assumed to be identical to the PV cell temperature measured at the manufacturer test condition: 323 K. The effect of this assumption on the simulation results will be examined.

The performance of FSEC system throughout the four non-consecutive days is illustrated in Figures 3.4.1-16. For each day, four plots of the system variables are presented: *Q*, *H*, *V* and *I* as functions of time, consecutively. Each plot includes both the results of the PV pumping model and the measured data. As seen in the figures, the PV pumping model is able to reproduce the performance of the FSEC system with good accuracy. However, two observations can be made. They are:

1) Throughout the simulation, the PV pumping model overestimated the flow rate at low solar radiation levels. However, the overestimated amount of flow rate when compared to the total daily flow rate was found to be small (~2%).

2) During September 3rd, the model accurately estimated *H*; however, it overestimated *Q* by 8%. On the other hand, during September 7th, the model accurately estimated *Q* and underestimated *H* by 16%. This is in contrary to the known piping system characteristic relation: *H* and *Q* are directly proportional to each other. If the model overestimated *H* then the model should overestimate *Q* as well, and visa versa. Inspection of the measured values of FSEC system's *H* and *Q*

reveled that they did not constitute an exact relation to each other suggesting that the experimental data are in error. Figure 3.4.17 is a plot of the measured *H* as a function of the measured *Q* for the four days. The characteristic *H*-*Q* correlation was found to vary from one day to the next, and from one hour to the next. The reason for this discrepancy may lie in the experimental technique. The measured data are not instantaneous; the solar radiation and the head are averaged throughout the hour and the flow is additive throughout the hour. Therefore, the reported *Q* may not necessarily correspond to the reported *H* at the reported value of *G*. Secondly, additional uncounted for flow resistances might have been present at some times.

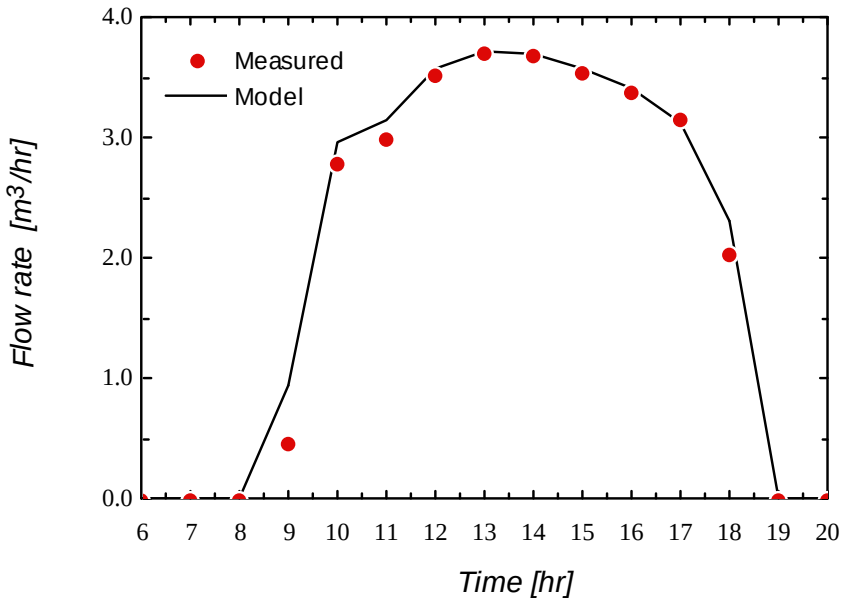

Figure 3.4.1 Flow rate produced by FSEC PV pumping system as a function of time. Data measured on August 23rd, 1987. Data reported by FSEC.

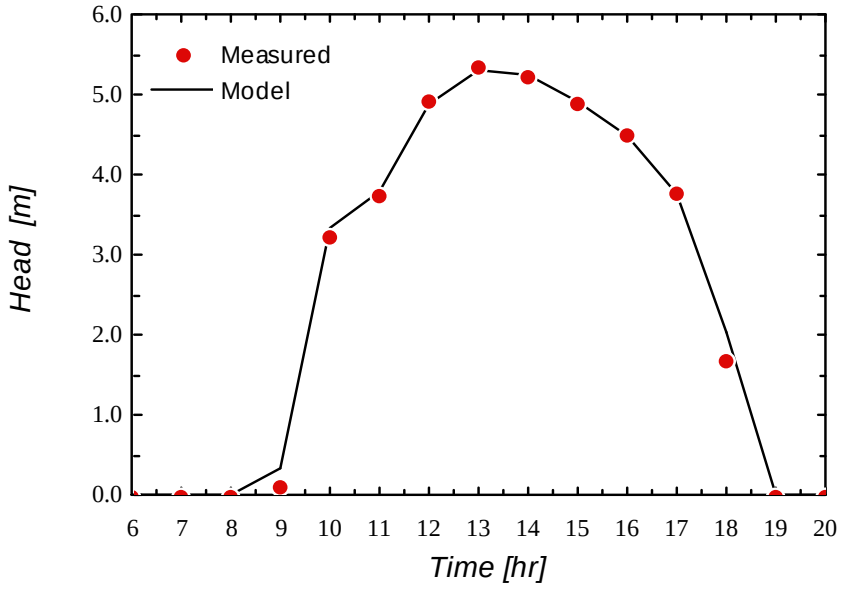

Figure 3.4.2 Head of FSEC PV pumping system as a function of time. Data measured on August 23rd, 1987. Data reported by FSEC.

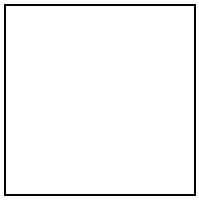

Figure 3.4.3 Voltage of FSEC PV pumping system as a function of time. Data measured on August 23rd, 1987. Data reported by FSEC.

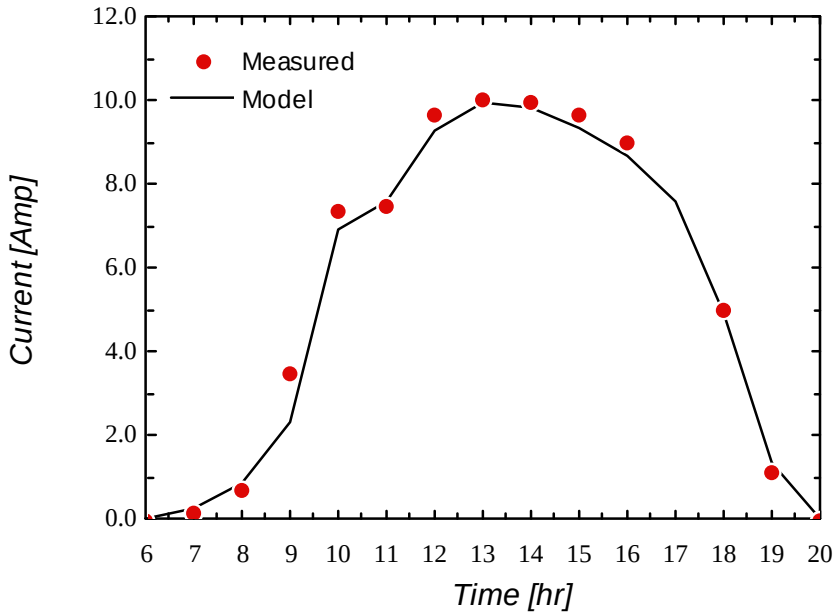

Figure 3.4.4 Current of FSEC PV pumping system as a function of time. Data measured on August 23rd, 1987. Data reported by FSEC.

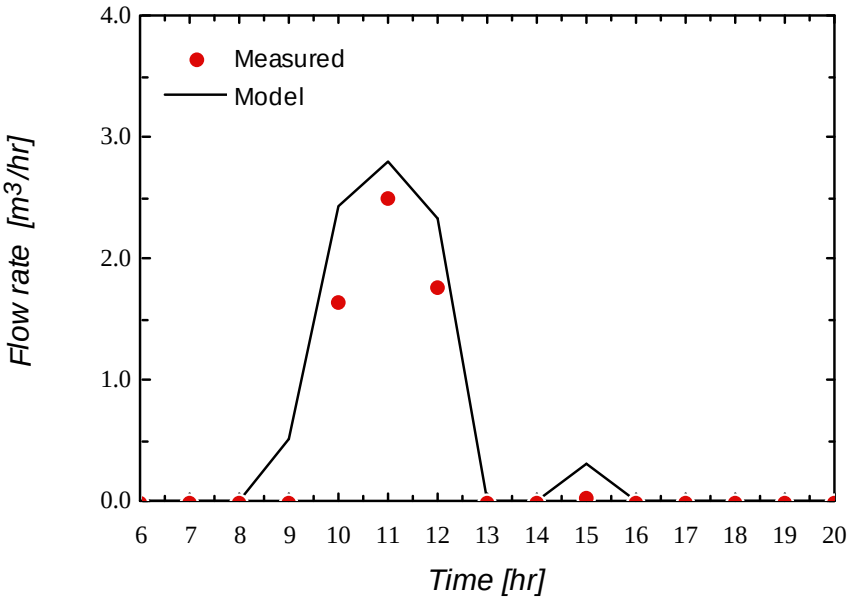

Figure 3.4.5 Flow rate of FSEC PV pumping system as a function of time. Data measured on September 3rd, 1987. Data reported by FSEC.

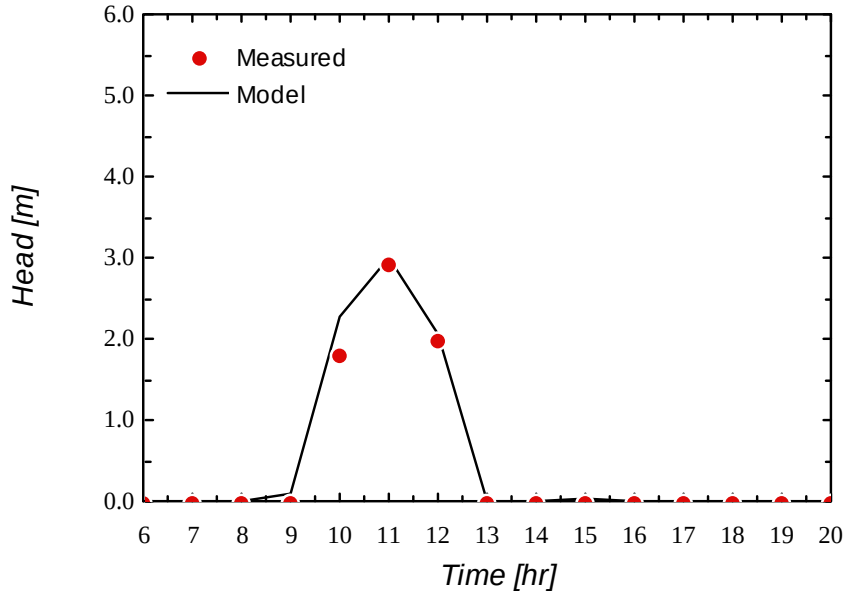

Figure 3.4.6 Head of FSEC PV pumping system as a function of time. Data measured on September 3rd, 1987. Data reported by FSEC.

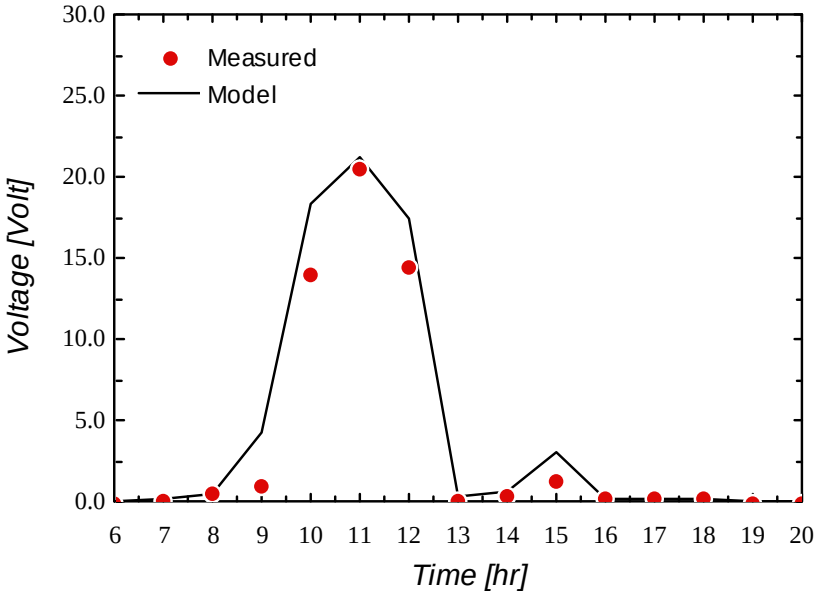

Figure 3.4.7 Voltage of FSEC PV pumping system as a function of time. Data measured on September 3rd, 1987. Data reported by FSEC.

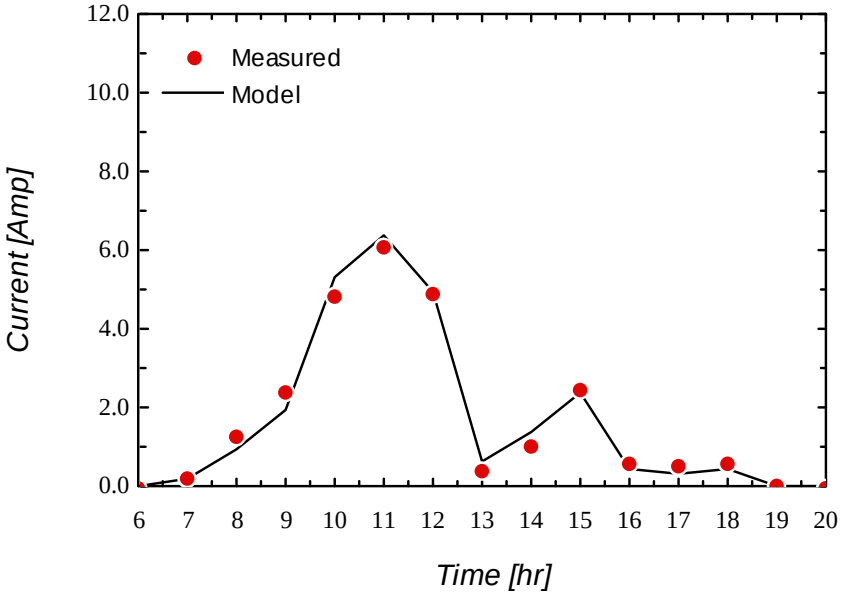

Figure 3.4.8 Current of FSEC PV pumping system as a function of time. Data measured on September 3rd, 1987. Data reported by FSEC.

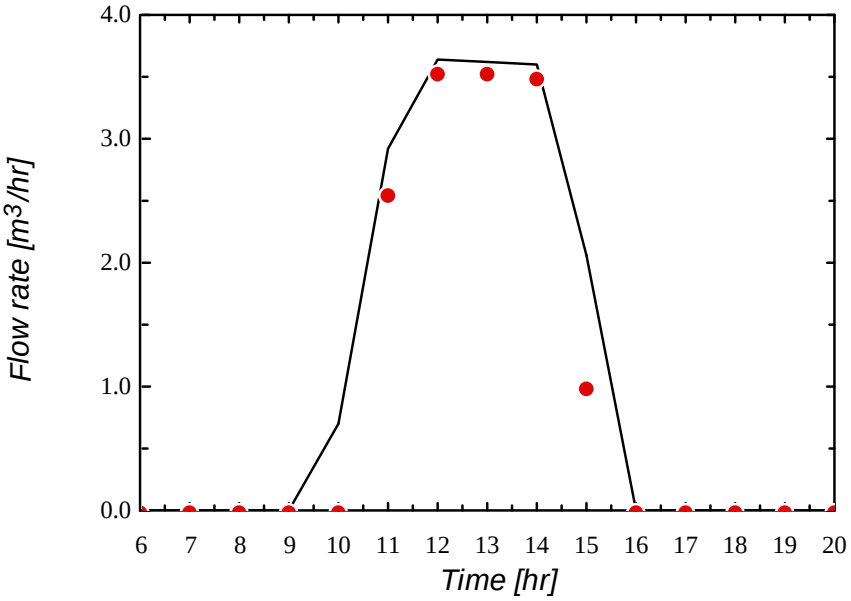

Figure 3.4.9 Flow rate of FSEC PV pumping system as a function of time. Data measured on September 5th, 1987. Data reported by FSEC.

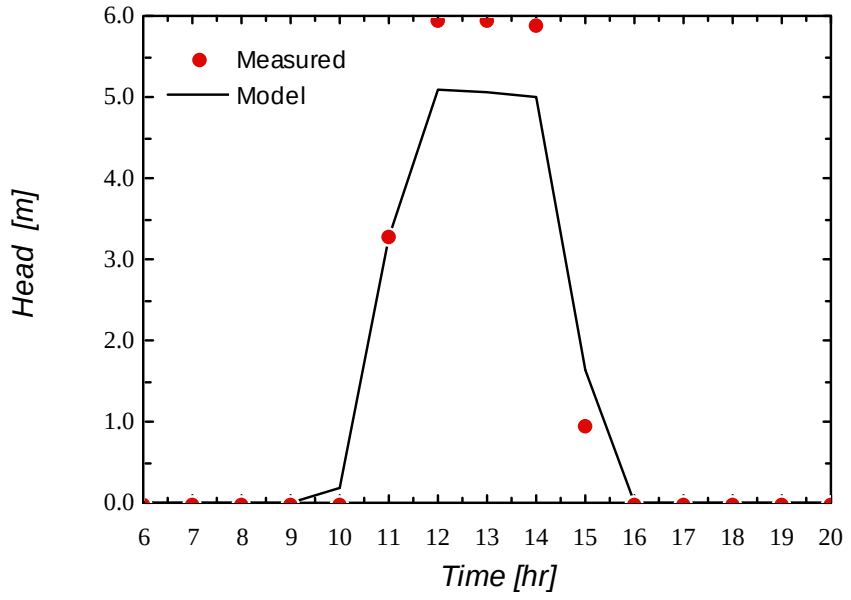

Figure 3.4.10 Head of FSEC PV pumping system as a function of time. Data measured on September 5th, 1987. Data reported by FSEC.

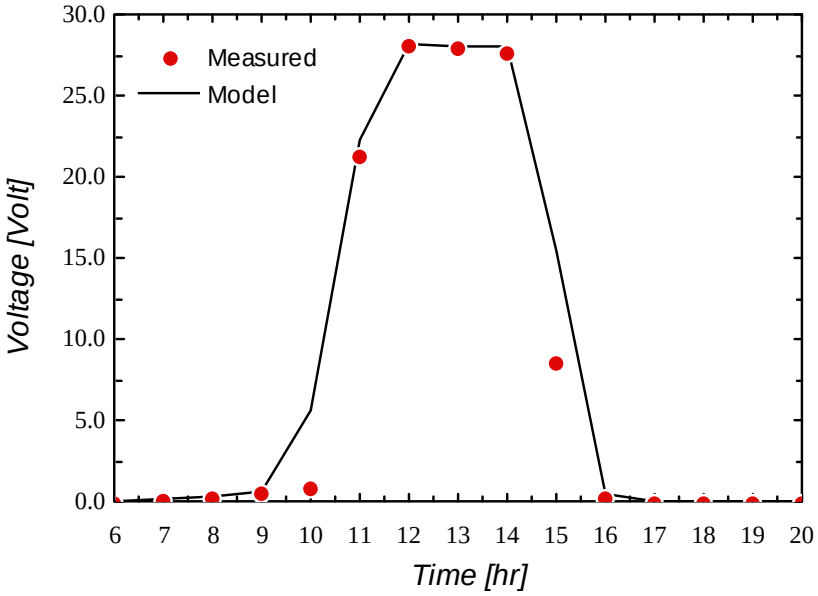

Figure 3.4.11 Voltage of FSEC PV pumping system as a function of time. Data measured on September 5th, 1987. Data reported by FSEC.

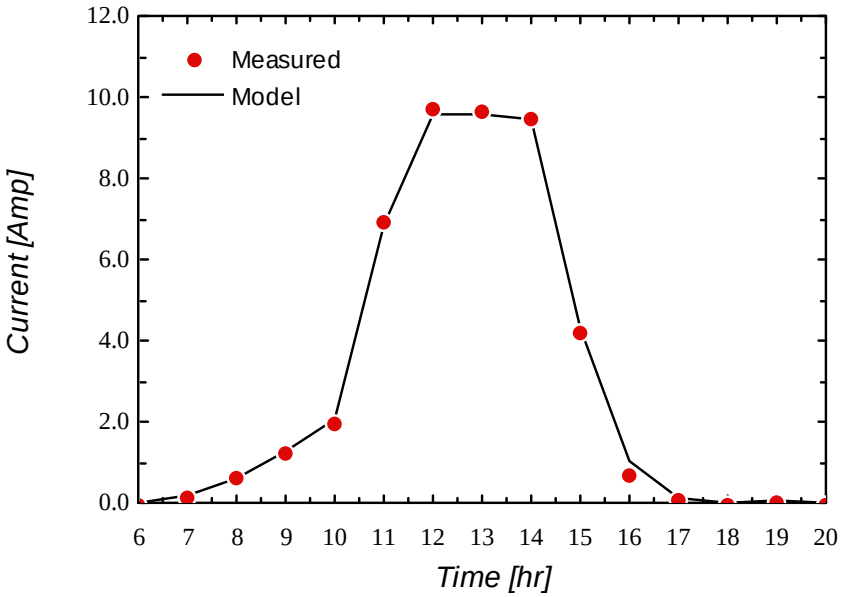

Figure 3.4.12 Current of FSEC PV pumping system as a function of time. Data measured on September 5th, 1987. Data reported by FSEC.

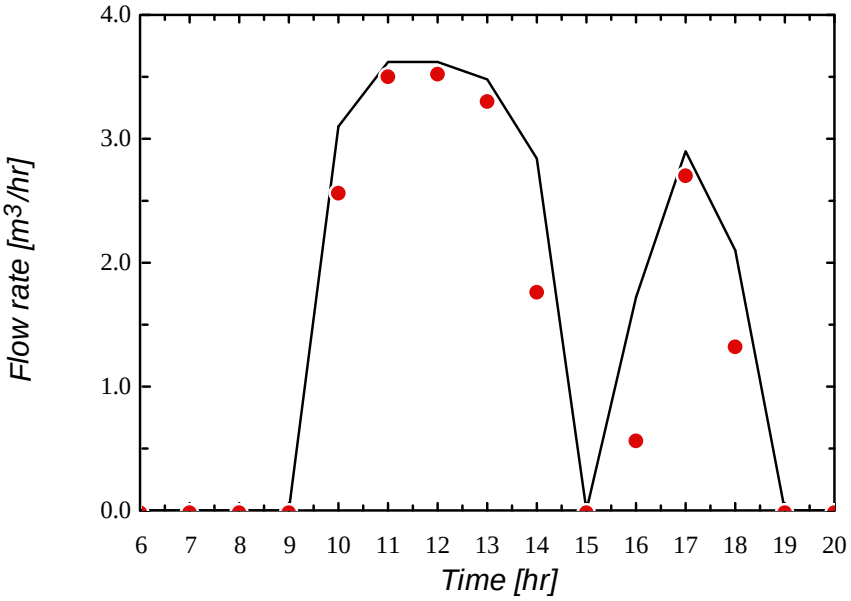

Figure 3.4.13 Flow rate of FSEC PV pumping system as a function of time. Data measured on September 7th, 1987. Data reported by FSEC.

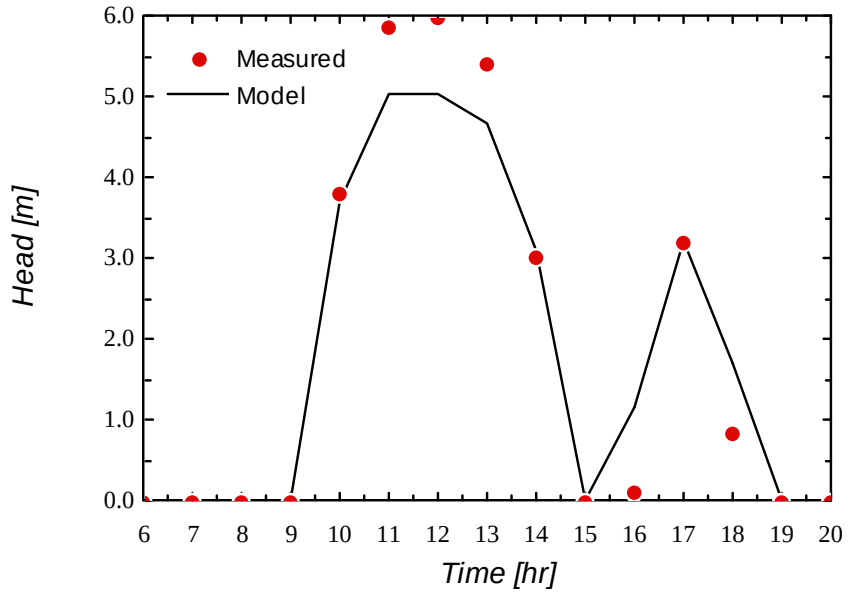

Figure 3.4.14 Head of FSEC PV pumping system as a function of time. Data measured on September 7th, 1987. Data reported by FSEC.

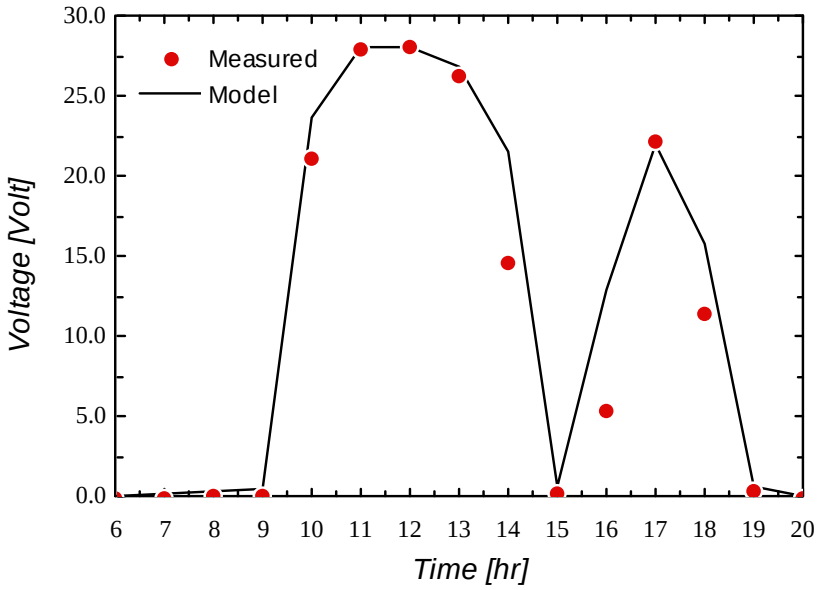

Figure 3.4.15 Voltage of FSEC PV pumping system as a function of time. Data measured on September 7th, 1987. Data reported by FSEC.

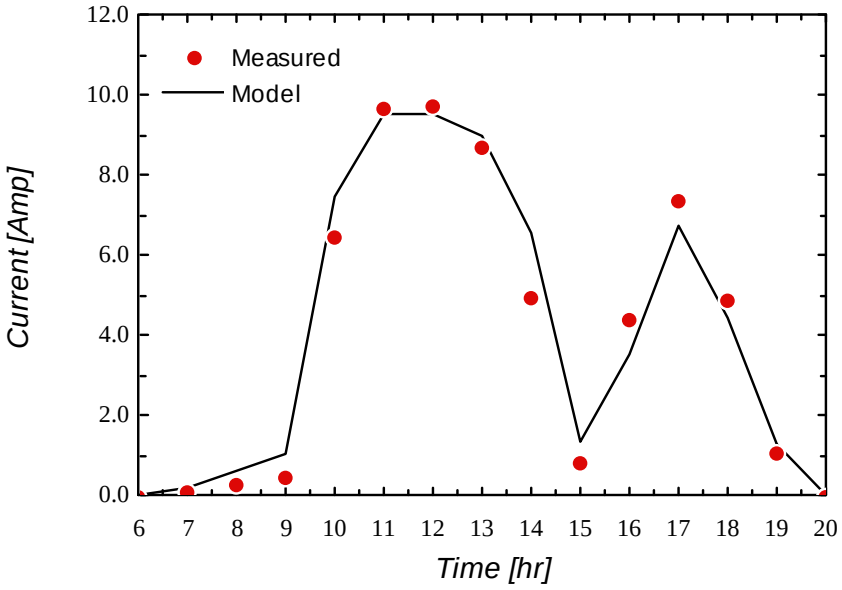

Figure 3.4.16 Current of FSEC PV pumping system as a function of time. Data measured on September 7th, 1987. Data reported by FSEC.

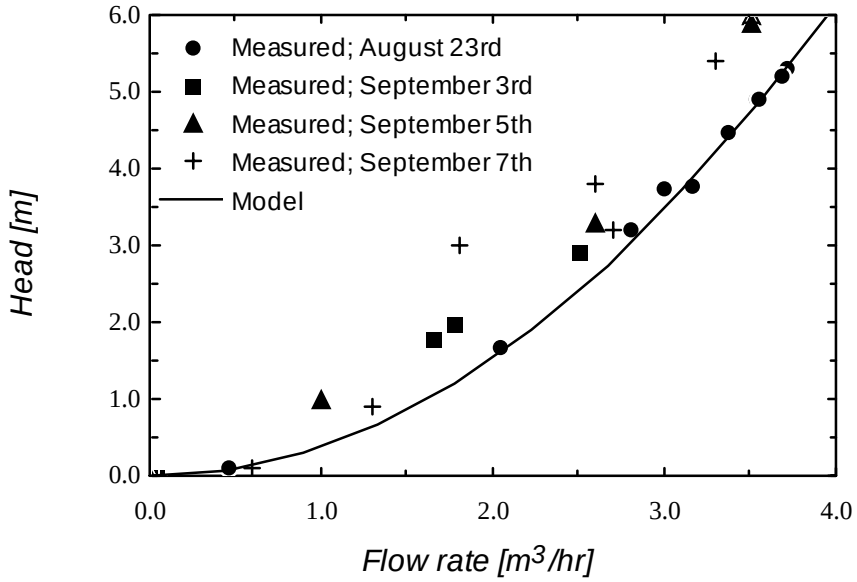

Figure 3.4.17 FSEC system head for the four days as a function of the flow rate of FSEC system. Data reported by FSEC.

To examine the effect of the PV cell temperature, the simulation of FSEC system were repeated for August 23rd, using a lower PV cell temperature: 298 K. Figure 3.4.18 depicts the flow rate as a function of time using two PV cell temperatures: 323 K and 298 K. The difference in flow rate is insignificant.

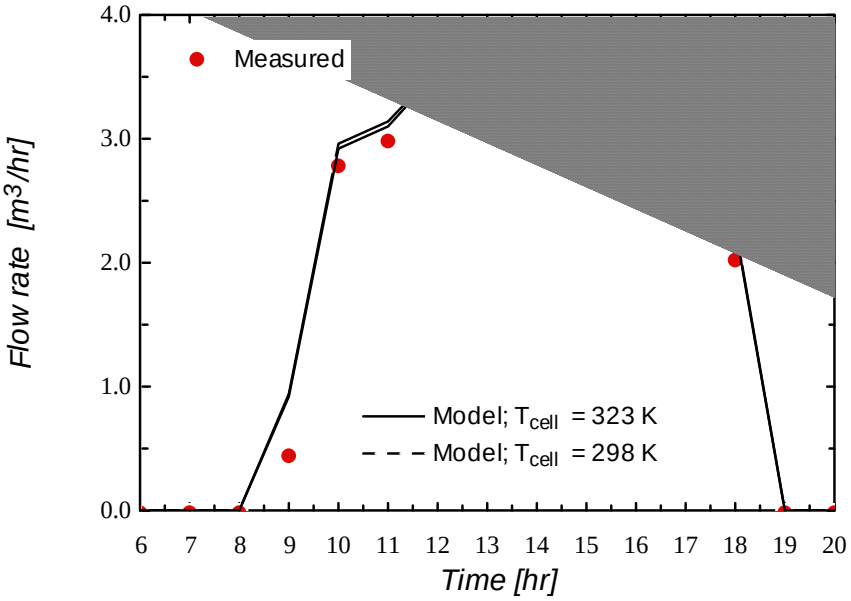

Figure 3.4.18 The effect of the PV cell temperature on the flow rate of FSEC system. Data reported by FSEC.

For comparison purposes, the results of the preceding PV pumping model, Eckstein *et al.*'s (1990), were compared against the results obtained using the proposed PV pumping model (Equations 3.2.1-30). The proposed PV pumping model predicted the performance of the FSEC system with better accuracy than Eckstein *et al.*'s model. Figures 3.4.19-20 illustrate the flow rate and the head of FSEC system as a function of time, respectively.

In conclusion, a mathematical model for PV pumping systems has been developed and experimentally validated. The proposed PV pumping system model will be coupled with the available and validated SDHW system model to constitute the PV-SDHW system model.

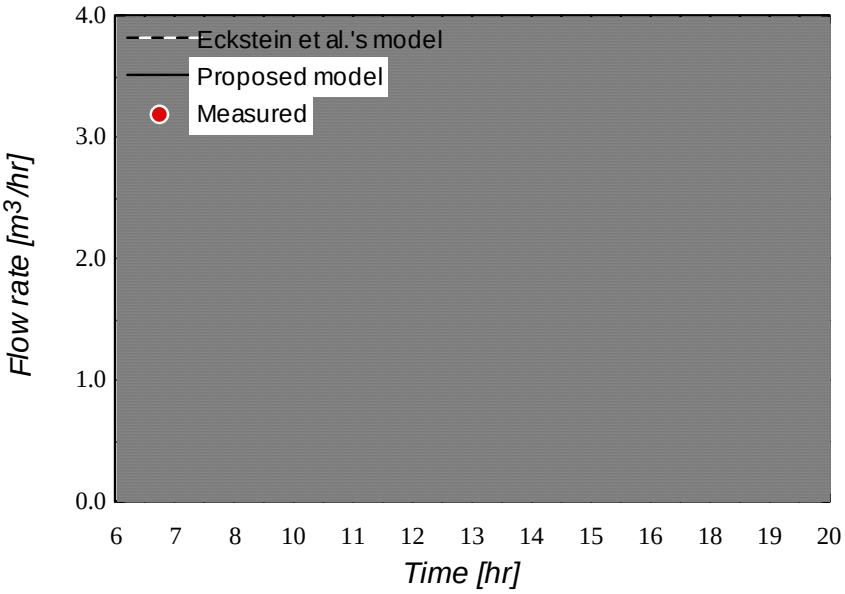

Figure 3.4.19 A comparison of the flow rates obtained by the proposed PV pumping system and the preceding PV pumping model developed by Eckstein *et al.* (1990).

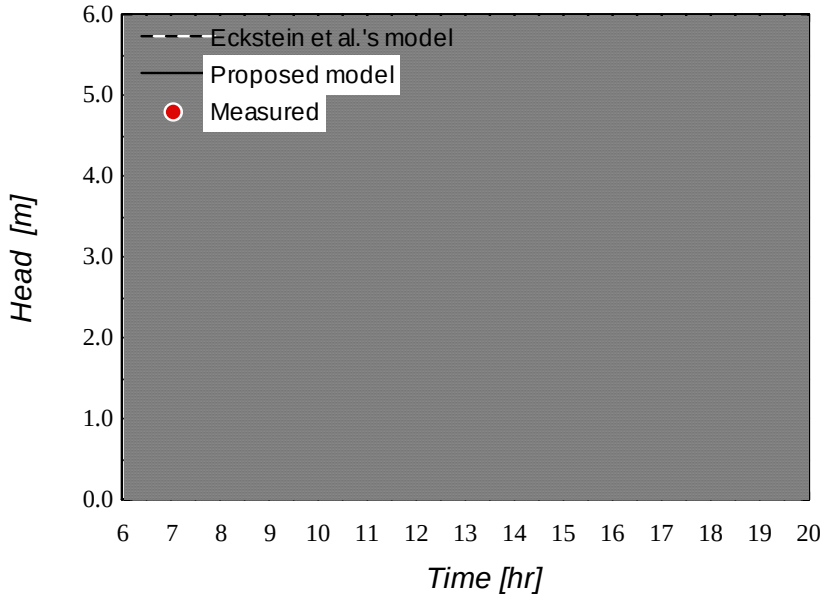

Figure 3.4.20 A comparison of the system head obtained by the proposed PV pumping system and the preceding PV pumping model developed by Eckstein *et al.* (1990).

Chapter 4 Optimum Search Methodology

This chapter presents the search procedure used to select an optimum direct-coupled PV pumping system in SDHW systems. The first and the second section introduce the objective function chosen to optimize the performance of PV-SDHW systems. The third section identifies the parameters that significantly affect the performance of PV-SDHW systems. The fourth section summarizes the optimization strategy for the optimum selection procedure. Finally, the fifth section briefly reviews the optimization algorithm used to identify the optimum solution.

4.1 Prologue

Due to the complex nature of PV-SDHW systems, a closed form mathematical expression for the efficiency of the system cannot be obtained. Therefore, the methodology for the optimization will be based on a numerical analysis. The parameters having a significant effect on the efficiency of the system will be identified, and the efficiency of the PV-SDHW system will be considered as a function of these parameters.

4.2 PV-SDHW Systems Performance Indicator

The output of a PV-SDHW system varies with time. Therefore, a time-integral quantity will be adopted to quantifies the PV-SDHW system performance. In SDHW systems, it is widely accepted that the performance is measured by its contribution of energy to meet a specific load profile (Duffie and Beckman, 1991). In this regard, SDHW systems and PV-SDHW systems are identical. The performance indicator is referred to as the solar fraction $\mathcal{F}$. If L_s denotes the energy delivered from the SDHW system, L_a denotes the energy delivered from the auxiliary source, and L_o is the total energy required by the load, then

$$F = \frac{L_s}{L_o} = \frac{L_o - L_a}{L_o} \qquad 4.2.1$$

where $\mathcal{F}$ is a dimensionless quantity.

4.3 Significant Parameters Affecting the Efficiency of PV-SDHW Systems

The flow rate profile (the flow rate, Q, as a function of the solar radiation, G) was found by the reviewed literature in chapter 1 and 2 to be the most significant factor in the efficiency of PV-SDHW systems.

A visual inspection of measured and simulated flow rate profiles reveals that all the flow rate profiles follow a general trend. PV pumping systems require a threshold radiation level, G_t, to start pumping. The value of G_t varies from one system to

another. As G increases beyond G_t, Q rapidly increases. However, the rate of increase in Q decreases as G increases.

A curve-fitting procedure, of three sets of measured flow rate profiles from the available literature, showed that a square root function of the form

$$Q = \begin{cases} 0.0 & \text{for } G \le G_t \\ \dfrac{-b + \sqrt{b^2 + 4\,a\,(G - c)}}{2\,a} & \text{for } G > G_t \end{cases} \qquad 4.3.1$$

reproduces the measured data with a correlation coefficient, R^2, in all three cases higher than 96%. Figures 4.3.1-3 present the three measured flow rate profiles obtained from the available literature along with their curve-fitted lines. Hence, each flow rate profile can be completely determined by the values of the three parameters a, b, and c.

The form of Equation 4.3.1 contains parameters that can be related to physical variables of a PV pumping system. The parameter c represents the threshold radiation level below which no flow occurs. The parameter b is the reciprocal of the rate of increase of Q as a function of G at G_t. At a given G, a smaller value of the parameter a gives a higher flow rate. The parameter b was restricted to be non-negative since Q would not increase for a decreasing G. Figures 4.3.4-6 illustrate the effect of the parameters a, b and c on the general flow rate profile of PV pumping systems.

The change in the ambient temperature has an effect only on the PV cells within the PV pumping system. A 1°C increase in the ambient temperature produces a slight *decrease* in the open circuit voltage and an even smaller *increase* in the short circuit current. In the three measured flow rate profiles shown in Figures 3.4.1-3 the ambient temperature changed during the course of the day, but the resultant change in Q was insignificant.[11]

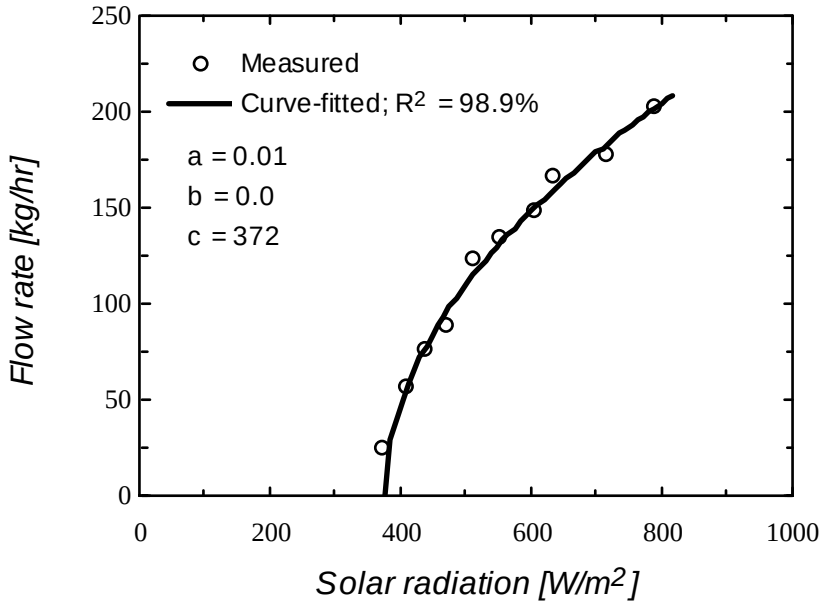

Figure 4.3.1 Measured and curve-fitted flow rate profile of a PV pumping system. Data obtained from Litka and Chandra (1979).

[11]However, the change in the ambient temperature has a significant effect on the operation of PV systems that include batteries, whose operating voltage may become higher than the open circuit voltage as a consequence of a temperature increase. In this case, the batteries will never be charged.

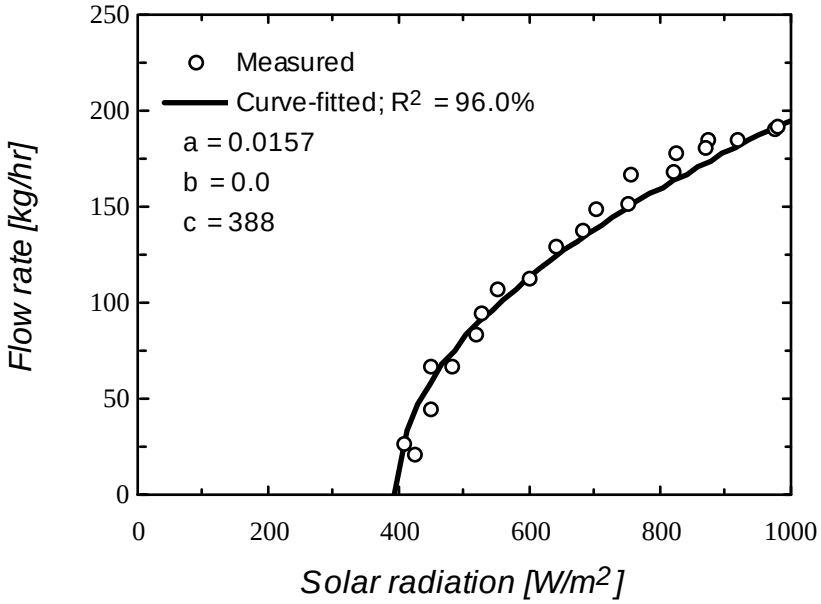

Figure 4.3.2 Measured and curve-fitted flow rate profile of a PV pumping system. Data obtained from Cromer (1983).

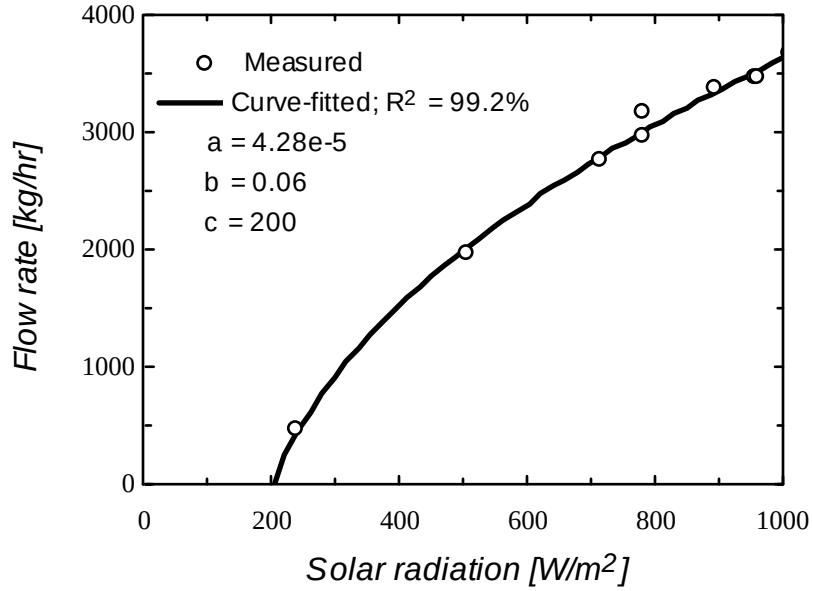

Figure 4.3.3 Measured and curve-fitted flow rate profile of a PV pumping system. Data reported by FSEC (August 23rd, 1987).

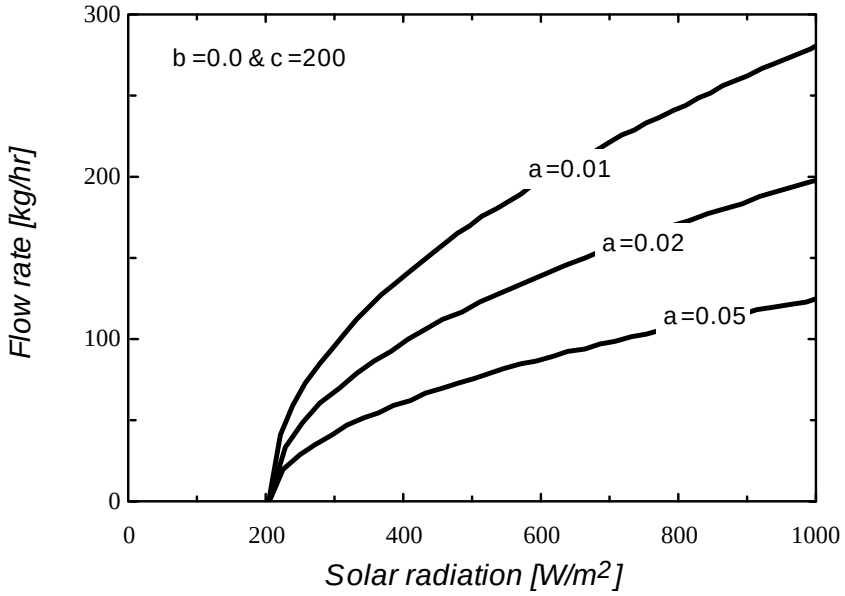

Figure 4.3.4 The effect of the parameter *a* on the general flow rate profile of PV pumping systems.

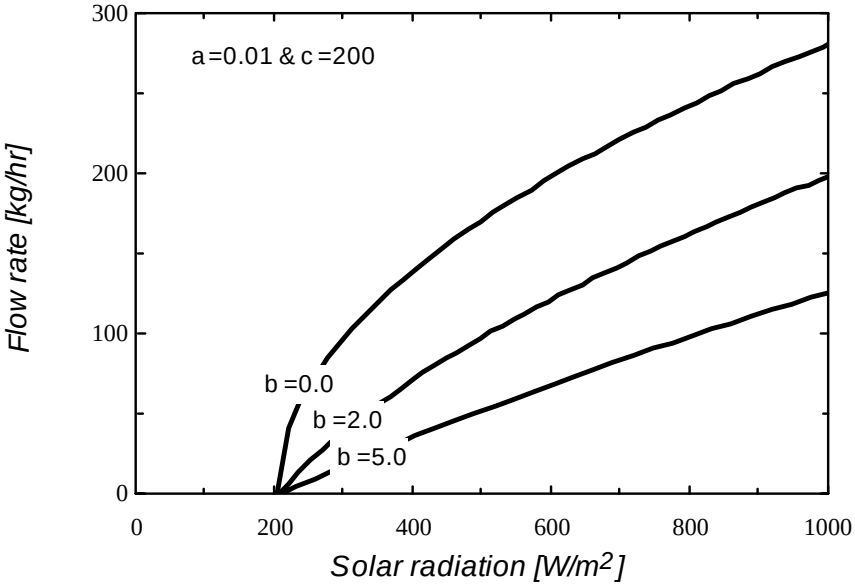

Figure 4.3.5 The effect of the parameter *b* on the general flow rate profile of PV pumping systems.

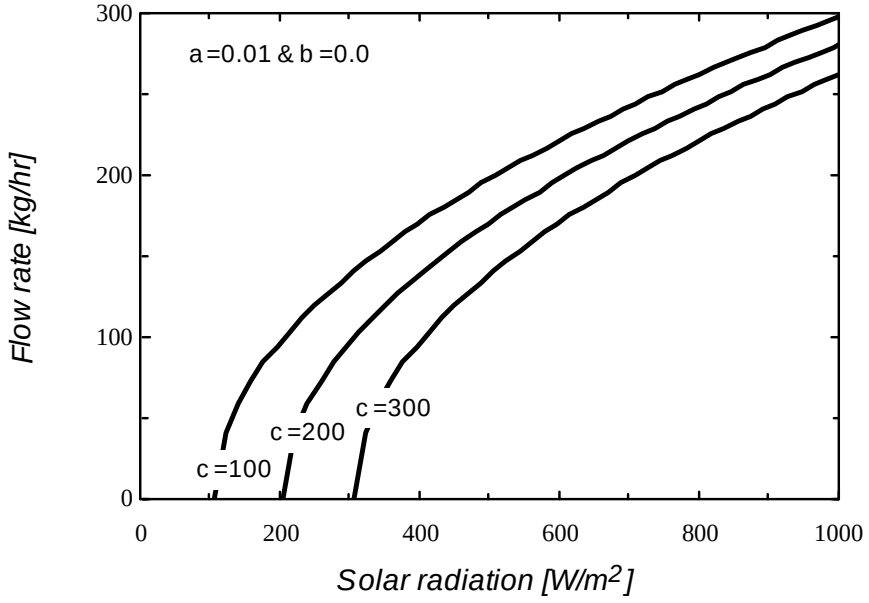

Figure 4.3.6 The effect of the parameter *c* on the general flow rate profile of PV pumping systems.

4.4 Optimum Search Strategy

The search methodology for optimizing the PV-SDHW system's components will be performed using a two-phase procedure. In phase one a direct solution is sought. The goal is to find, among the possible PV pumping systems' flow rate profiles, the flow rate profile that maximizes the performance of a given SDHW system. In phase two, the goal is to select the components of the PV pumping system. Each combination of PV cell(s), DC-motor and pump exhibits a unique flow rate profile. Therefore, the problem in this phase is an inverse problem; that is to identify the PV pumping system's components that results in the best match to the optimum profile found in phase one.

An alternate route could have been taken; that is to maximize $\mathcal{F}$ with respect to the parameters of the PV pumping system. However, the two-phase procedure alternative was chosen because of two reasons:

1) The issue of the optimum flow rate of SDHW system has not been fully addressed in the reviewed literature. The results of phase one of the current investigation will add more information to the issue of the optimum SDHW flow rate profile among the possible PV pumping system's flow rate profiles.

2) The performance of SDHW systems is location dependent; it depends upon the magnitude of the weather variables as well as their frequency distribution. On the other hand, the flow rate profile (the significant parameter that affect the performance of PV-SDHW system and the only output of the PV pumping systems) is location independent; $Q = f(G)$ only. Therefore, performing repetitive annual simulations of PV pumping systems in conjunction with SDHW systems is more costly than repetitive annual simulations of SDHW systems alone followed by repetitive calculation of PV pumping systems using a fixed solar radiation increment. (~100 runs each as opposed to an hourly annual simulation of 8760 runs).

The following two sections briefly describe the tasks of phase one and phase two of the two-phase procedure.

4.4.1 Phase One

Main Task: *Finding the optimum flow rate profile of a given SDHW system*

The objective function that needs to be optimized in this phase is the annual solar fraction, $\mathcal{F}$, of the SDHW system. For a given SDHW system configuration, the task is to find the values of the three parameters (a, b and c) determining the flow rate profile that produce maximum $\mathcal{F}$. In mathematical form, the problem in phase one can be written as:

$$\textbf{maximize} \quad \mathrm{F}(a,b,c) \tag{4.4.1}$$

where $a \geq 0$, $b \geq 0$ and $c \geq 0$.

4.4.2 Phase Two

Main Task: *Finding the optimum configuration of the direct-coupled PV pumping system*

The goal of this phase is to find the configuration of the PV pumping system that results in a flow rate profile that is closest to the optimum flow rate profile found in phase one. The objective function chosen to be minimized is the square of the area, ϕ, between the flow rate profile resulted by a PV pumping system and the optimum flow rate profile. Hence, the problem in phase two is to minimize ϕ with respect to the PV pumping system components.

$$C_{stat1} = \begin{cases} 0.1CI_{mp,ref}^{2} P & \text{for Type = 1} \\ 0.1CI_{mp,ref} P & \text{for Type = 2} \end{cases}$$

$$C_{stat2} = 0.5C_{stat1}$$

$$C_{visc} = 0.0$$

Therefore, the flow rate profile resulted by a PV pumping system can be looked at as a function of five parameters:

I) Two integer parameters: P and S, corresponding to the parallel and serial arrangement of the given PV cell.

II) Three parameters describing the performance of the DC-motor; as follows:

- An integer parameter, Type, representing the type of the DC-motor: series excited DC-motors (Type = 1) or permanent magnet and separately excited DC-motors (Type = 2)

- Two real parameters corresponding to the values of the coefficient, C, and the resistance, R, of the DC-motor.

This is a mixed integer optimization problem with five independent parameters. In mathematical form, the problem in phase two can be written as:

minimize ϕ(Type, P, S, C, R) 4.4.2

where

$$\phi = \int_{G=0}^{G=G_{\max}} (Q_{PV} - Q_{optimum})^2 \, dG \qquad 4.4.3$$

and P>=1, S>=1, Type = 1 or 2, C>=0, R>=0, and G_{max} is the maximum solar radiation. G_{max} is set to be 1000 W/m^2.

and $P \geq 1$, $S \geq 1$, $Type = 1$ or 2, $C \geq 0$, $R \geq 0$, and G_{max} is the maximum solar radiation. G is linearly varied from 0 to 1000 W/m^2.

4.5 Optimization Algorithm

The optimization problem encountered in this investigation is classified among the combinatorial optimization class: There is an objective function to be maximized ($\mathcal{F}$) or minimized (ϕ)but the space over which that function is defined is the N-dimensional space of N continuously (a, b, c, R, and C) and discrete ($Type$, P and S) variable parameters.

Among the available method of solving combinatory optimization is the method of simulated annealing. The method of simulated annealing is a statistically based method that has recently attracted significant attention as suitable for optimization problems of very large scale (Press *et al.*, 1989). It has effectively solved the famous salesman problem and has also been used successfully for designing complex integrated circuits.

Press *et al.* (1989) indicated that the method of simulated annealing has two unique features when compared to other optimization techniques. First, it is not easily fooled by the quick payoff achieved by falling into unfavorable local minimum. Second, configuration decisions tend to proceed in a global order. The algorithm initially explores the objective function with course detail over a wide region, progress to finer detail in regions where a global optimum may likely exist (Flake, 1994). The primary disadvantage, however, is that the algorithm is computationally expensive.

Flake (1994) indicated that the first version of the simulated annealing algorithm is attributed to Kirkpatrick *et al.* (1983) who originally proposed the algorithm to solve large combinatorial problems. Later, Corana *et al.* (1987) modified Kirkpatrick *et al.*'s algorithm to handle functions of continuous variables. Most recently, Goeffe *et al.* (1994) introduced extensions of the Corana *et al.*'s algorithm which help in reducing execution time. Flake (1994) modified Goeffe *et al.*'s algorithm for use with the TRNSYS simulation program.

The TRNSYS component of the simulated annealing algorithm, TYPE 74, requires the objective function as an input evaluated at the control variables which are its outputs.

Further information on the simulated annealing algorithm can be found in Kirkpatrick *et al.* (1983), Corana *et al.* (1987), Press *et al.* (1989), Flake (1994) and Goeffe *et al.* (1994).

Chapter 5 Direct PV-SDHW Systems

This chapter presents the results of the analysis of selecting the optimum PV pumping system in Direct SDHW system (direct PV-SDHW system). The two-phase procedure that was explained in the previous chapter has been applied. The first section presents the results of phase one and the second section presents the results of phase two. In each section, a base system will be defined followed by the analysis results and other parametric analysis.

5.1 Phase One

5.1.1 Base System

The following section presents a brief description of the base SDHW system used in phase one. Detailed information about the system is given in Appendix C.

The system chosen is composed of a flat-plate collector, a hot water storage tank, an in-line auxiliary heater and a variable flow pump. The pump flow rate will be varied using the general flow rate profile equation presented in the previous chapter. Figure 5.1.1 illustrates a schematic drawing of the base system used in phase one.

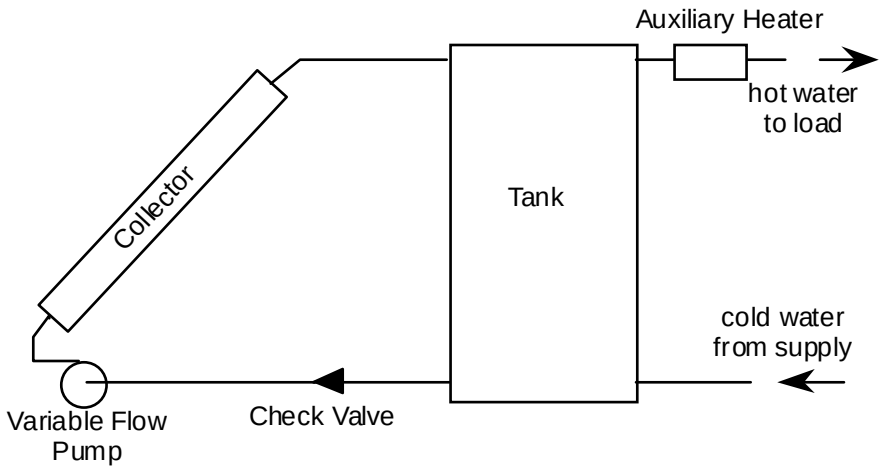

Figure 5.1.1 Schematic drawing of the base system in phase one.

The flat-plate collector consists of one glass cover with an area of 6.5 m^2. The working fluid is water. The collector has a slope of 40° and points due South. As per ASHRAE standards, the collector has a curve intercept, $F_R(\quad)$, of 0.7 and a line slope, $-F_R U_L$, of 15 kJ/hr-m^2. The ASHRAE test was performed under the manufacturer recommended flow rates of 325 kg/hr.

The thermal storage tank has a volume of 0.39 m^3. The tank is located indoors with an all year around envelope temperature of 21°C.

The load for which the initial optimization was computed has a demand of 300 kg of water per day evenly distributed over the day from 7:00 to 21:00 hours with a set temperature of 60°C. Figure 5.1.2 depicts the load flow rate profile over the course of one day. If the tank water outlet temperature falls below the set temperature, an in-line auxiliary heater will compensate for the difference.

The system is designed to partially supply the hot water needs for a house located in Madison, WI. TMY data will be used to represent the weather data of the location. In a second stage, the load profile was varied and the corresponding optimum computed. Among the load profiles studied, the standard RAND load profile was considered. The results are presented in section 5.1.2.1. Afterwards, the effect of the location was studied and the optimum computed for different locations. These results are presented in section 5.1.2.2.

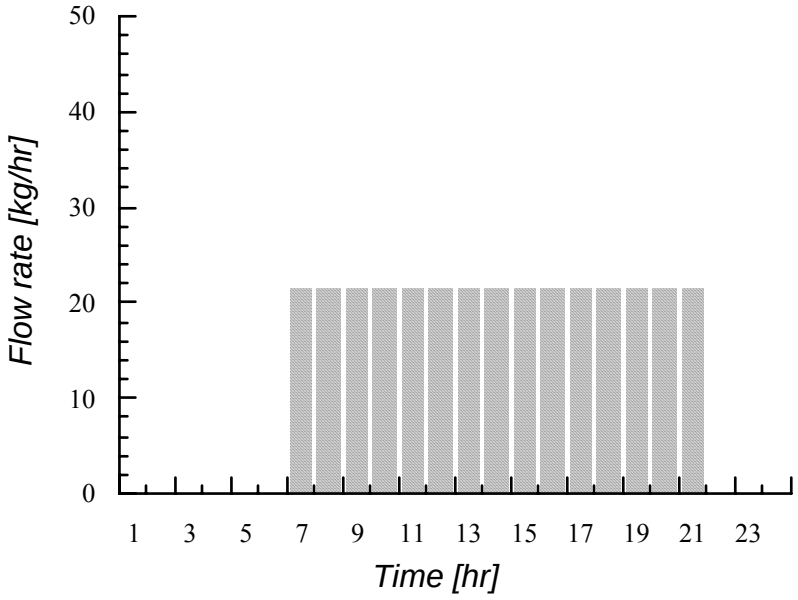

Figure 5.1.2 Base system load flow rate profile over the course of one day.

5.1.2 Results

The simulated annealing algorithm (Flake, 1994) was used to search for the flow rate profile parameter set (a, b, c)[12] that maximizes the annual solar fraction, $\mathcal{F}$, of the base system. The optimum annual solar fraction was found to be 0.699 and the optimum parameter set, which yields this maximum performance, was found to be

$$(a, b, c) = (1.0302, 0.0575, 287)$$

The optimum system hence has a threshold radiation level, G_t, of 287 kJ/hr-m^2 (71 W/m^2) and a rate of change of the flow rate at G_t equal to 1/0.0575 kg/hr/kJ/hr-m^2 (5.75E-5 kg/s/W/m^2). Figure 5.1.3 shows the optimum flow rate profile.

A second method for finding the optimum value was also used. It consists of evaluating the objective function at the nodes of a prescribed grid in the space of parameters (a, b, c). This method led to the same optimum values found by the simulated annealing algorithm. It has the advantage though of being much faster in producing the optimum.[13]

---

[12](a, b, c) define the load profile via equation $Q = \frac{-b + \sqrt{b^2 + 4\,a\,(G - c)}}{2\,a}$ *for* $G > G_t$

[13]The simulated annealing algorithm needed 35,101 annual hourly simulations before attaining the forgoing optimum! On the other hand, 300 annual hourly simulations using of the direct evaluation method was sufficient to reach to the optimum and to describe the objective function around this optimum.

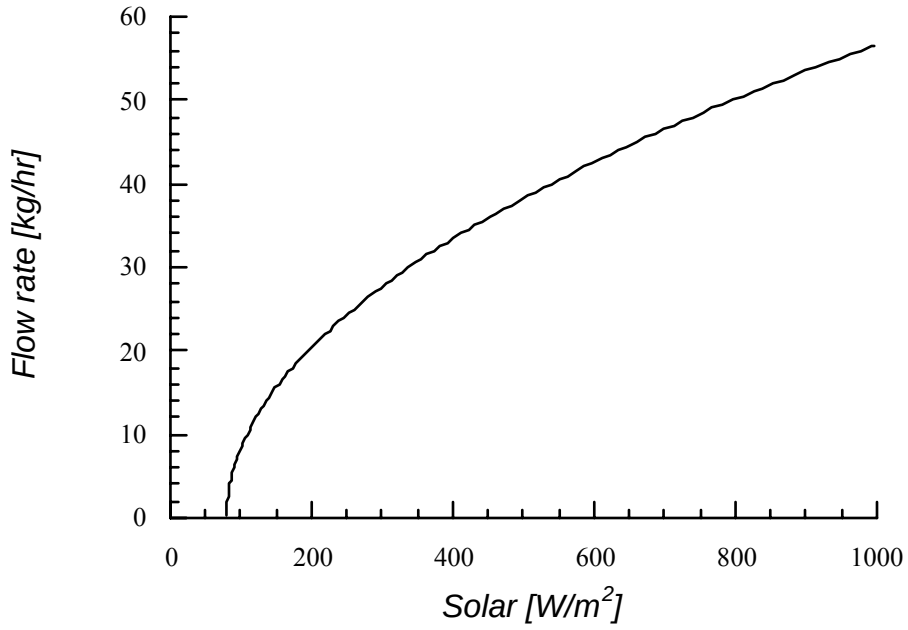

Figure 5.1.3 The optimum flow rate profile of the base system.

A closer examination of the graph of the objective function reveals that the objective function, $\mathcal{F}$, is not sensitive to the value of the parameter *b*. Figure 5.1.4 shows that for a fixed value of *a* (*a*=1.0), if the value of *c* is fixed, the objective function, $\mathcal{F}$, shows almost no variation with respect to *b*. Similarly, Figure 5.1.5 shows that for a fixed value of *c* (*c*=300.0), if the value of *a* is fixed, the objective function, $\mathcal{F}$, shows almost no variation with respect to *b*.

On the other hand, the objective function is quite sensitive to the values of both *a* and *c*. This can be observed from Figure 5.1.6 in which the parameter *b* was fixed to be

zero. The surface hence obtained shows some variation in the value of $\mathcal{F}$ when either a or c varies.

The only region in which changes in a and c induce only small changes in $\mathcal{F}$ is around the optimum point. This can be seen in Figure 5.1.6 where the surface $\mathcal{F}(a,c)$ is almost flat around the optimum point. This has important practical consequences in the sense that it allows the reproduction of the optimum flow rate profile with a relatively large range of (a,c) values.

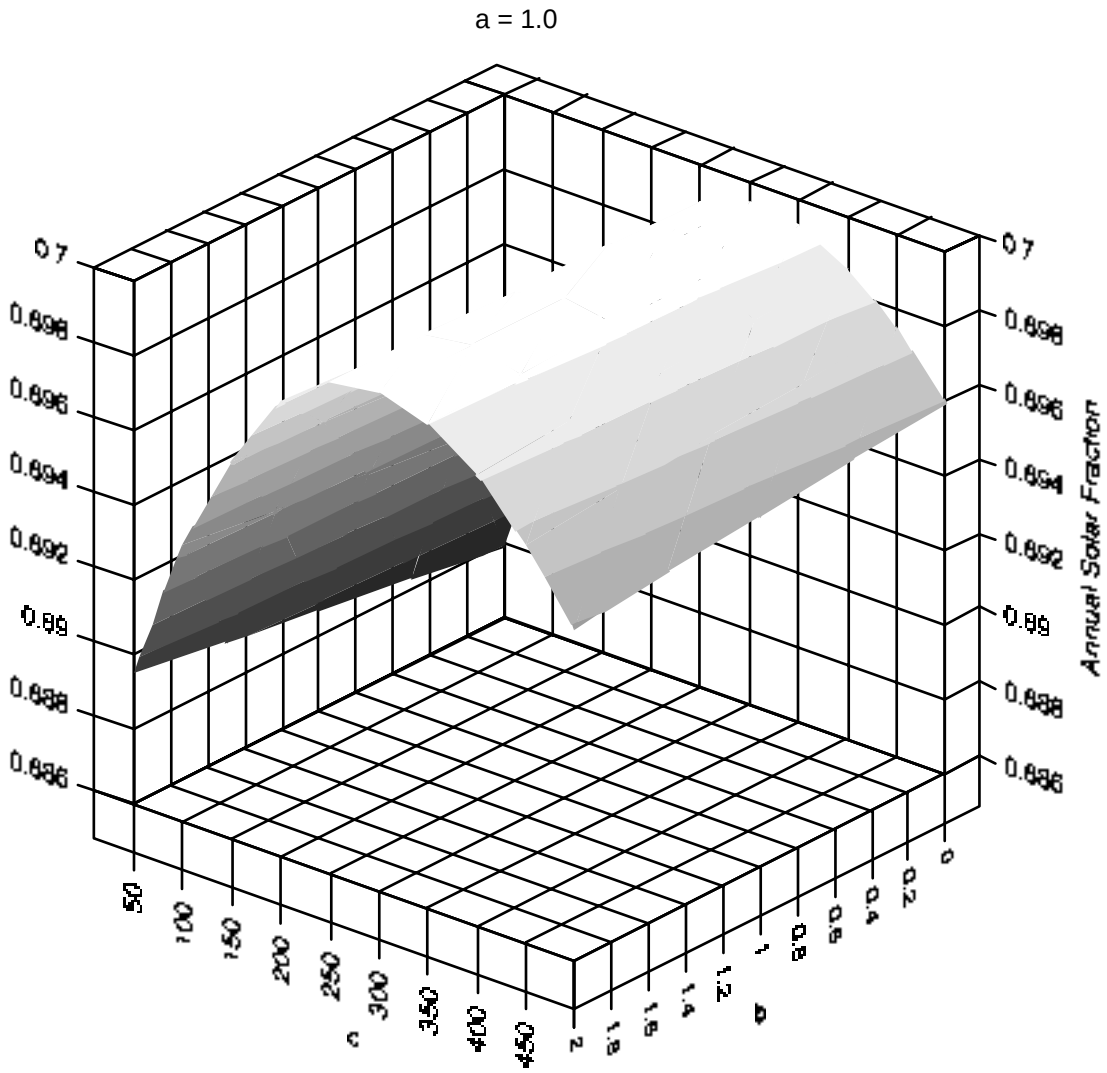

Figure 5.1.4 Graph of the annual solar fraction of the base system as a function of the parameters *b* and *c*. The value of the parameter *a* is set to 1.

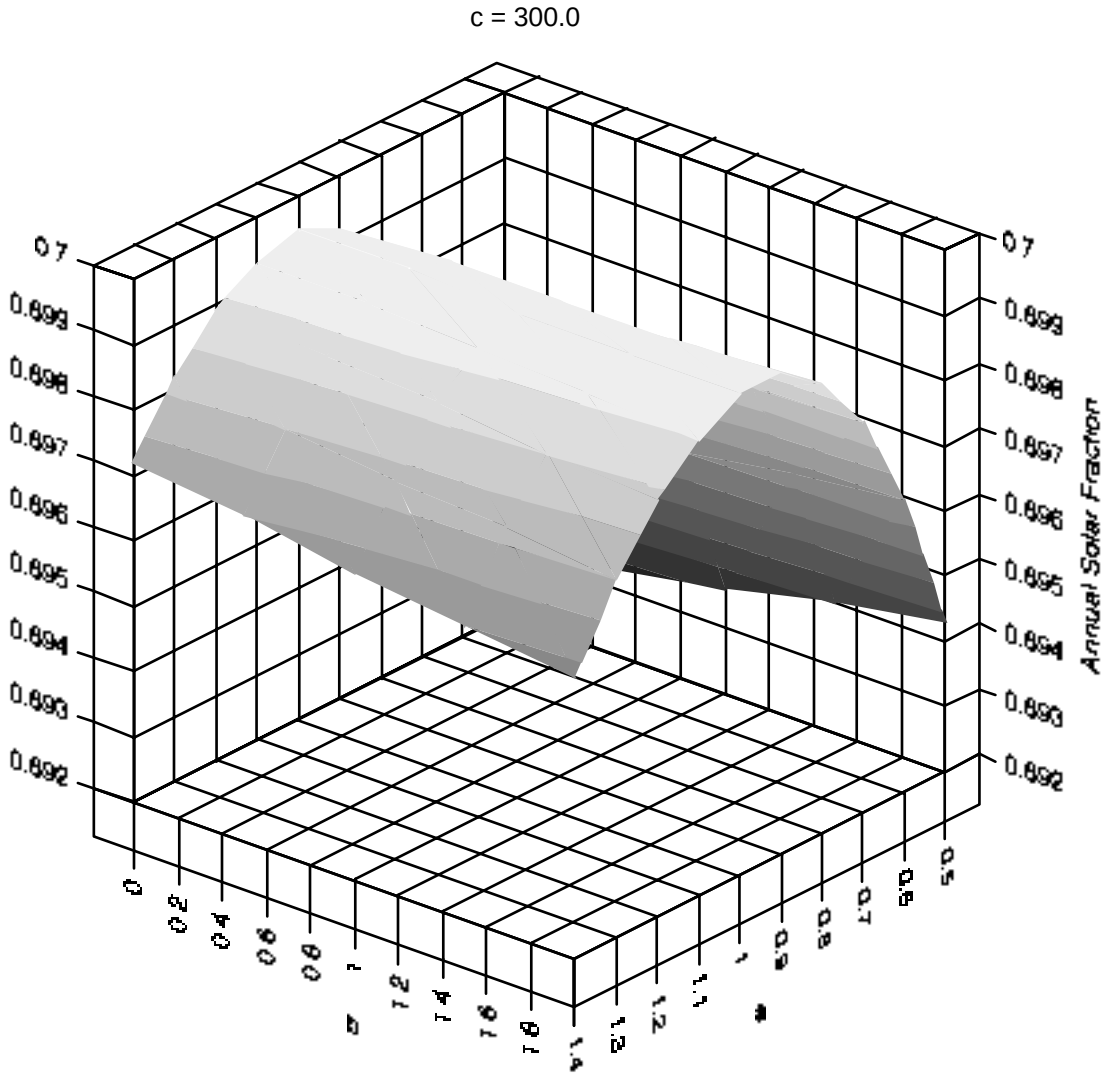

Figure 5.1.5 Graph of the annual solar fraction of the base system as a function of the parameters *a* and *b*. The value of the parameter *c* is set to 300.

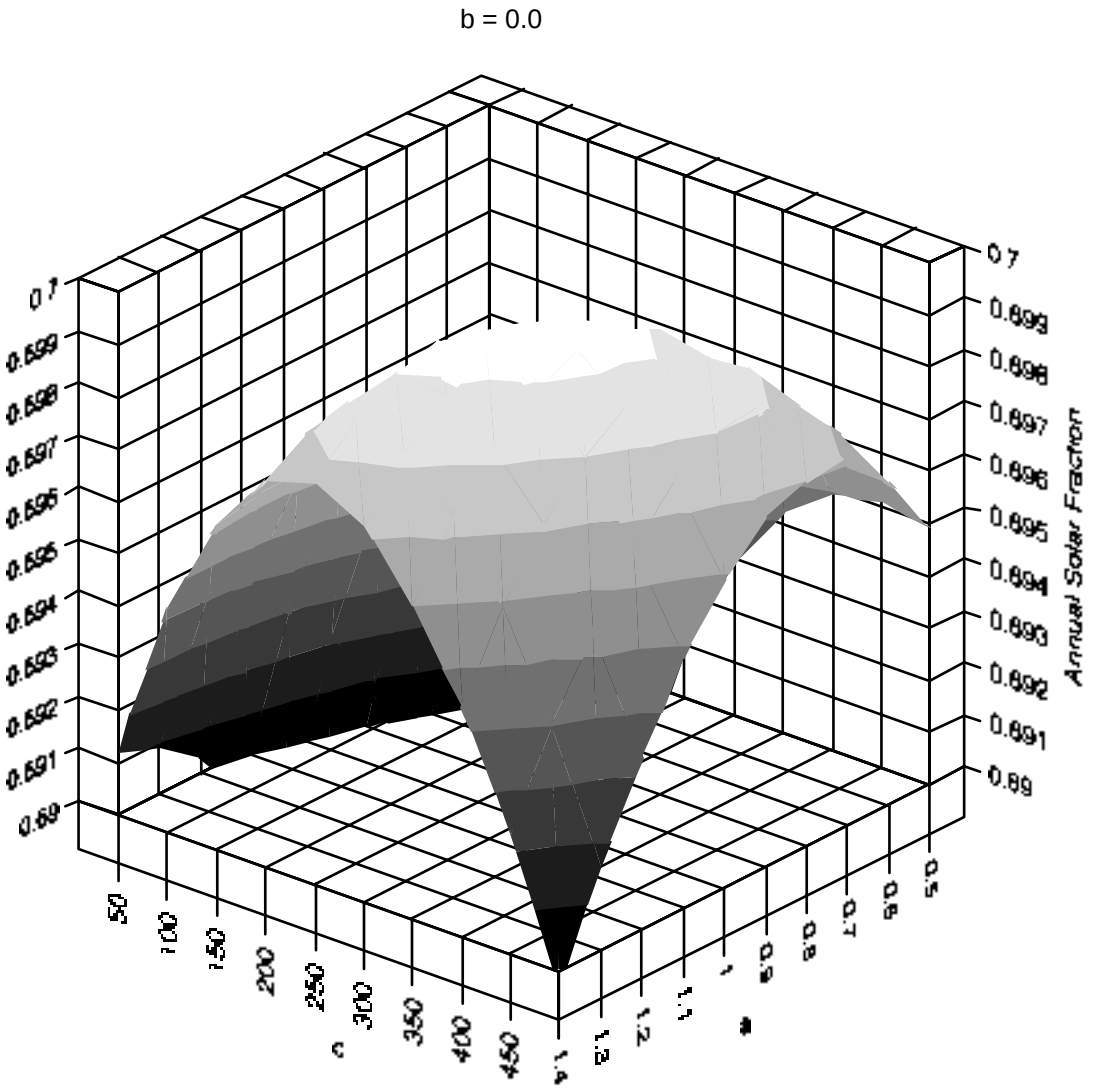

Figure 5.1.6 Graph of the annual solar fraction of the base system as a function of the parameters *a* and *c*. The value of the parameter *b* is set to 0.

Mathematically, the optimum flow rate profile found earlier is unique and can theoretically be met by a unique PV pumping system. However, in reality, the discrete selection of the different PV pumping system components may not allow a

perfect match with that optimum. Therefore, it is necessary and useful to identify the possible range of flow profiles that can yield an annual solar fraction close enough to the optimum. This possible range will be referred to as the "window" of possible flow rate profiles. Figure 5.1.7a shows the contour-lines $\mathcal{F}(a,c)$ = constant. Points (a,c) in the interior of the contour line $\mathcal{F} = 0.69$ produce an annual solar fraction of at least that amount. Hence, any set of system components that produces values of a and c inside that region is for all practical purposes an optimum system. Such a region can be defined as "the optimum region". By translating the values of c to the values of the threshold radiation level, G_t, it appears that the value of G_t for the optimum PV-SDHW system is allowed to range in a wide interval between 20 W/m^2 and 180 W/m^2. Similarly, by translating the values of a to the values of Q_{noon}, the flow rate at 1000 W/m^2, it appears that the values of Q_{noon} for the optimum system range between 40 kg/hr and 100 kg/hr. Figure 5.1.7b shows the corresponding contour-lines $\mathcal{F}(Q_{noon},G_t)$ = constant.

Another way of looking at this is by drawing all the flow rate profiles produced by the (a,c) values within the optimum region. These profiles have an upper envelope and a lower envelope which bound the "window" of the optimum flow rate profiles. Figure 5.1.8 shows the optimum flow rate profile and the window of the optimum flow rate profiles that will yield an annual solar fraction of at least 0.69.

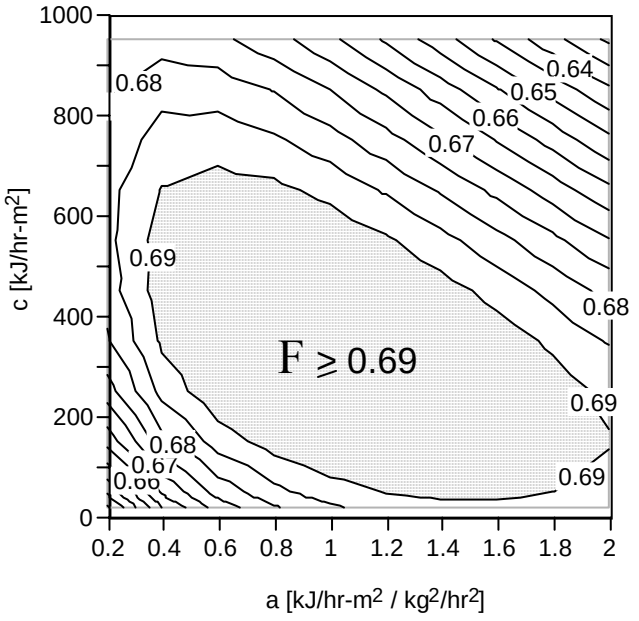

(a)

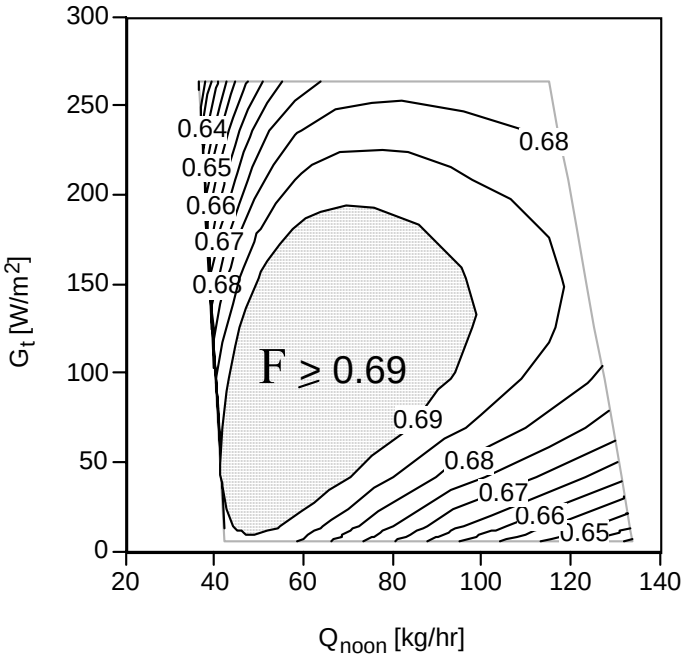

(b)

Figure 5.1.7 (a) Contour plot of the annual solar fraction of the base system as a function of the parameters *a* and *c*. (b) Contour plot of the annual solar fraction of the base system as a function of the parameters Q_{noon} and G_t. The value of the parameter *b* for both is set to zero.

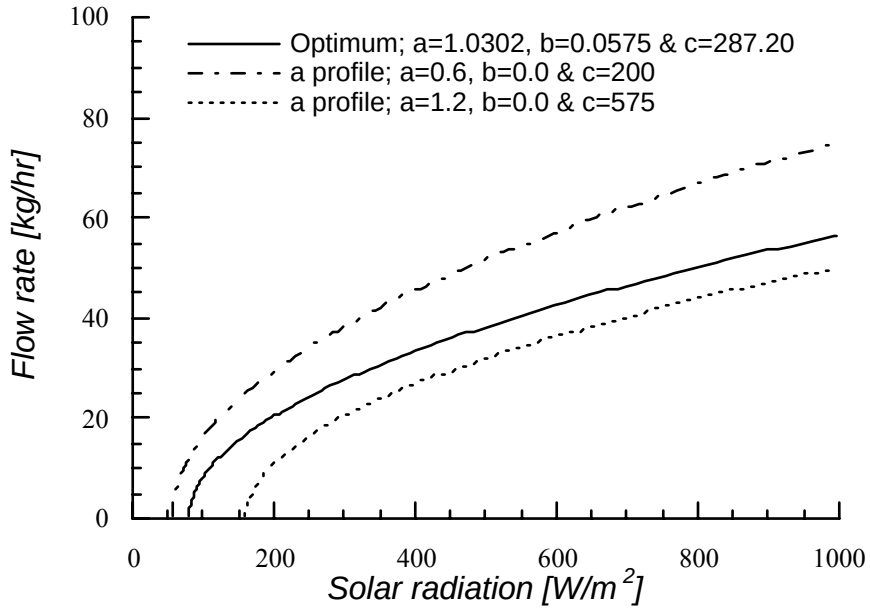

Figure 5.1.8 The window of the optimum flow rate profiles that will yield an annual solar fraction of at least 0.69.

5.1.2.1 Effect of the Load Profile on the Optimum Set

Further analysis has been carried out to examine the effect of the pattern and the daily integral quantity of the load profile to be met by the system under investigation. The results indicate that the optimum annual solar fraction shows little sensitivity with respect to the pattern of the load profile. However, its magnitude was found to be dependent upon the amount of the daily integral quantity of the load.

Three load profiles other than the one used in the base system were studied and the optimum computed. In all three cases the optimum was within 2.5% of the standard

optimum, the optimum resulting from the standard load profile of the base system. This proves that there is little sensitivity of $\mathcal{F}$ to load distributions. Figure 5.1.9 shows the standard load profile and the corresponding contour plot of the objective function. Figure 5.1.10 depicts a triangular load profile with a daily integral value of 300 kg of water and an early morning peak demand, and the corresponding contour plot of the objective function. Figure 5.1.11 depicts a triangular load profile with a daily integral value of 300 kg of water and a late evening peak demand, and the corresponding contour plot of the objective function. Figure 5.1.12 depicts the standard RAND load profile with a total daily integral value of 300 kg of water, and the corresponding contour plot of the objective function.

The effect of the daily integral quantity was studied by computing the optimum for a load profile which differed from the standard profile only by its integral quantity (440 kg instead of 300 kg for the standard profile). The optimum found was within 1.5% of the value of the annual solar fraction that the optimum parameters of the base system would have produced. Hence, the optimum parameters are not sensitive to the value of the daily integral quantity of the load profile. Figure 5.1.13 depicts the load profile with a total daily integral value of 440 kg of water, and the corresponding contour plot of the objective function.

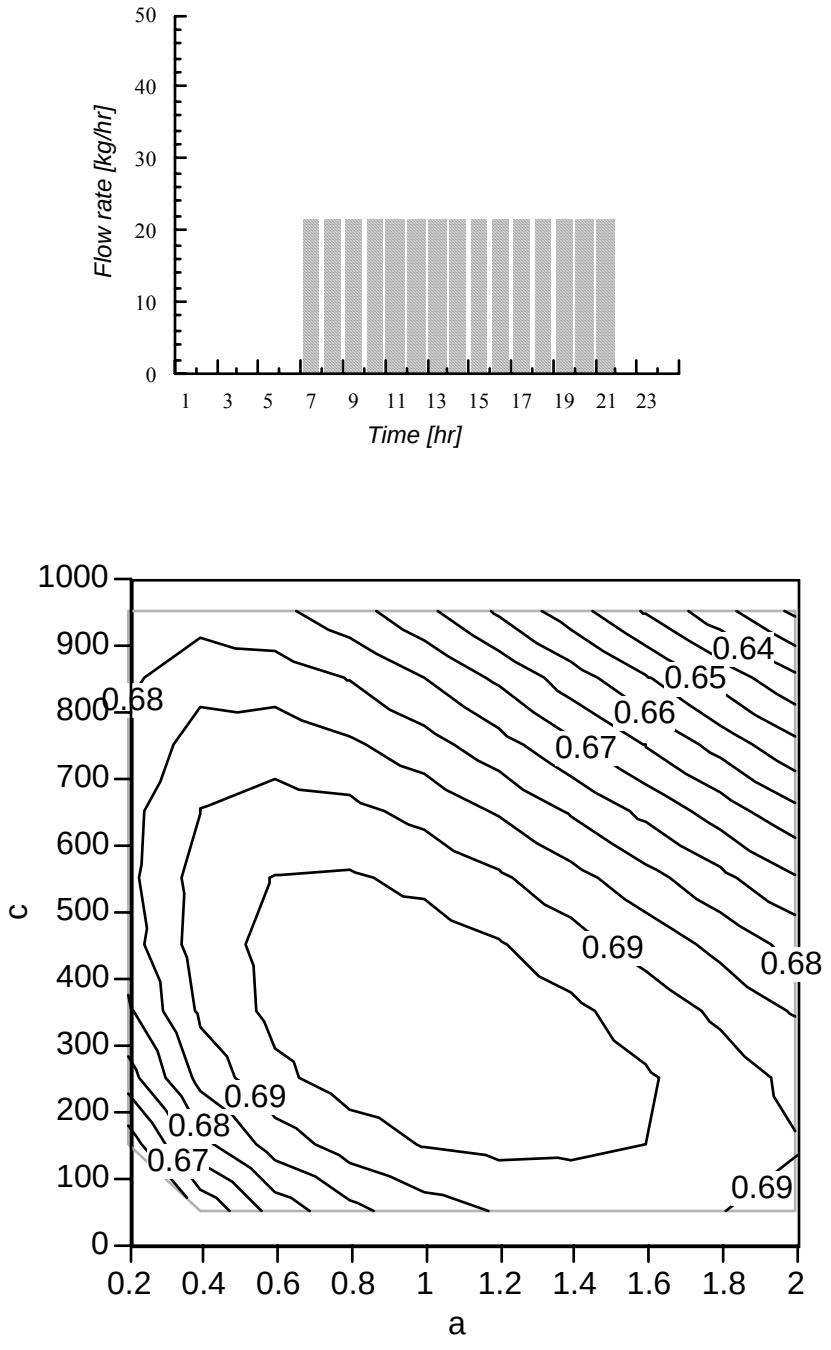

Figure 5.1.9 Contour plot of the annual solar fraction of the base system as a function of the parameters *a* and *c*. The load profile is defined as a square function with a daily integral value of 300 kg of water.

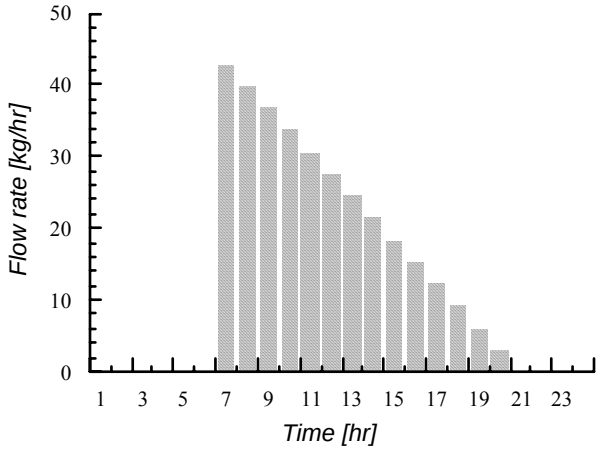

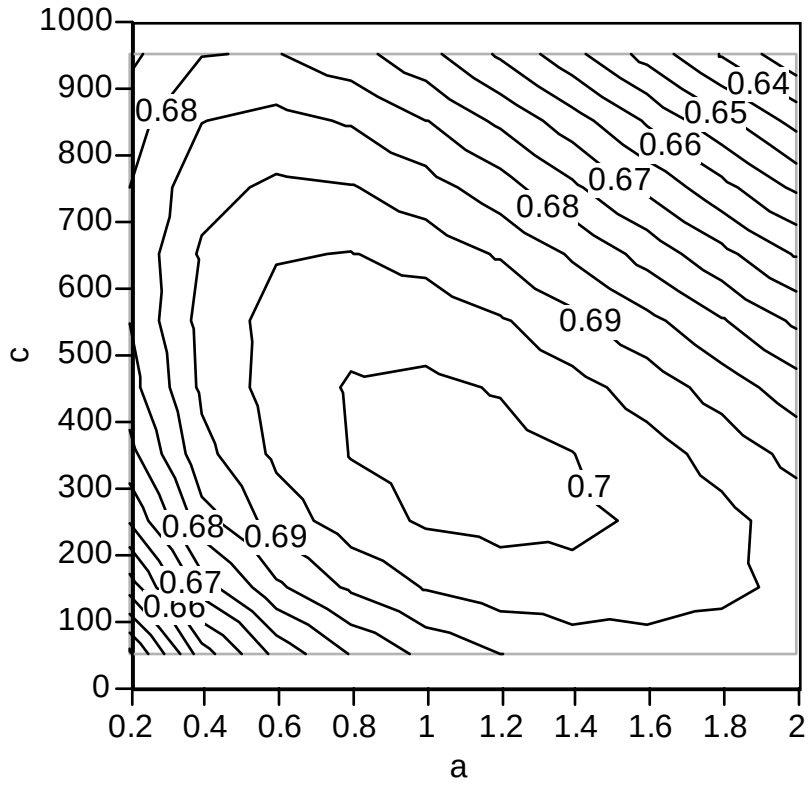

Figure 5.1.10 Contour plot of the annual solar fraction of the base system as a function of the parameters *a* and *c*. The load profile is defined as a triangular

function with a daily integral value of 300 kg of water and an early morning peak demand.

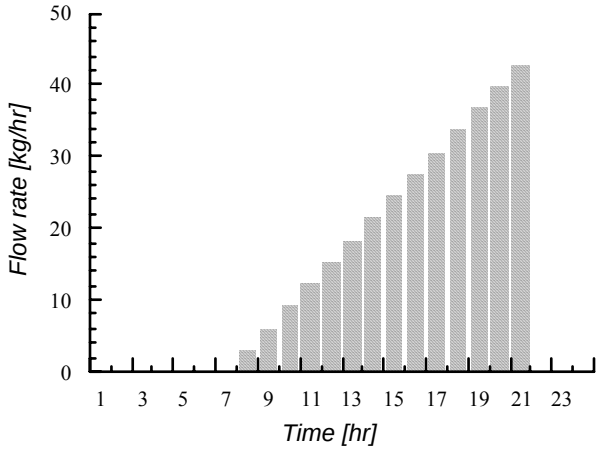

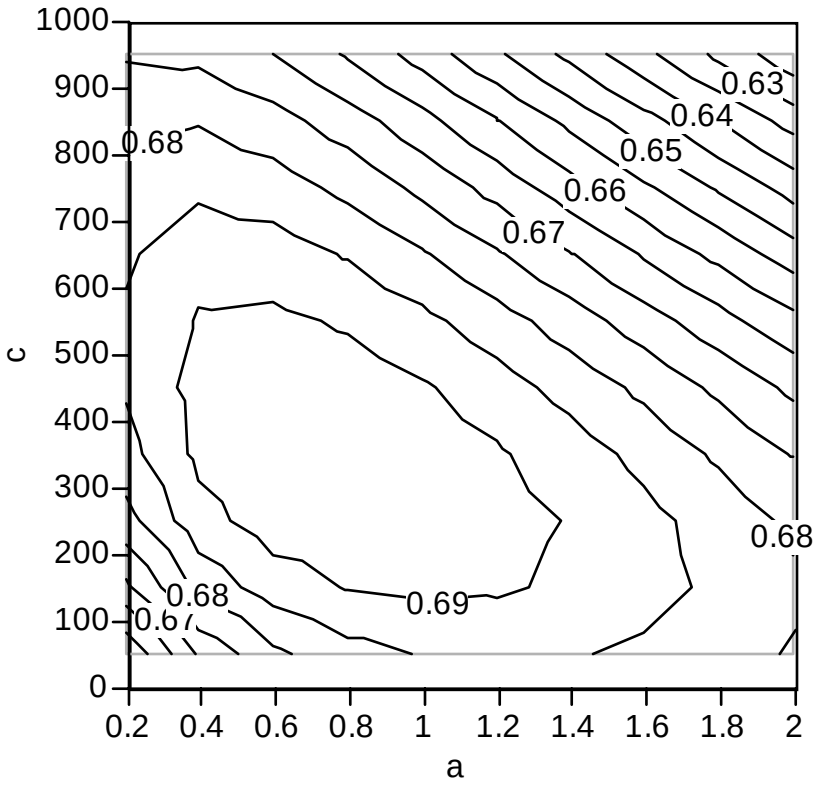

Figure 5.1.11 Contour plot of the annual solar fraction of the base system as a function of the parameters *a* and *c*. The load profile is defined as a triangular

function with a daily integral value of 300 kg of water and a late evening peak demand.

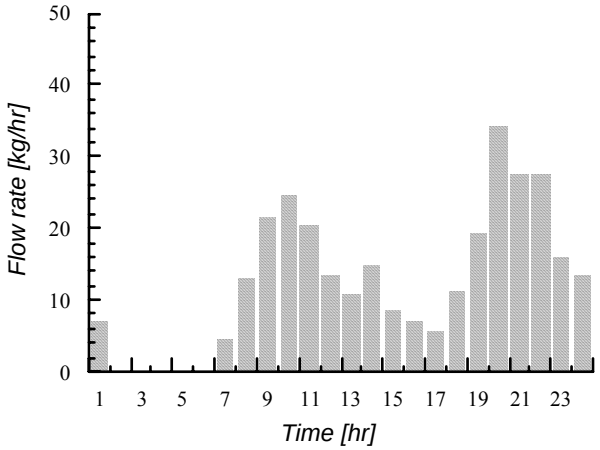

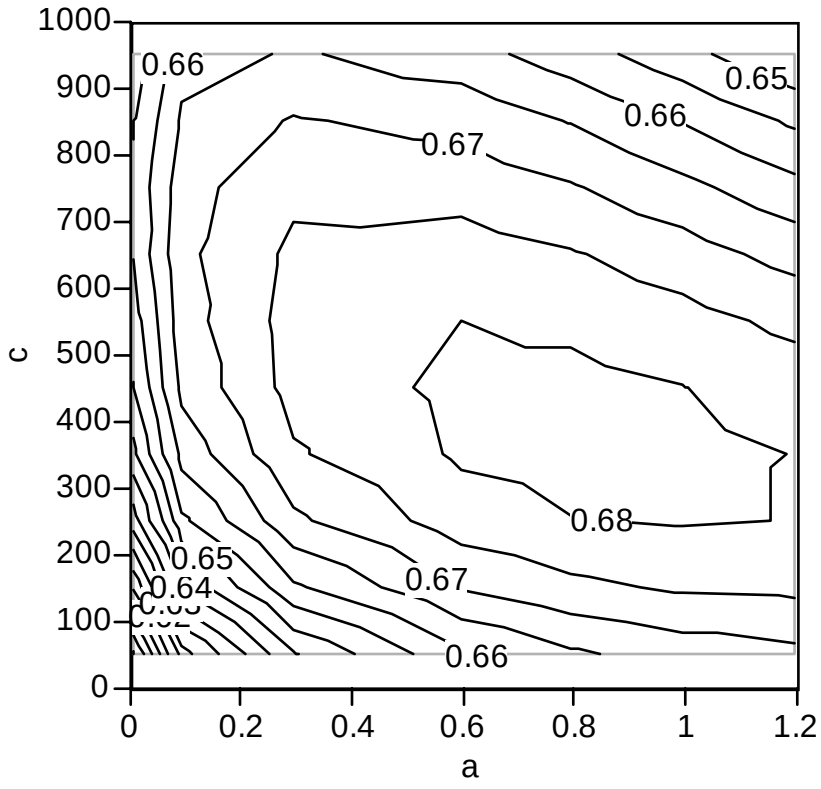

Figure 5.1.12 Contour plot of the annual solar fraction of the base system as a function of the parameters *a* and *c*. The load profile is represented by the standard RAND flow profile with a total daily water draw of 300 kg.

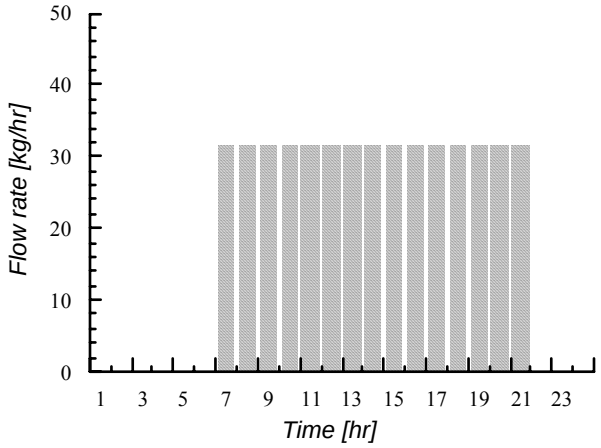

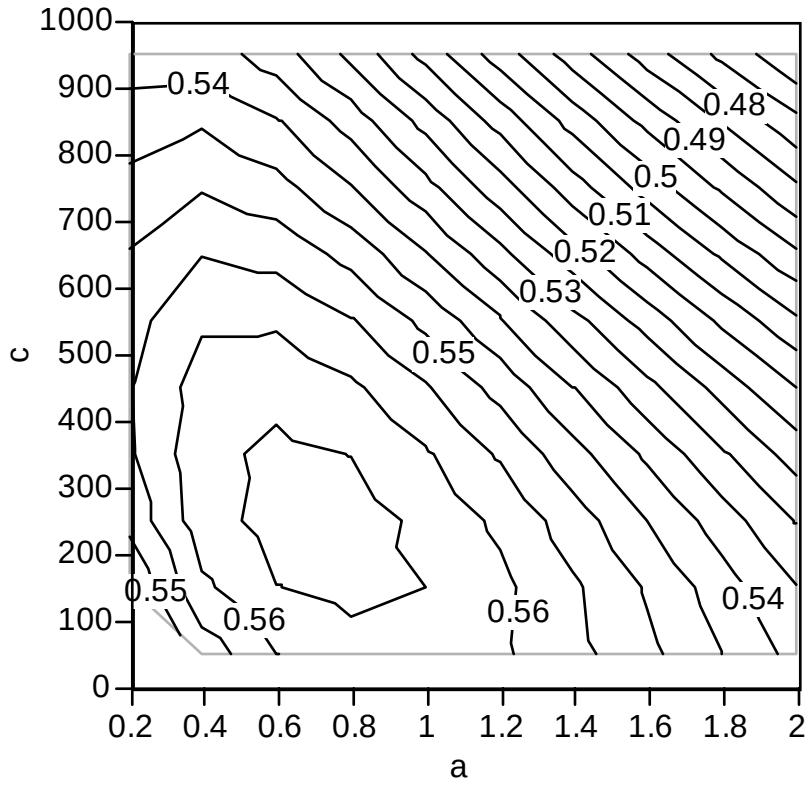

Figure 5.1.13 Contour plot of the annual solar fraction of the base system as a function of the parameters *a* and *c*. The load profile is defined as a square function with a daily integral value of 440 kg of water.

Furthermore, the investigation examined the effect of the time-lag between the load profile and the solar radiation profile. The search for the optimum parameters was repeated for five daily load profiles (Run # 2 through 6) that were obtained by translating the standard profile (Run # 1) in 2-hours increments. Results showed that the magnitude of the optimum annual solar fraction decreases as the mismatch increases but that such a decrease remains smaller than 4.3% of the standard optimum. Figures 5.1.14-19 depict the load profiles used in Run # 1 through 6 and the corresponding contour plots of the objective function.

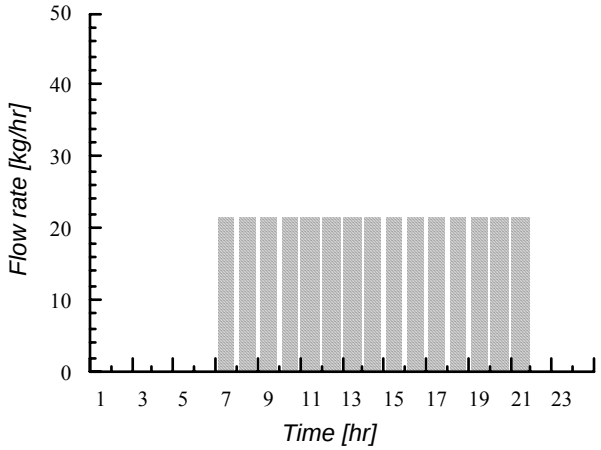

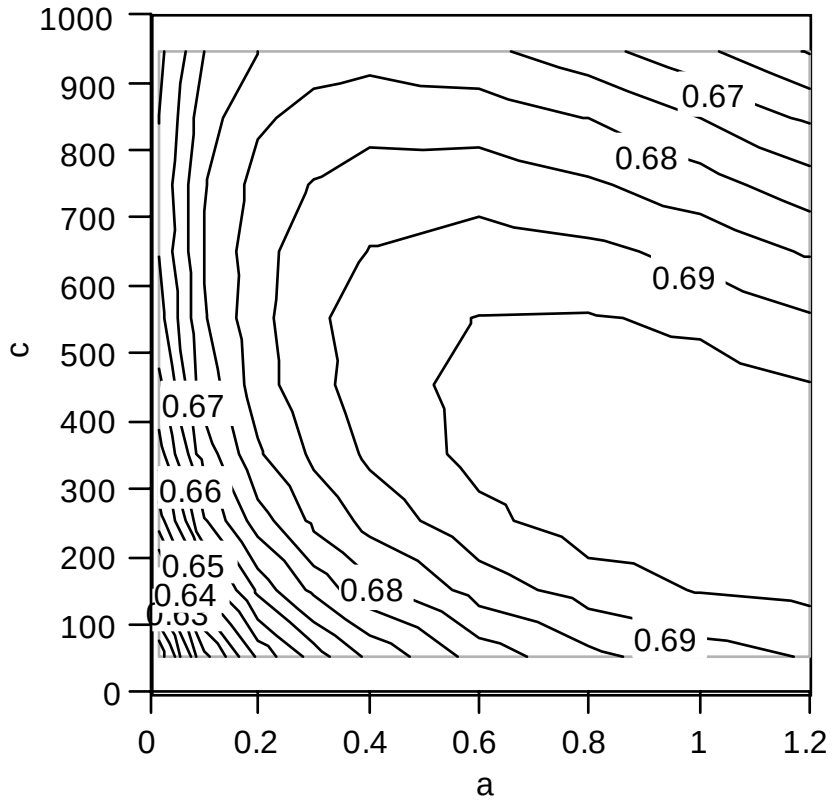

Figure 5.1.14 Contour plot of the annual solar fraction of the base system as a function of the parameters *a* and *c*. The standard system (Run # 1).

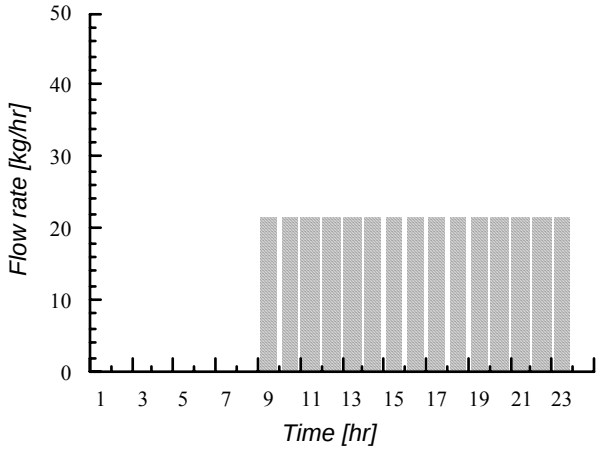

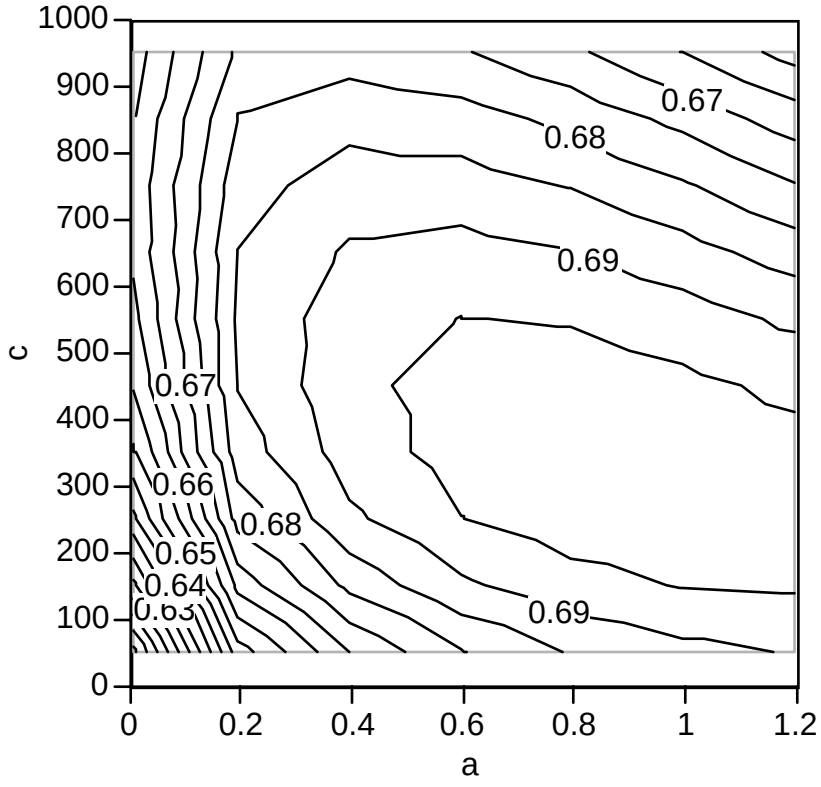

Figure 5.1.15 Contour plot of the annual solar fraction of the base system as a function of the parameters *a* and *c*. The load profile has a time-lag of 2 hours from the standard system (Run # 2).

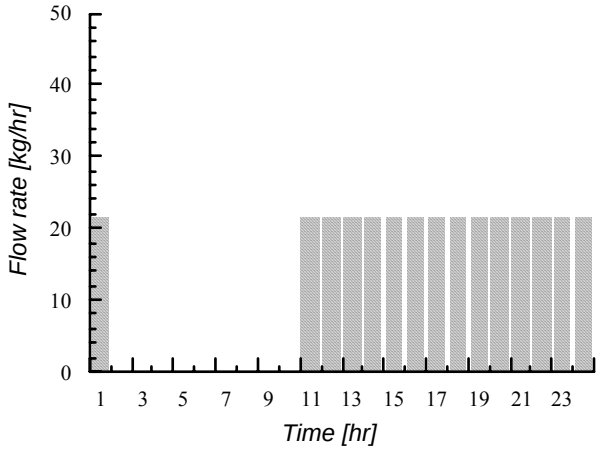

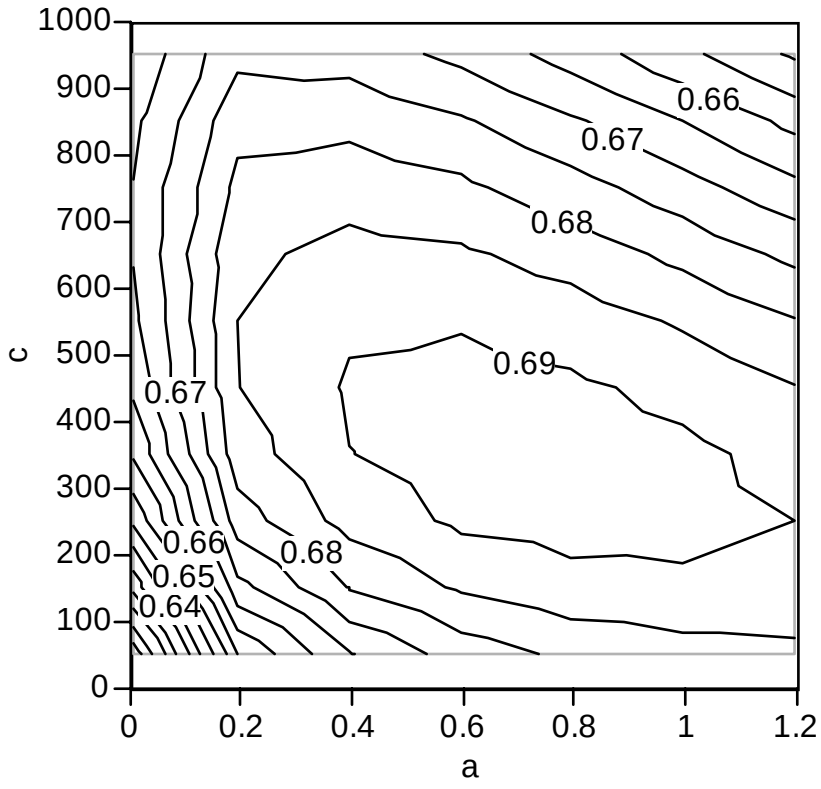

Figure 5.1.16 Contour plot of the annual solar fraction of the base system as a function of the parameters *a* and *c*. The load profile has a time-lag of 4 hours from the standard system (Run # 3).

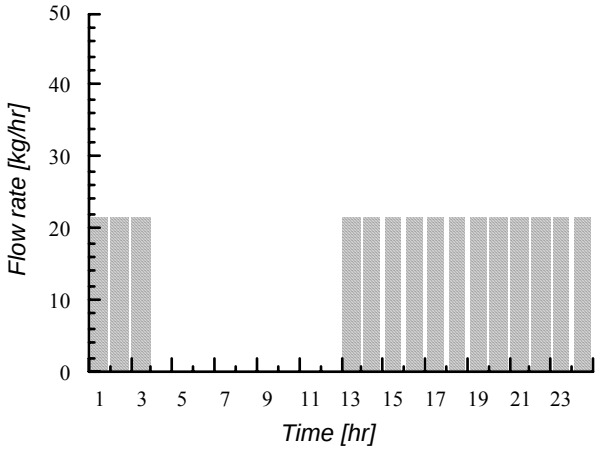

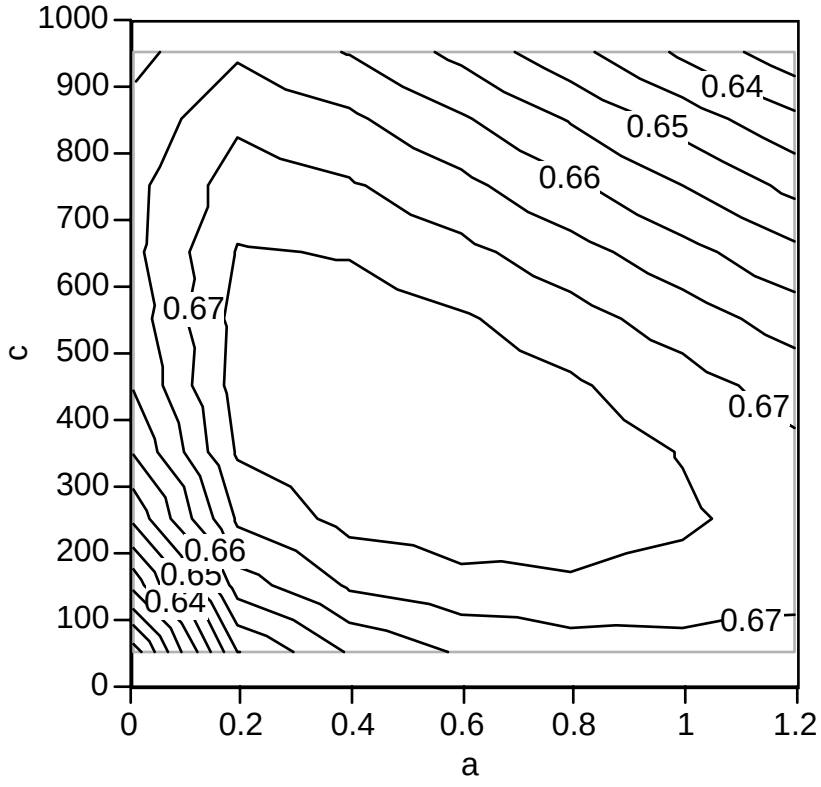

Figure 5.1.17 Contour plot of the annual solar fraction of the base system as a function of the parameters *a* and *c*. The load profile has a time-lag of 6 hours from the standard system (Run # 4).

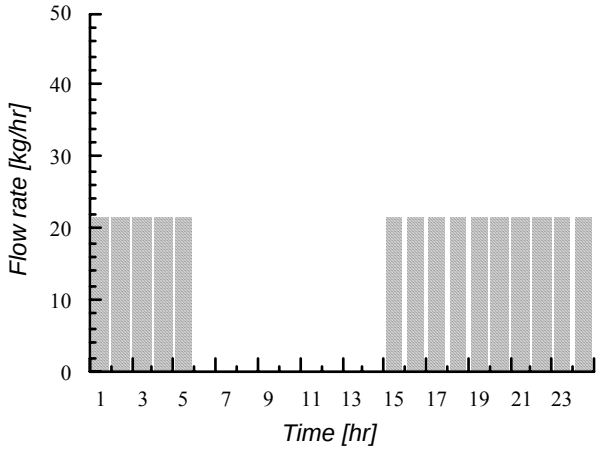

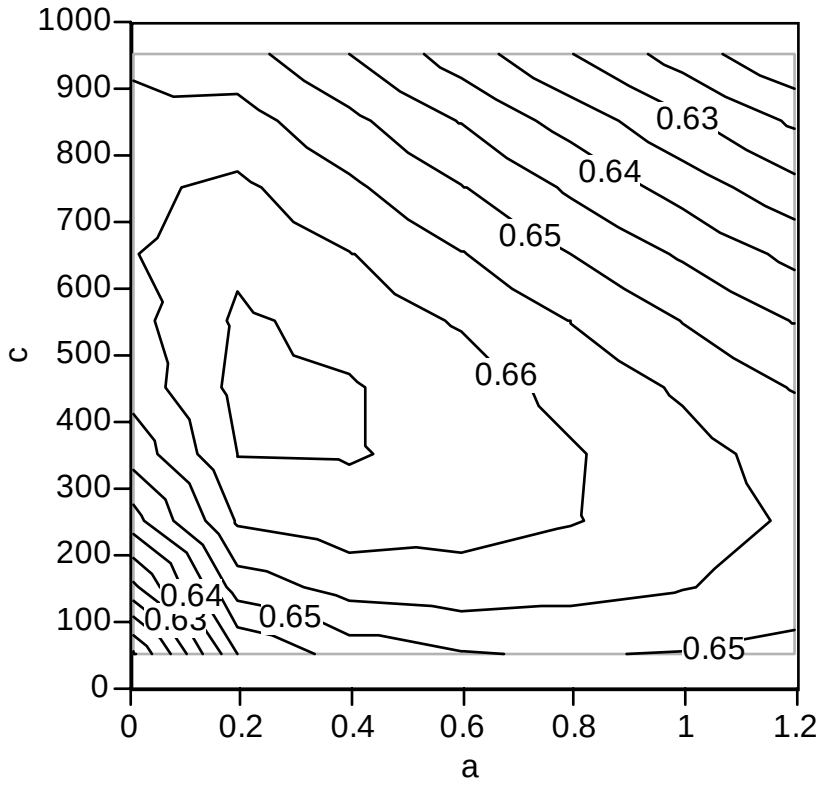

Figure 5.1.18 Contour plot of the annual solar fraction of the base system as a function of the parameters *a* and *c*. The load profile has a time-lag of 8 hours from the standard system (Run # 5).

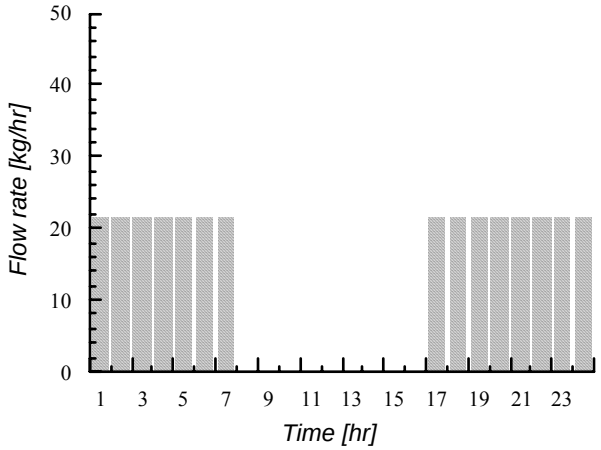

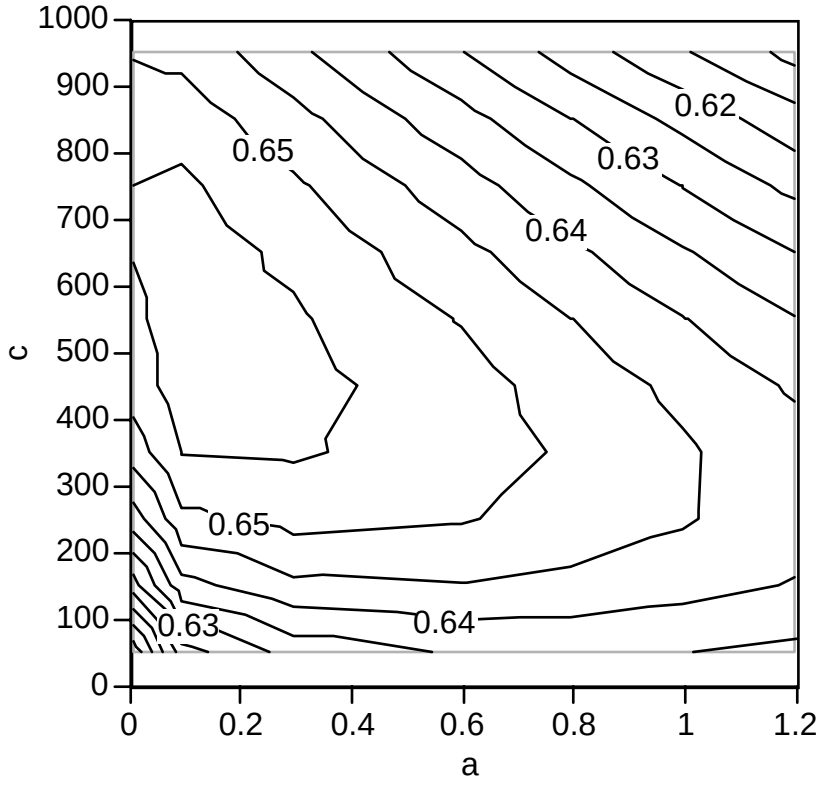

Figure 5.1.19 Contour plot of the annual solar fraction of the base system as a function of the parameters *a* and *c*. The load profile has a time-lag of 10 hours from the standard system (Run # 6).

5.1.2.2 Effect of the System Location on the Optimum Set

Three locations, other than the one used in the base system, were studied, the optimum parameter set computed and compared with the optimum parameters that resulted from the base system. The three locations (Seattle, WA; Albuquerque, NM; Washington, DC) were chosen to represent a wide variety of climates. In all three cases, the standard optimum set found for Madison, WI produced an annual solar fraction within 0.1% of the optimum annual solar fraction of the system at each of the three locations. Figures 5.1.20-23 present the annual solar fraction of the base system if located in Madison, WI; Seattle, WA; Albuquerque, NM; and Washington, DC; respectively.

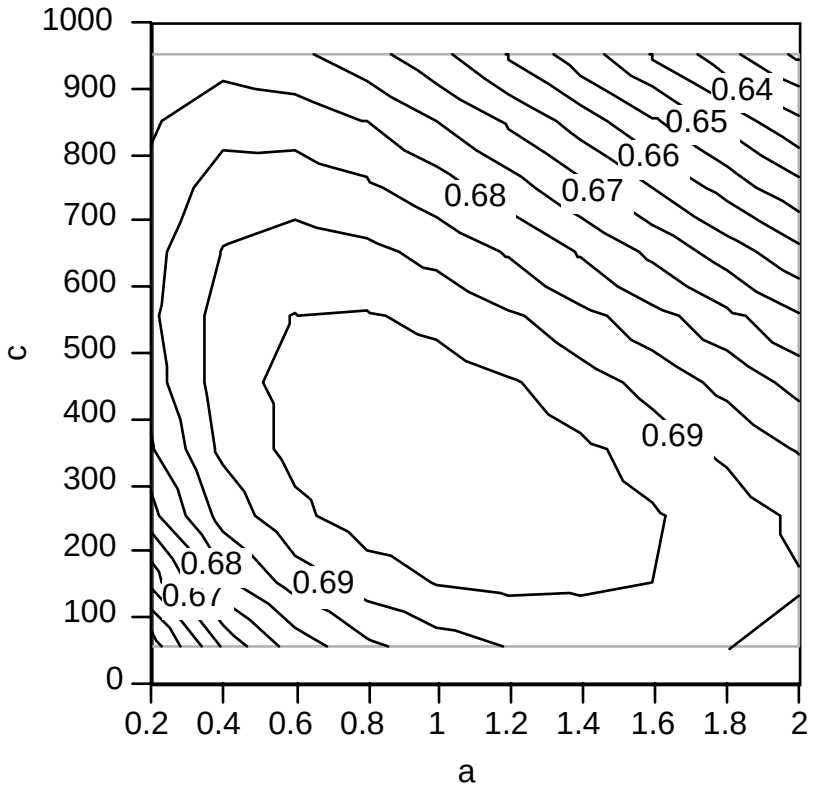

Figure 5.1.20 Contour plot of the annual solar fraction of the base system if located in Madison, WI.

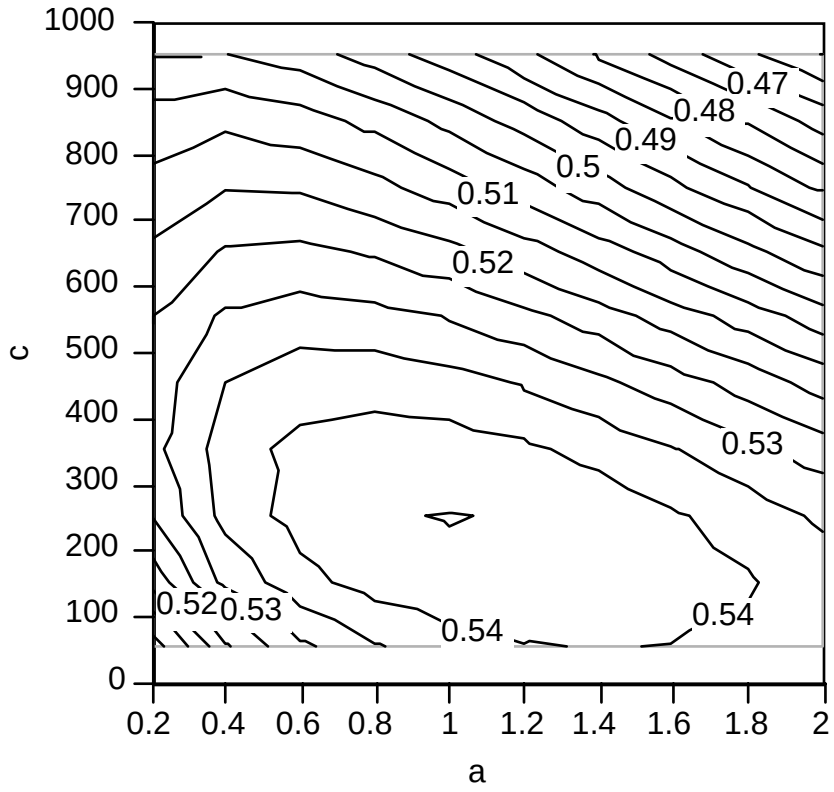

Figure 5.1.21 Contour plot of the annual solar fraction of the base system if located in Seattle, WA.

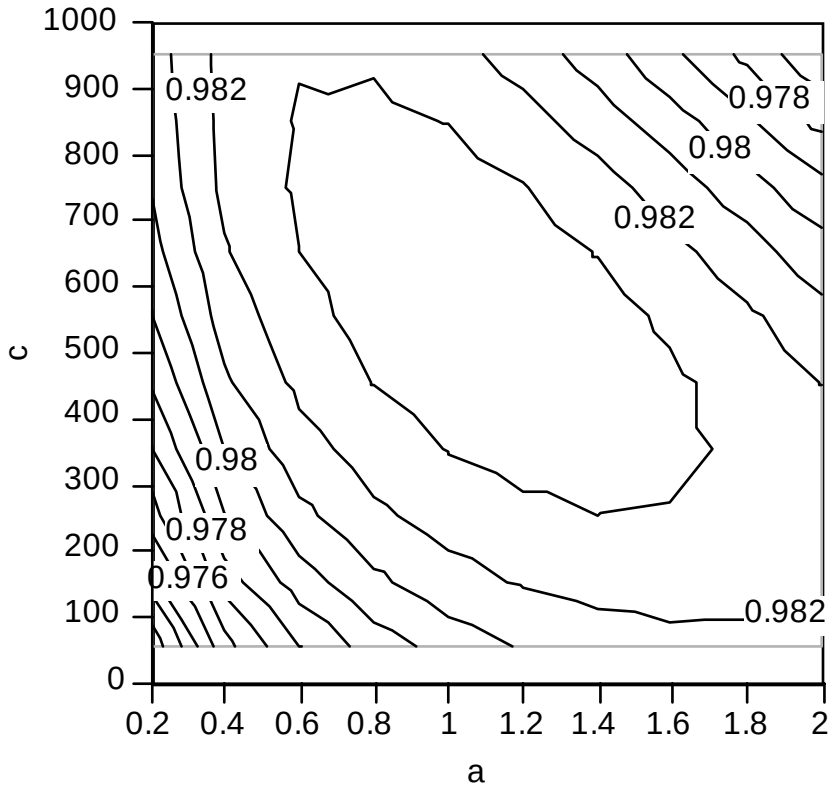

Figure 5.1.22 Contour plot of the annual solar fraction of the base system if located in Albuquerque, NM.

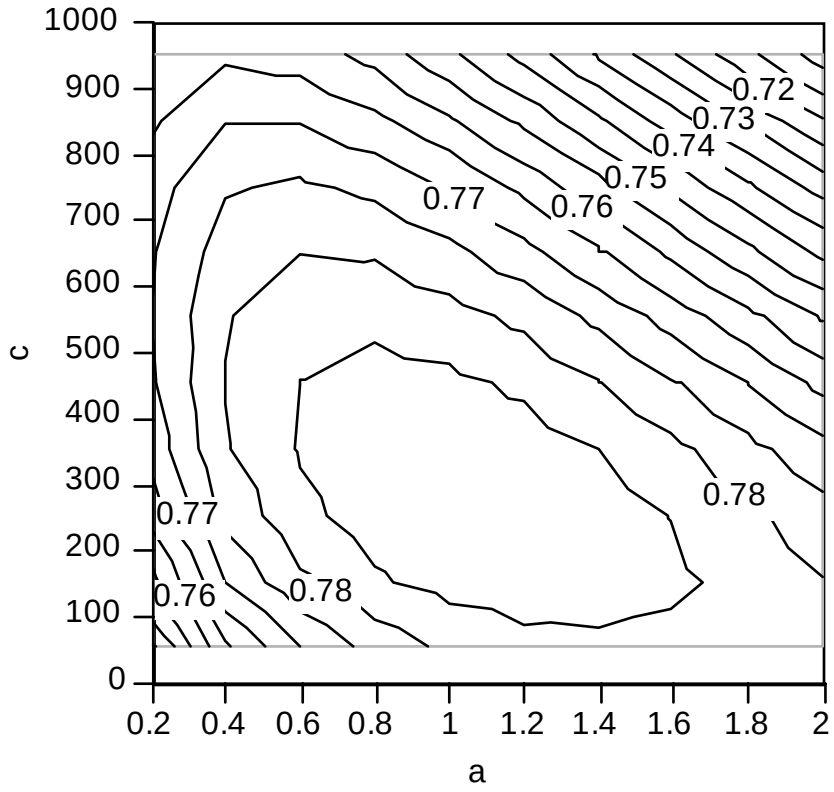

Figure 5.1.23 Contour plot of the annual solar fraction of the base system if located in Washington, DC.

In conclusion, the previous study shows that the optimum flow rate profile is practically independent of the load profile and the location. The optimum had no significant variation with respect to either the integral quantity, the load pattern or the load mismatch. It also showed no significant change with respect to location. This carries important consequences for the optimum design of PV-SDHW systems since it decreases significantly the variables that the designer has to take into account. Nevertheless, the insensitivity to location and load profile pattern is by no means an indication that F may be insensitive to the collector flow rate profile.

5.2 Phase Two

5.2.1 Base System

The following section presents a brief description of the base PV cell, the piping system and the centrifugal pump used in phase two. Detailed information about these components is presented in Appendix C.

The parameters of the base PV cell have been extracted from a PV module that has been tested by FSEC (ARCO M115). No catalogue data were available for this PV module. However, a reference *I-V* curve at a solar radiation of 895 W/m^2 and a cell temperature of 50.8 °C were reported. The PV module was assumed to have 40 cells connected in series. Accordingly, the parameters of the individual PV cell become: a short circuit current of 0.385 Amp, an open circuit voltage of 0.515 Volt, and is capable of delivering a maximum power of 0.143 W.

FSEC has created a standard SRCC[14] SDHW system *H-Q* curve with all of the required system components including nominal collector and heat exchanger pressure drops. Figure 5.2.1 shows the standard SRCC curve displayed within the operating range of the optimum flow rate found in phase one. The reference *Q* and *H* was chosen to be 1.3e-5 m^3/s and 0.051 m, respectively.

[14]SRCC stands for the Solar Rating & Certification Corporation.

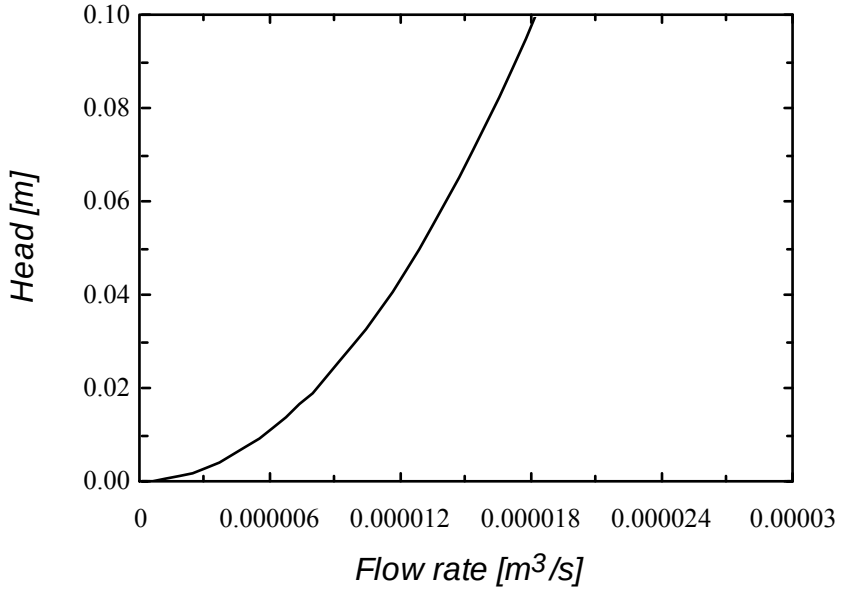

Figure 5.2.1 The standard SRCC *H*-*Q* curve.

The centrifugal pump has been selected such that the system operating flow rate is within the maximum pump efficiency. Unfortunately, no pump data were available that has a nominal operating flow rate of 1.4e-5 m^3/s (50 kg/hr). However, MARCH manufacturing, Inc. presented in their catalogue several small motor-pump units that have nominal flow rates of 1.e-4 to 1.5e-4 m^3/s (360 to 540 kg/hr). Their combined motor-pump efficiencies ranged from 5 to 10%. Accordingly, a data for a small flow rate pump was created. The pump has a maximum pump efficiency of 5% if operated at the reference flow rate of 1.3e-5 m^3/s and the reference head of 0.051 m. Figure 5.2.2 presents the characteristic relations of the centrifugal pump used in phase two.

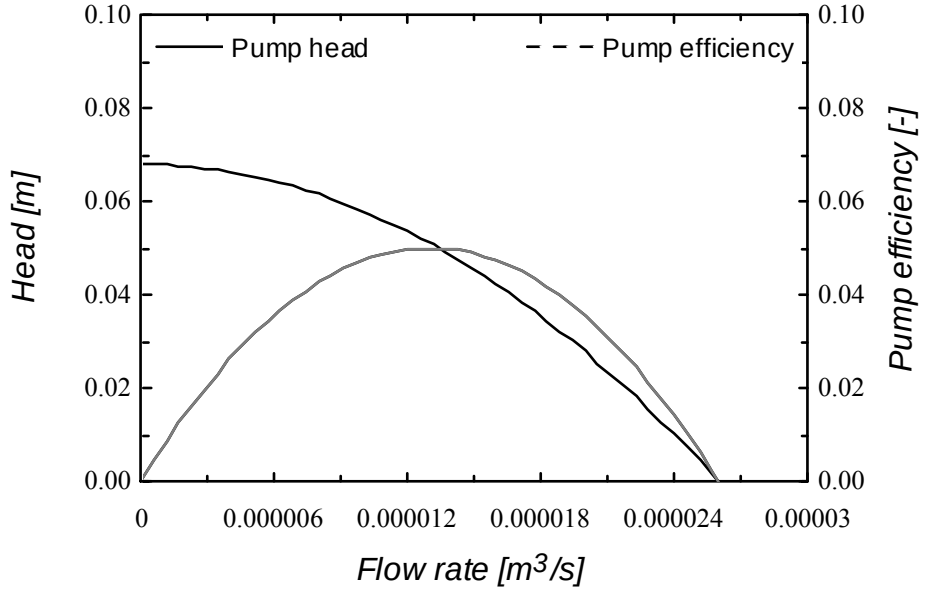

Figure 5.2.2 The *H*-*Q* and the $\tilde{Q}$ of the centrifugal pump used in phase two.

5.2.2 Results The PV pumping model presented in chapter 3 was used to simulate a PV pumping system that uses the described base PV cell, a DC-motor and the described centrifugal pump installed in the SRCC standard system. The number of PV cells in parallel, *P*, and in series, *S*, the DC-motor type, *Type*, and the DC-motor coefficient, *C*, and resistance, *R*, have been varied such that resultant PV pumping system's flow rate profile is closest to the optimum flow rate profile found in phase one (i.e., minimum ϕ).

For clarity, *Type* = 1 refers to the series excited DC-motor and *Type* = 2 refers to either the permanent magnet or the separately excited DC-motors. If *Type* = 1 then the parameter *C* refers to the mutual inductance of the series excited DC-motor, M_{af},

and the parameter *R* refers to the sum of the armature resistance and the field resistance, R_{a+f}. If *Type* = 2 then the parameter *C* refers to the torque coefficient (C_e for the permanent magnet DC-motor and k_f for the separately excited DC-motor) and the parameter *R* refers to the armature resistance, R_a.

The search for the optimum parameter set (*Type*, *P*, *S*, *C*, *R*)^{opt} has been performed in two steps. First, for a given value of the integer parameters *Type*, *P* and *S*, a grid is constructed containing 100 nodes of *C* and *R*. The space of *C* was chosen such that either of its extreme values reflects a poor system (no flow rate at any solar radiation level). *R* was varied from 0.01 to 0.9. *Type* was assigned the values of 1 or 2 and *P* and *S* were assigned the values of 1, 2 or 3. A total of 18 combination of *Type*, *P* and *S* were evaluated. The goal of the first step is to identify the optimum values of *Type*, *P* and *S* that yields the minimum objective function, ϕ. Later a finer grid is constructed containing 100 nodes of *C* and *R* in the neighborhood of the optimum value of *C* and *R* found in the first step. The goal of the second step is to identify the optimum values of *C* and *R* that yields the minimum ϕ.

The Results of the First Step

Table 5.2.1 presents the results of the first step for *Type* = 1 and Table 5.2.2 presents the results of the first step for *Type* = 2. The results shows that a minimum value of ϕ can be attained using *Type* = 2, *P* = 1 and *S* = 3. Moreover, for *Type* = 2 and *P* = 1, the difference between ϕ for *S* = 2 and *S* = 3 is insignificant ($\Delta\phi$ = 0.08). If *S* was increased to 4, then the difference in ϕ would even reduces to an even smaller values

($\Delta\phi$ = 0.001). Therefore, the optimum value of *S* can be selected as 2 with no loss in the closeness of the resultant flow rate profile to the optimum flow rate profile.

The conclusion of the first step is that a close match to the optimum flow rate profile found in phase one can be attained using a PV pumping system employing two PV cells connected in series and an either of a permanent magnet DC-motor or a separately excited DC-motor.

Table 5.2.1 Summary of the results of the first step in phase two. *Type* = 1.

P	*S*	ϕ_{min}	*C**	*R**
1	1	14195	0.012	0.01
1	2	10774	0.018	0.1
1	3	12307	0.018	0.9
2	1	5698	0.004	0.9
2	2	5578	0.004	0.9
2	3	8170	0.004	0.9
3	1	4214	0.002	0.9
3	2	4365	0.002	0.9
3	3	8184	0.002	0.9

Table 5.2.2 Summary of the results of the first step in phase two. *Type* = 2.

P	*S*	ϕ_{min}	*C**	*R**
1	1	1963	0.00275	0.01
1	2	189.1	0.00350	0.01
1	3	189.0	0.00350	0.01
2	1	801.3	0.00200	0.3
2	2	915.6	0.00200	0.9
2	3	1125	0.00200	0.9
3	1	488.1	0.00125	0.01
3	2	467.4	0.00125	0.9
3	3	481.0	0.00125	0.9

The Results of the Second Step

For *Type* = 2, *P* = 1 and *S* = 2, a very fine grid of *C* and *R*, containing 100 nodes, was constructed centering around their optimum values found in the first step, and the objective function, ϕ, computed. The minimum value of ϕ (ϕ = 173.43) was achieved at *C* = 0.00345 and *R* = 0.01. Figure 5.2.3 depicts the objective function ϕ as a function of *C* and *R*. Within the neighborhood of the optimum region, ϕ was found to be significantly dependent on the value of *C* and is not sensitive to the value of *R*. This does not rule out the role of *R* on ϕ. A closer look at ϕ as a function of *R*, for the optimum *C*, shows that ϕ increases exponentially as *R* increases. As *R* increased from 0.01 to 0.9, ϕ increased by 31%. Figure 5.2.4 shows the effect of *R* on ϕ for the optimum value of *C* (= 0.00345).

The flow of energy within the components of this optimum PV pumping system can be seen by examining the input-output energy of each component at a reference operating condition. When *G* is 1000 W/m^2 and T_c is 25 °C, the energy delivered to the PV cells[15] is 3.5 W, the energy generated from the PV cells is 0.232 W, the output energy from the DC-motor is 0.222 W and the output energy from the pump is 0.011 W. This reflects a PV cell efficiency of 6.6%, a DC-motor efficiency of 95% and a pump efficiency of 4.95%. The PV cell efficiency is slightly less than the maximum

[15]Exact PV cell area is not available. However, an area of a PV module similar to the one used, manufactured by a sister company (SIEMENS M10), was used to find a reasonable estimate of the area. By no mean, the value of the area affects the accuracy of the current optimality analysis as the PV model does not require the area to compute *I* and *V*. The model uses the area to compute the operating efficiency, only, which is not monitored in the current optimality analysis.

PV cell efficiency (= 8.1%) at this value of G and T_C. The high DC-motor efficiency reflects the proper selection of the DC-motor's parameters C and R.

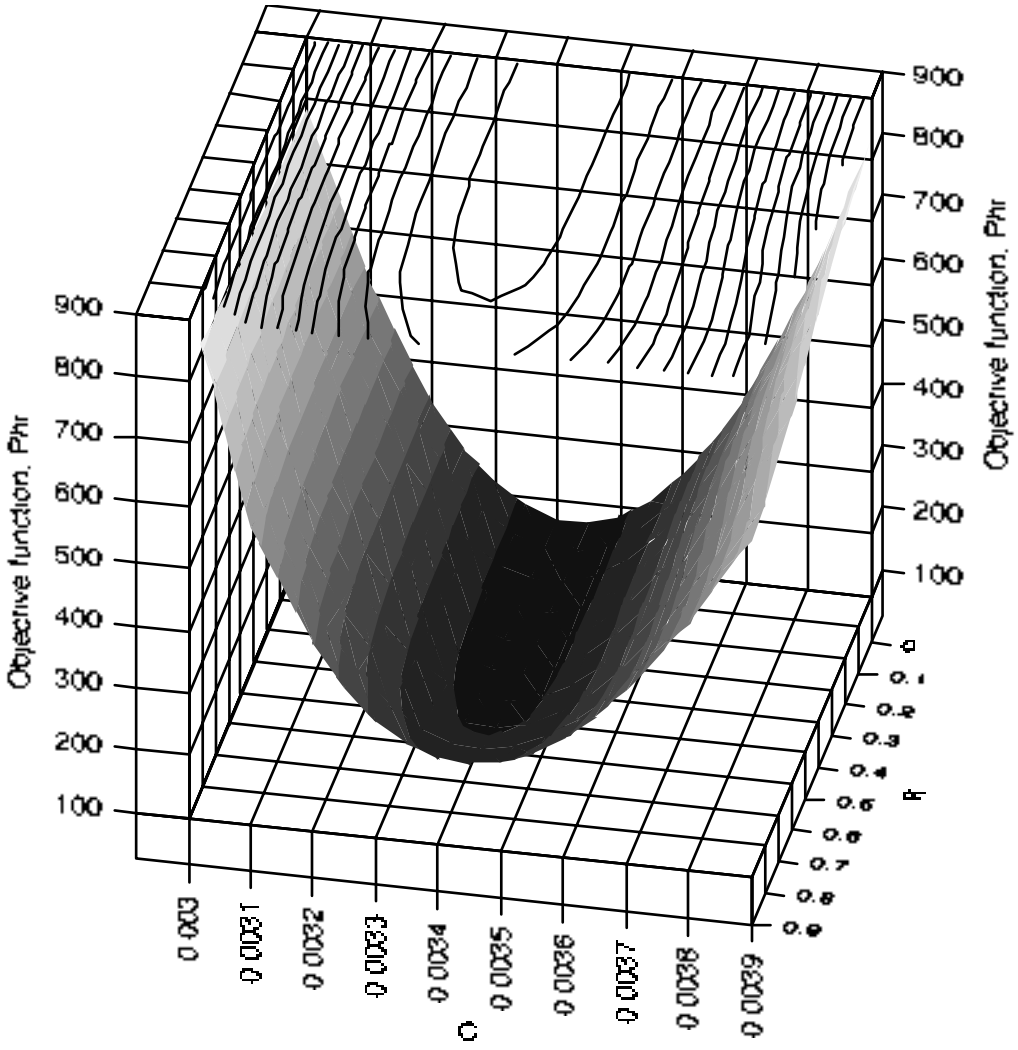

Figure 5.2.3 The objective function in phase two, ϕ, as a function of C and R. *Type* = 2, P = 1 and S = 2.ϕ

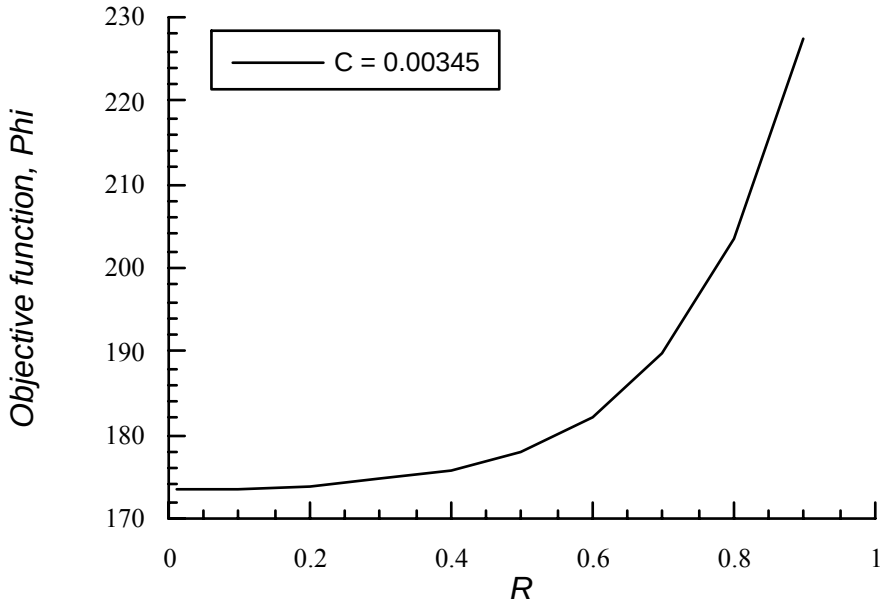

Figure 5.2.4 The objective function in phase two, ϕ, as a function of R. C = 0.00345, *Type* = 2, P = 1 and S = 2.ϕ

To further investigate the gain in increasing the number of PV cells in series from 2 to 3, the previous analysis of step two was repeated using S = 3. The reduction in ϕ was less than 0.16% and the increase in the generated torque at the optimum set was less than 0.07% when compared to the S = 2 case. Figure 5.2.5 depicts the objective function ϕ as a function of C and R for the case of S = 3. The effect of R on ϕ was found to reduce as S increased from 2 to 3. The exponential increase in ϕ as a function of R has been also observed; however, ϕ increased by 0.1% as R increased from 0.01 to 0.9. Figure 5.2.6 shows the effect of R on ϕ for the optimum value of C = 0.00345 and S = 3.

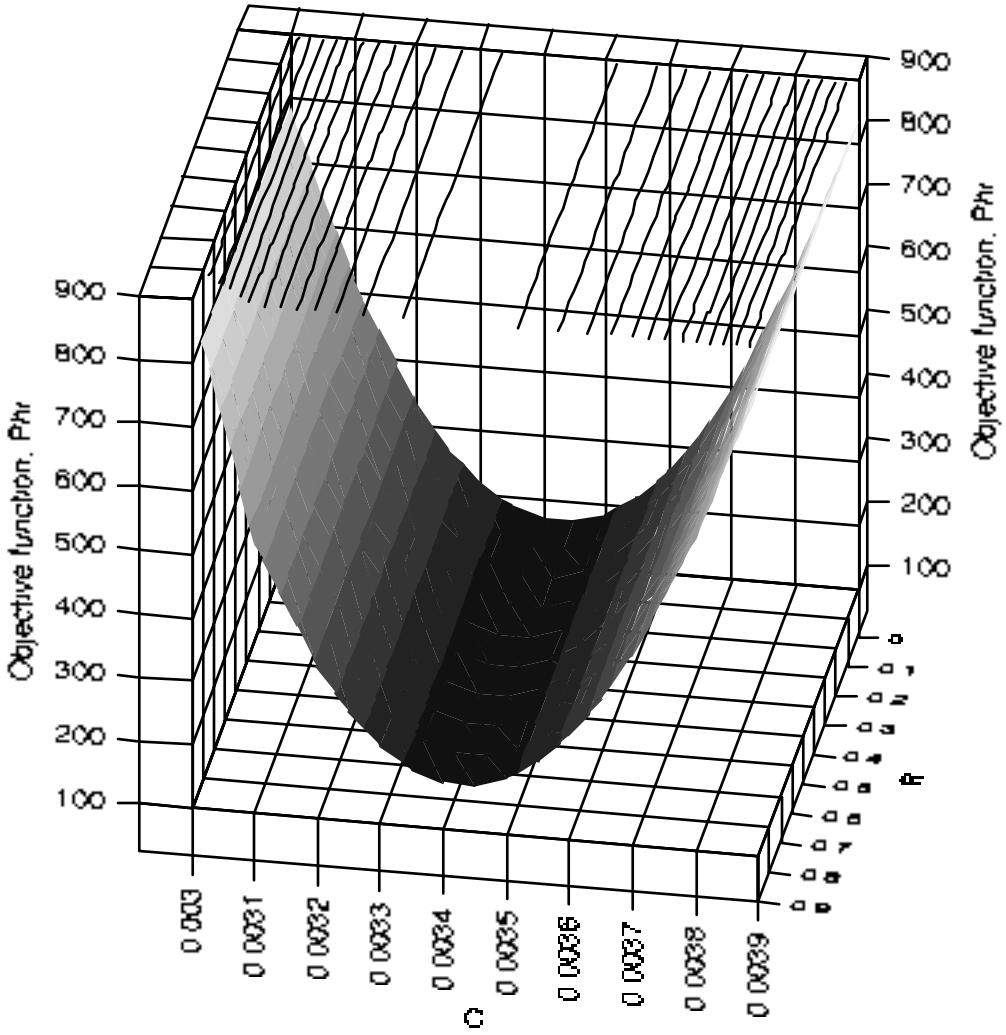

Figure 5.2.5 The objective function in phase two, ϕ, as a function of C and R. *Type* = 2, $P = 1$ and $S = 3$.ϕ

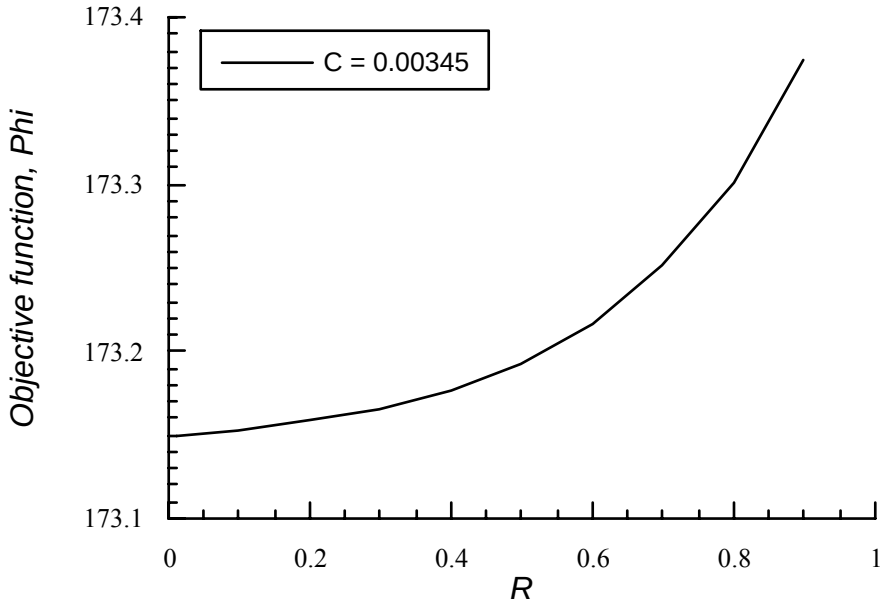

Figure 5.2.6 The objective function in phase two, ϕ, as a function of R. C = 0.00345, *Type* = 2, P = 1 and S = 3.ϕ

Figure 5.2.7 shows the flow rate profile produced by the proposed optimum PV pumping system compared to the optimum flow rate profile found in phase one. Figure 5.2.7 also shows the flow rate profile when the optimum PV pumping system has 3 PV cells in series instead of 2. The optimum PV pumping system exhibit a delay in the DC-motor starting. The DC-motor starts[16] when G exceeds 100 W/m^2 and it

[16]The minimum requirement for the FSEC PV pumping system approval protocol requires that the DC-motor-pump start pumping by the time G reaches 350 W/m^2.

exhibits torque losses constants, C_{stat1} and C_{stat2} of 1.18e-4 N-m and 5.90e-5 N-m, respectively. The generated torque, T, at G of 1000 W/m^2 is 1.19e-3 N-m.

In conclusion, a very close match to the optimum flow rate profile found in phase one can be attained using a PV pumping system employing two PV cells connected in series and either a separately excited DC-motor or a permanent magnet DC-motor having C = 0.00345 N-m/Amp and R = 0.01 □.

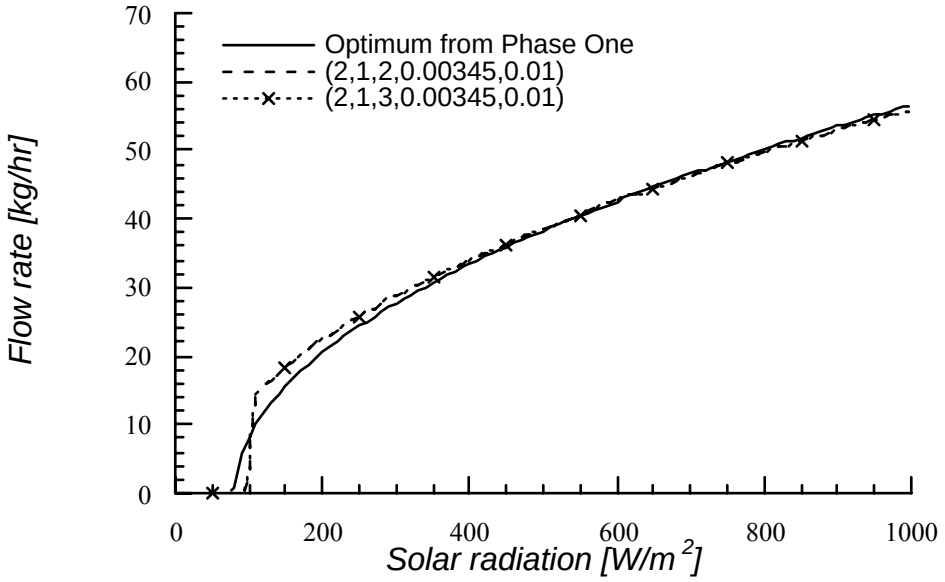

Figure 5.2.7 The flow rate profile generated from the proposed optimum PV pumping system using S = 2 and 3 compared to the optimum flow rate profile found in phase one.

The reason for the very small gain in the power of the PV pumping system as *S* increases from 2 to 3 or higher can be explained as follows. The output of a PV pumping system at a given *G* is determined by the operating current, *I*, and voltage, *V*. The operating *I* and *V* is determined by superimposing the *I*-*V* curve of the PV cells and the *I*-*V* curve of the attached load (DC-motor and pump in the present case). The operating *I* and *V* is the point at which the two curves match. Figure 5.2.8 shows three *I*-*V* curves of three PV cells (for *S* = 1, 2 and 3), calculated at *G* of 800 W/m^2, along with the *I*-*V* curve of the attached DC-motor-pump load. The parameters of the system components are identical to those of the proposed optimum PV pumping system. For these PV cells and the attached DC-motor-pump load, as *S* increases from 1 to 2, *I* increases as well as *V*. However, as *S* increases from 2 to 3 or higher, the increase in *I* or *V* diminishes. Similarly, the power output of the PV cells increases as *S* increases from 1 to 2. As *S* increases from 2 to 3 or higher, the power output remains nearly constant. At lower radiation levels, the increase in *I* or *V* as *S* increases from 2 to 3 is even smaller. The asymptotic value of *S* varies from one system to another, and depends upon the *I*-*V* curves of the PV cells and the attached load. Similar discussion can be drawn for the case of increasing the number of modules in parallel, *P*, as well. The issue of the optimum size of *P* and *S* is an essential topic as proper matching of PV system components may be achieved using the proper combination of *P* and *S*.

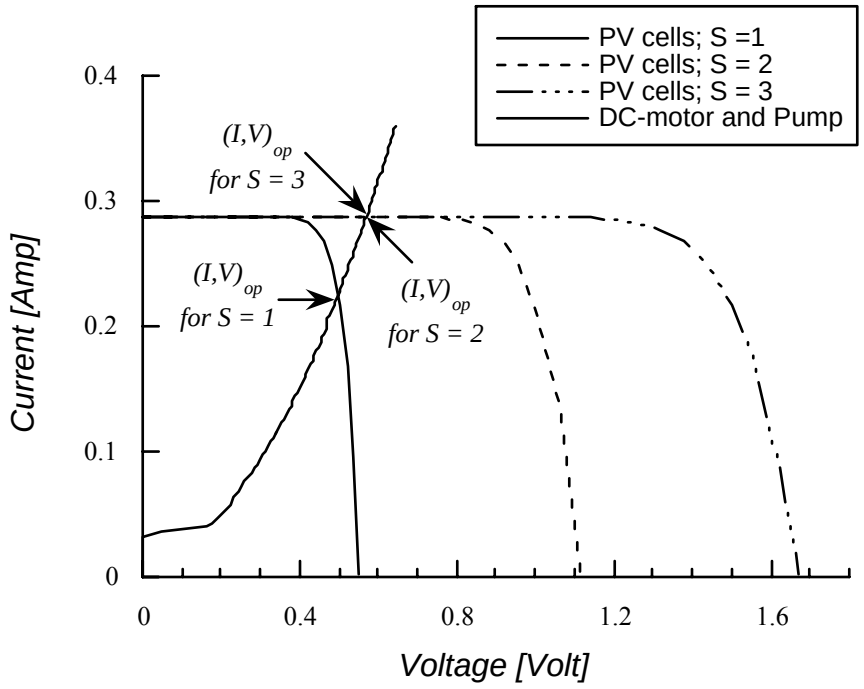

Figure 5.2.8 Three *I-V* curves of three PV cells (for *S* = 1, 2 and 3) and the *I-V* curve of the attached DC-motor-pump load.

Figure 5.2.9 shows the flow rates of two off-optimum PV pumping system compared to the optimum flow rate found in phase one. The system employing series excited DC-motor (*Type* = 1) exhibit a larger delay in pump starting than the other system. Figure 5.2.10 shows the *I-V* curve of the two off-optimum PV pumping system shown in Figure 5.2.9 compared to the *I-V* curve of the proposed optimum PV pumping system.

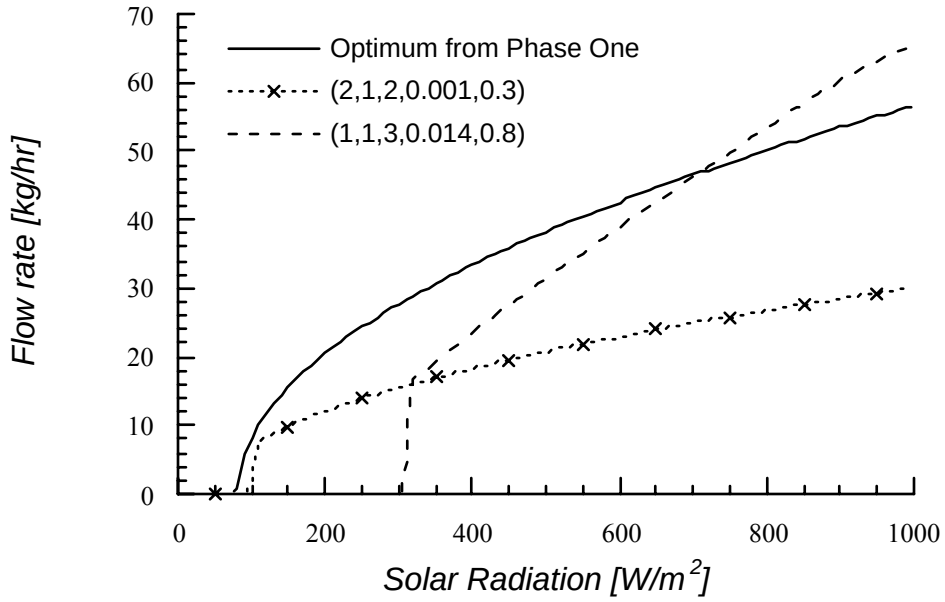

Figure 5.2.9 The flow rate profile of two off-optimum PV pumping system compared to the optimum flow rate profile found in phase one.

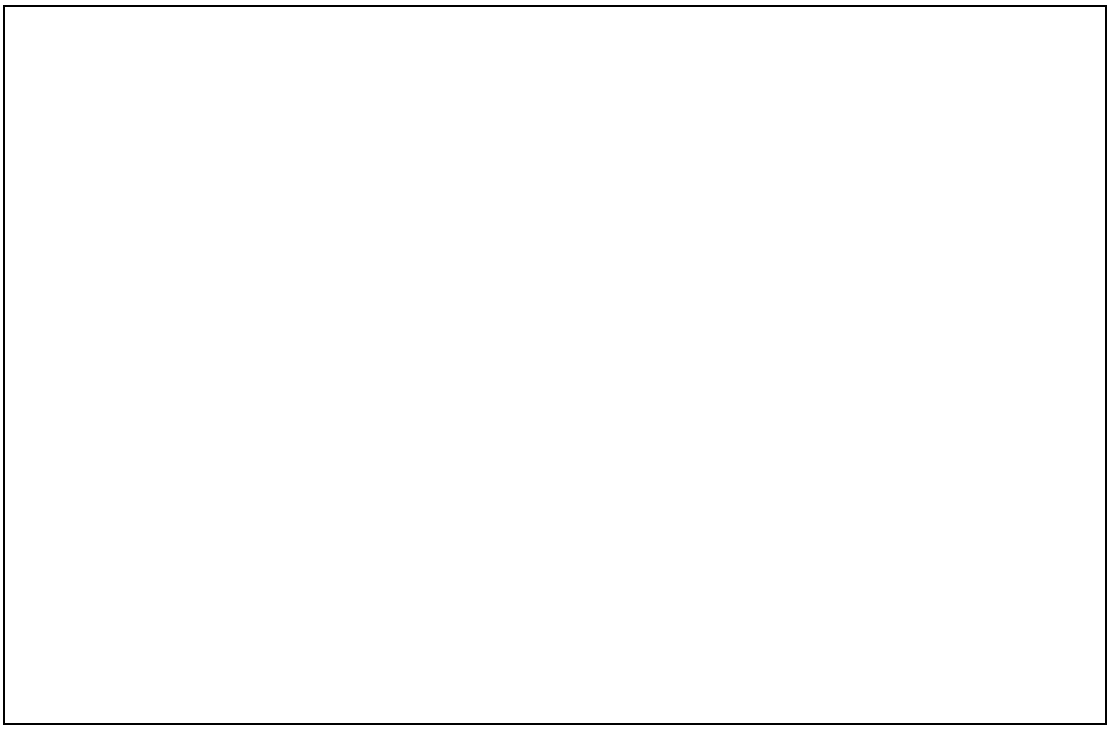

Figure 5.2.10 The *I-V* curves of two off-optimum PV pumping system compared to the *I-V* curve of the proposed optimum PV pumping system.

The concept of the "window" of possible flow rate profiles that produce an annual solar fraction of at least 0.69, which was presented in the previous section, has been related there to the flow rate profile parameters *a* and *c*. In the context of PV-SDHW systems, given the optimum value of *Type*, *P* and *S* (2,1,2), the "window" can be directly related to the DC-motor physical parameters *C* and *R*. The PV pumping model was combined with the SDHW model to simulate a PV-SDHW system. A grid containing 100 nodes in the space of *C* and *R* is constructed. A series of annual simulation of PV-SDHW system were performed and the annual solar fraction computed. Figure 5.2.11 depicts the annual solar fraction of the PV-SDHW system as

a function of *C* and *R*. Similar to the case of the objective function in phase two, ϕ, the annual solar fraction was found to be highly influenced by the value of *C* and is not sensitive to the value of *R*. It appears also that value of *C* for the optimum PV SDHW system is allowed to range from 0.002 to 0.005 and the values of *R* is allowed to range in a wide interval from as low as 0.01 to as high as 1.4 □ or more. This range of *C* and *R* will yields an annual solar fraction of at least 0.69.

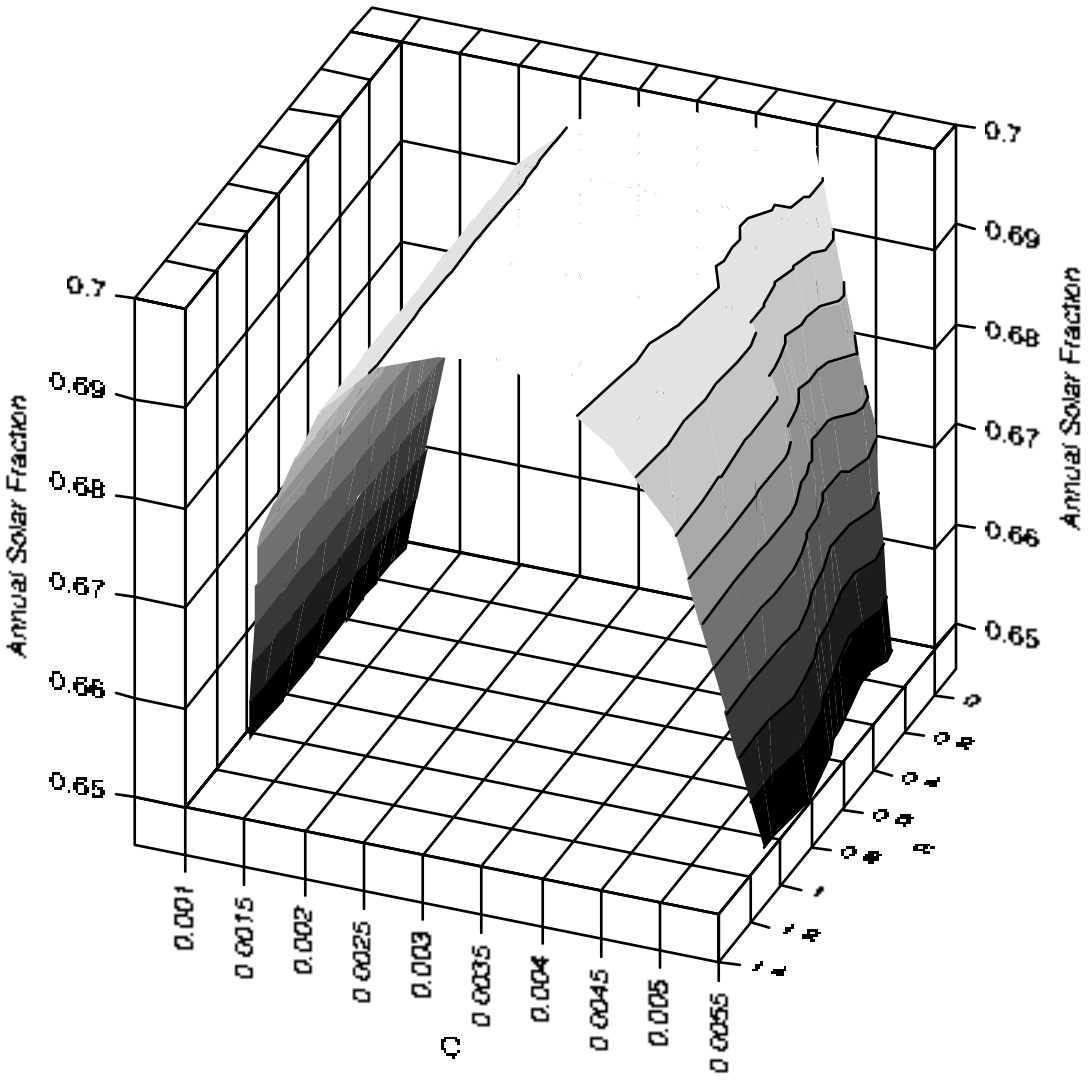

Figure 5.2.11 The annual solar fraction of a PV-SDHW system as a function of *C* and *R*. *Type* = 2, *P* = 1 and *S* = 2.

The optimum direct PV-SDHW system was compared to three SDHW systems that share identical SDHW components to the one of the optimum PV-SDHW system, however, the three systems vary in their flow control strategy; (i) an ON/OFF flow operating at the manufacturer recommended constant flow rate, (ii) an ON/OFF flow operating at the constant optimum flow rate, and (iii) a flow rate proportional to the solar radiation operating under the optimum proportionality. The optimum PV-SDHW system was ranked first, followed by the system with the optimum proportionality, then the system with the constant optimum flow rate, and lastly, the system with the manufacturer recommended constant flow rate. Figure 5.2.12 shows the results of this comparative analysis.

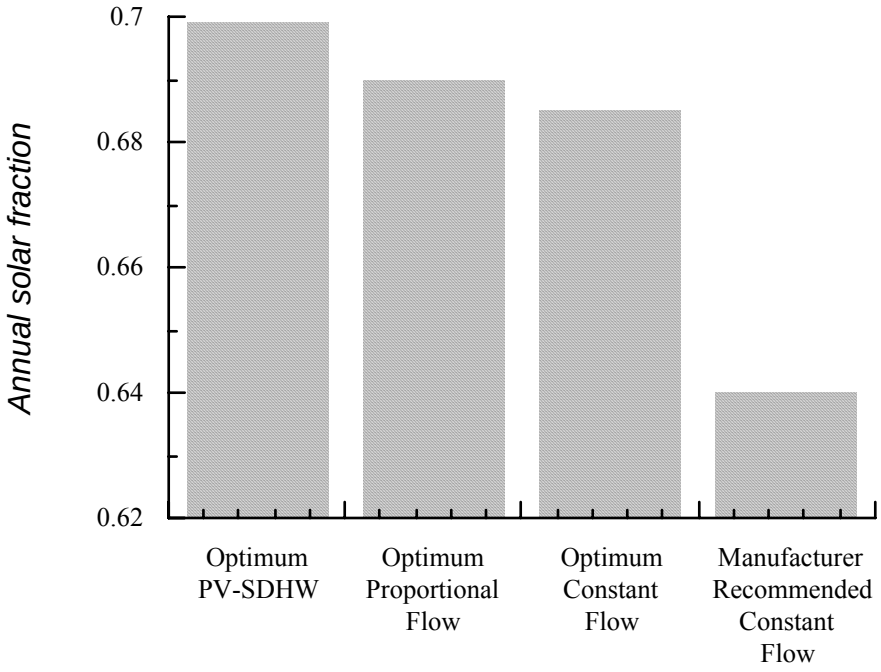

Figure 5.2.12 The annual solar fraction of the optimum direct PV-SDHW system compared to three SDHW systems operating under different control strategies.

Chapter 6 Indirect PV-SDHW Systems

This chapter presents the results of the analysis of selecting the optimum PV pumping systems in indirect SDHW systems (indirect PV-SDHW systems). It comprises two main sections. The first section presents the results of phase one and phase two optimizations applied to indirect PV-SDHW systems employing forced convection heat exchangers (FCHE). The second section presents the results of phase one and phase two optimizations applied to indirect PV-SDHW systems employing natural convection heat exchangers (NCHE). Each section includes information about its base system and relative parameteric analysis.

6.1 PV-SDHW with FCHE

6.1.1 Phase One

6.1.1.1 Base System

The base system chosen for this analysis is identical to the one used in the direct SDHW system analysis except that a forced convection heat exchanger was inserted between the collector and the storage tank. The effectiveness of the heat exchanger employed ranged from 0.2 at a collector flow rate of 600 kg/hr to 0.6 at a collector flow rate of 100 kg/hr. At a later stage, a heat exchanger with a larger effectiveness was used and the optimum computed. The tank side flow rate were controlled such that the flow is ON if the collector outlet temperature exceeds the tank bottom

temperature and OFF otherwise. Figure 6.1.1 illustrates a schematic drawing of the base system used in phase one.

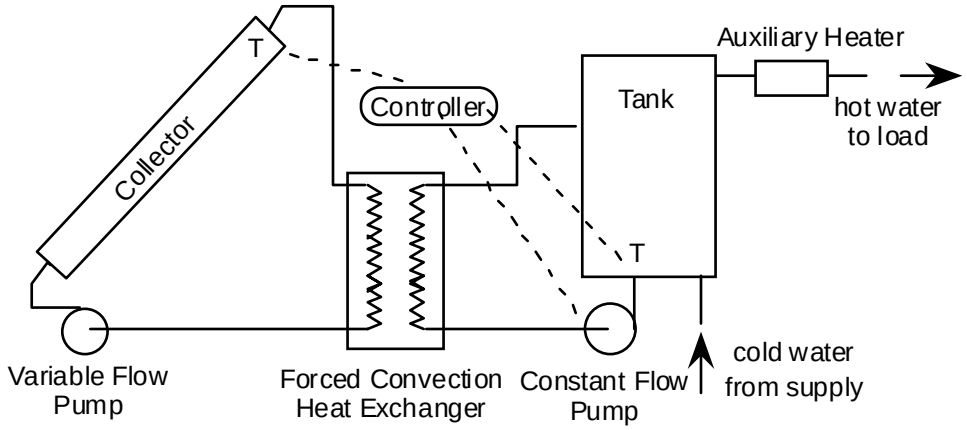

Figure 6.1.1 Schematic drawing of the base system used in phase one.

In order to execute phase one of the optimization, a preliminary analysis, aimed at determining the value of the forced flow of the tank loop side that leads to the maximum annual solar fraction, was initially undertaken. In phase one of the optimization, the value of the forced flow in the tank loop side was assumed to remain constant, while the flow in the collector loop side was allowed to vary within the family of curves determined by Equation 4.3.1.

In order to determine a reasonable value for the constant flow rate of the tank loop side, an optimization was conducted assuming that the flow in the collector side was also constant. The collector side flow rate, $Q_{collector}$, and the tank side flow rate Q_{tank}, were varied and the annual solar fraction, $\mathcal{F}$, computed. The flow rates on both

sides were controlled to be ON if the collector outlet temperature exceeds the tank bottom temperature and OFF otherwise. Figure 6.1.2 depicts the contour plots of the objective function $\mathcal{F}(Q_{collector},Q_{tank})$. The optimum $\mathcal{F}$ was obtained for Q_{tank} between 400 and 600 kg/hr regardless of the value of $Q_{collector}$ if chosen to be higher than 300 kg/hr. Consequently, the flow of the tank loop side was fixed to be constant at 500 kg/hr.

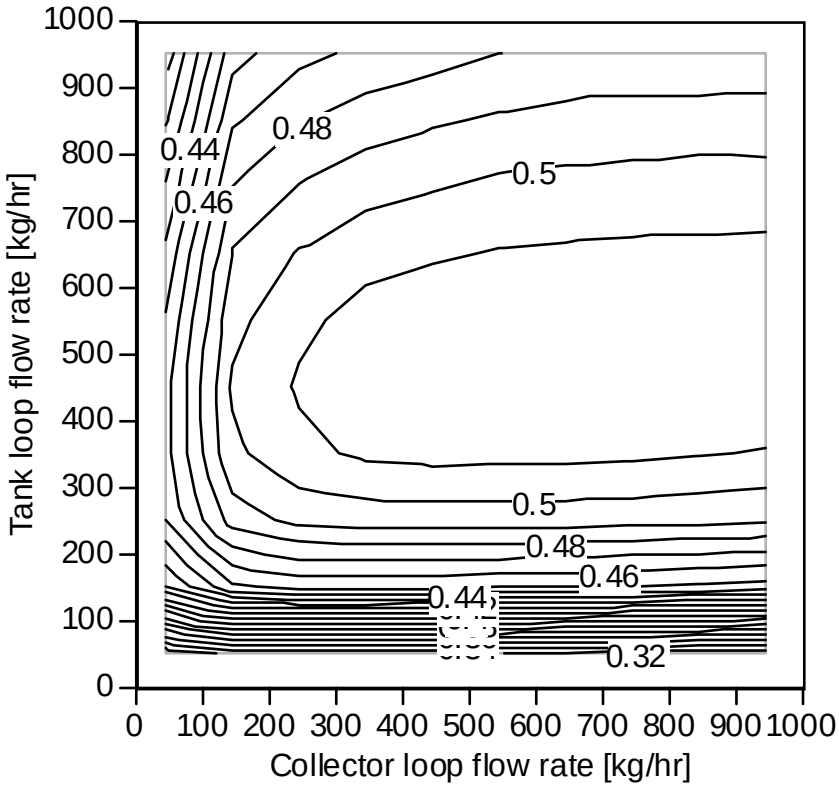

Figure 6.1.2 Contour plot of the annual solar fraction as a function of the constant collector loop flow rate and the constant tank loop flow rate.

6.1.1.2 Results

The optimum flow rate profile in the collector side was found by the simulated annealing algorithm as well as the direct evaluation of the objective function, $\mathcal{F}$, at the nodes of a prescribed grid. The optimum value of $\mathcal{F}$ was found to be 0.504 and the optimum parameter set, which yields this maximum performance was found to be:

$$(a, b, c) = (0.014, 0.0, 0.0)$$

Figure 6.1.3 shows the optimum flow rate profile.

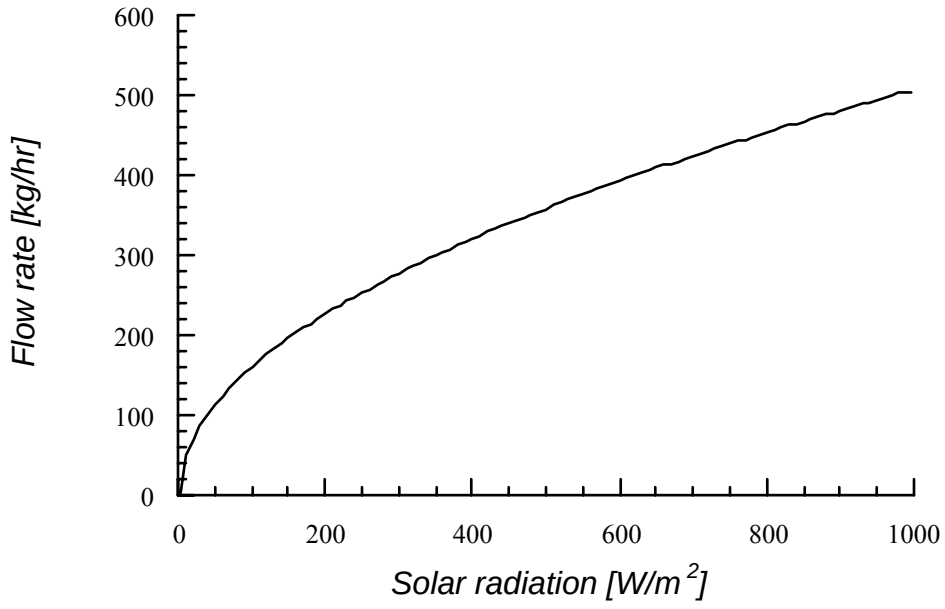

Figure 6.1.3 The optimum flow rate profile of the base system.

The graph of the objective function, $\mathcal{F}$, shows little variation with respect to the parameter b. Accordingly, the parameteric analysis will be made under the assumption that b is equal to zero and only a and c are allowed to vary. Figures 6.1.4-6 depict the surface $\mathcal{F}(a,b,c)$ where one of the parameters is fixed in each of the pictures.

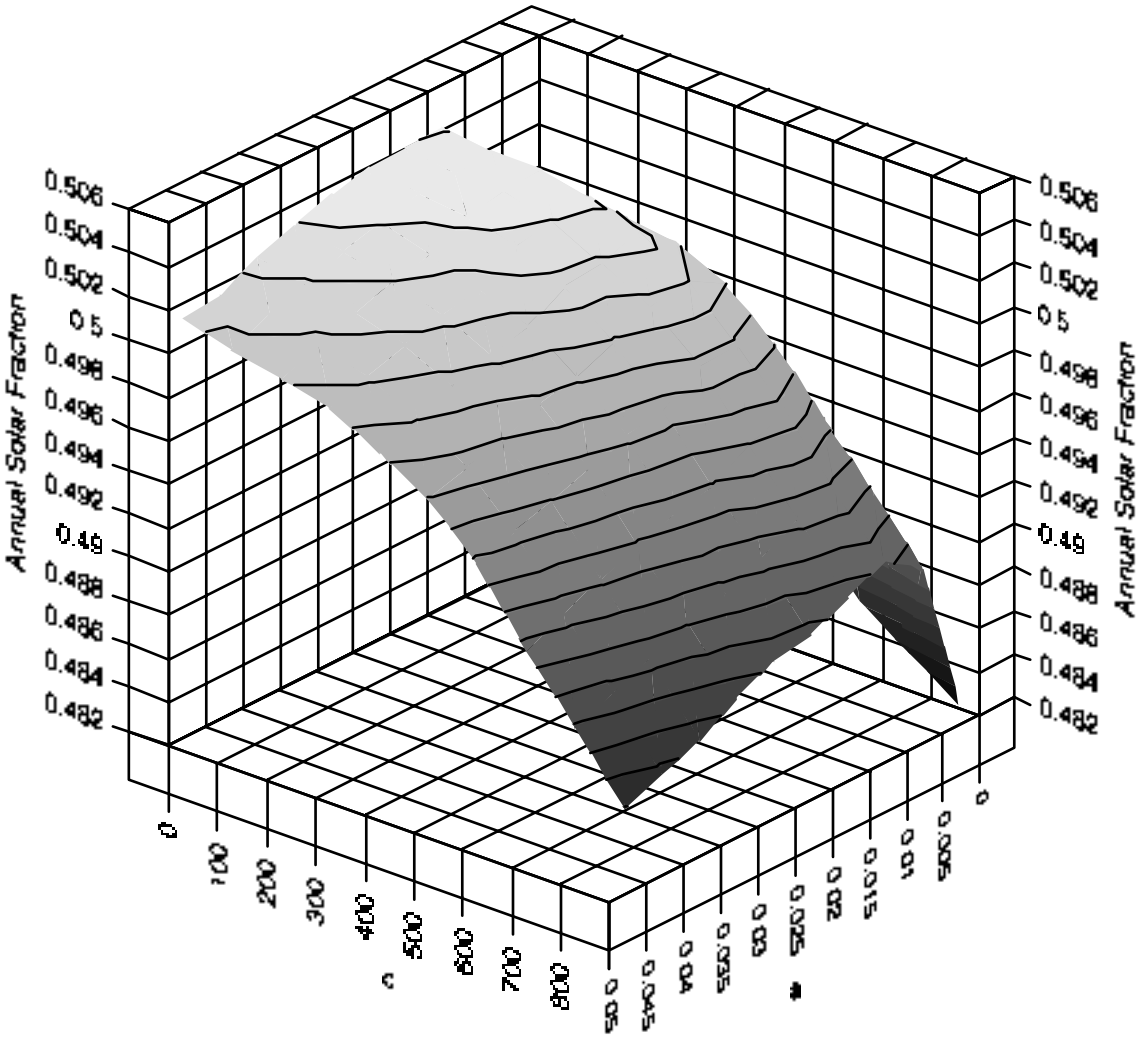

Figure 6.1.4 Graph of the annual solar fraction as a function of a and c, for b equal zero.

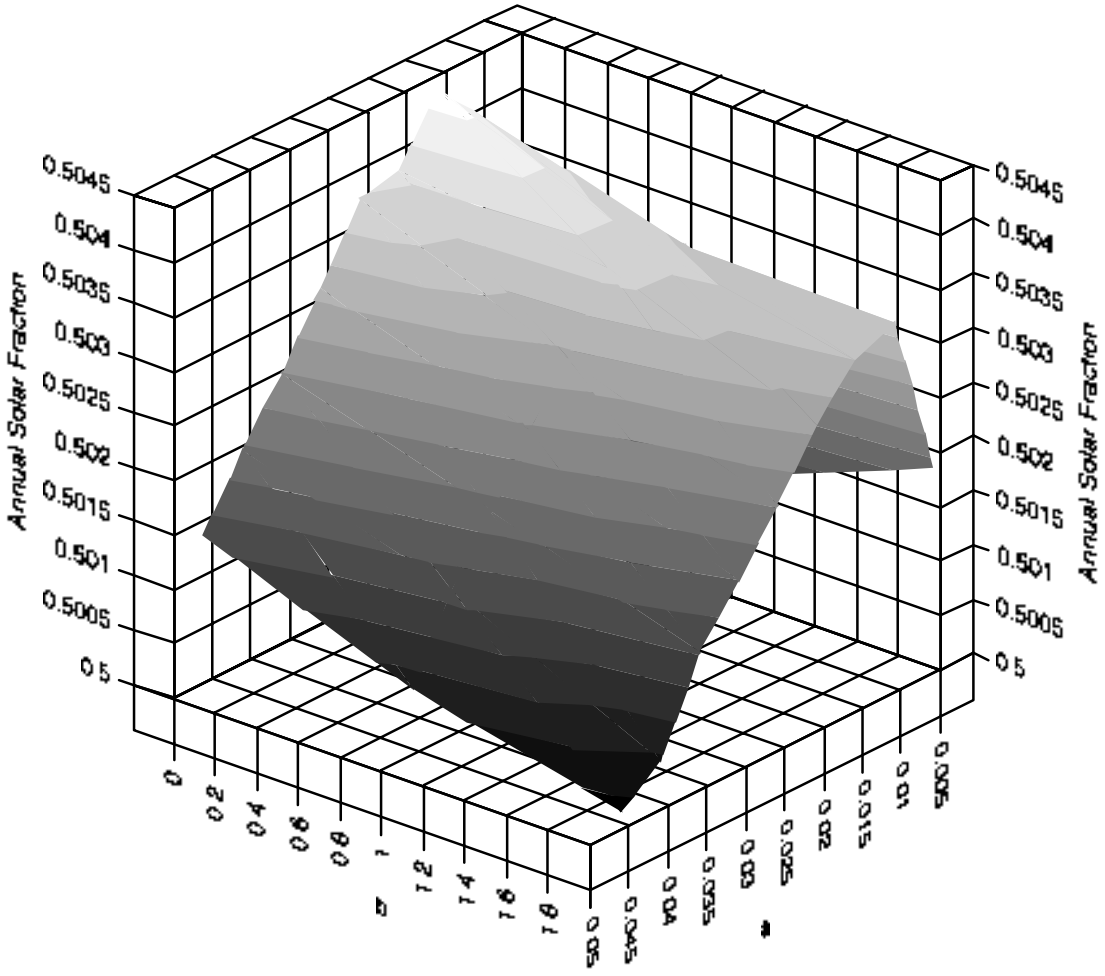

Figure 6.1.5 Graph of the annual solar fraction as a function of *a* and *b*, for *c* equal zero.

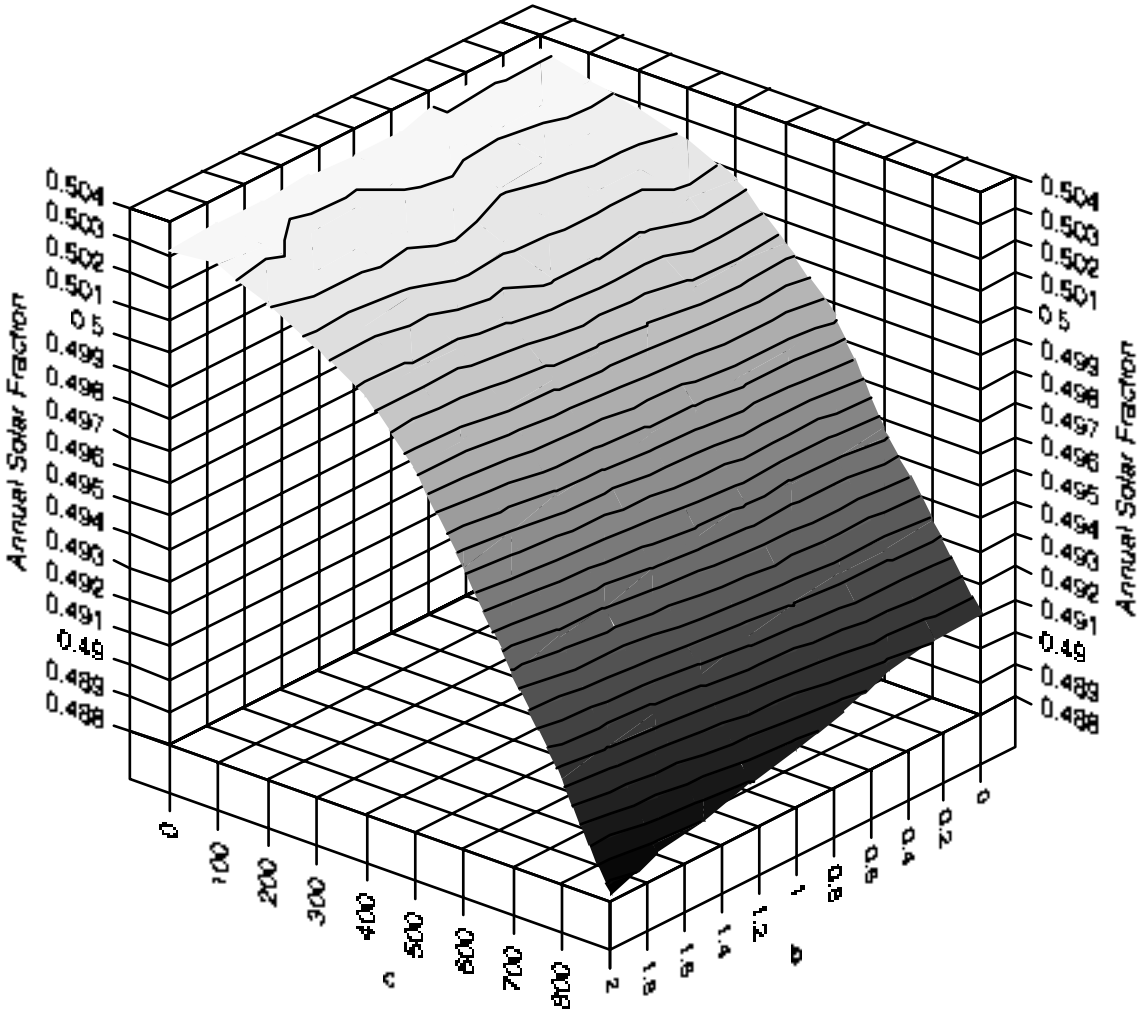

Figure 6.1.6 Graph of the annual solar fraction as a function of *b* and *c*, for *a* equal 0.014.

The optimum flow rate profile found earlier requires the collector-side pump to start very early. In conventional SDHW system, early pump starting may result in the reverse flow of energy from the hot fluid contained in the tank to the ambient via the collector. This phenomena occurs specifically when the solar radiation level is

insufficient to warm the collector structure, and the ambient temperature is lower than the collector inlet temperature. As a result, the circulating warm fluid is cooled rather than heated. On the other hand, for the case of the optimum indirect PV-SDHW system, although the optimum system requires the collector-side pump to start early, however, the tank-side pump is never activated unless the collector outlet temperature exceeds the tank bottom temperature. Hence, no exchange of energy occurs unless the collector outlet temperature is greater than the tank bottom temperature. The tank side flow in the base system is controller via a differential temperature ON/OFF controller.

If the this controller was replaced by a controller that turns the tank-side fluid ON only if the collector fluid is circulating, then the optimum flow rate profile would exhibit a delay in the pump starting to avoid the early starting penalty. The analysis of phase one for the base system was repeated for a system that uses this modified tank-side flow control strategy and the results are shown in Figure 6.1.7. The optimum flow rate profile for this modified system requires the pump to delay starting until a threshold radiation level of 160 W/m^2 is exceeded. The optimum value of the objective function of this modified system is slightly higher than the optimum value of the base system. Figure 6.1.8 shows the corresponding optimum collector-side flow rate profile along with the tank-side flow rate profile.

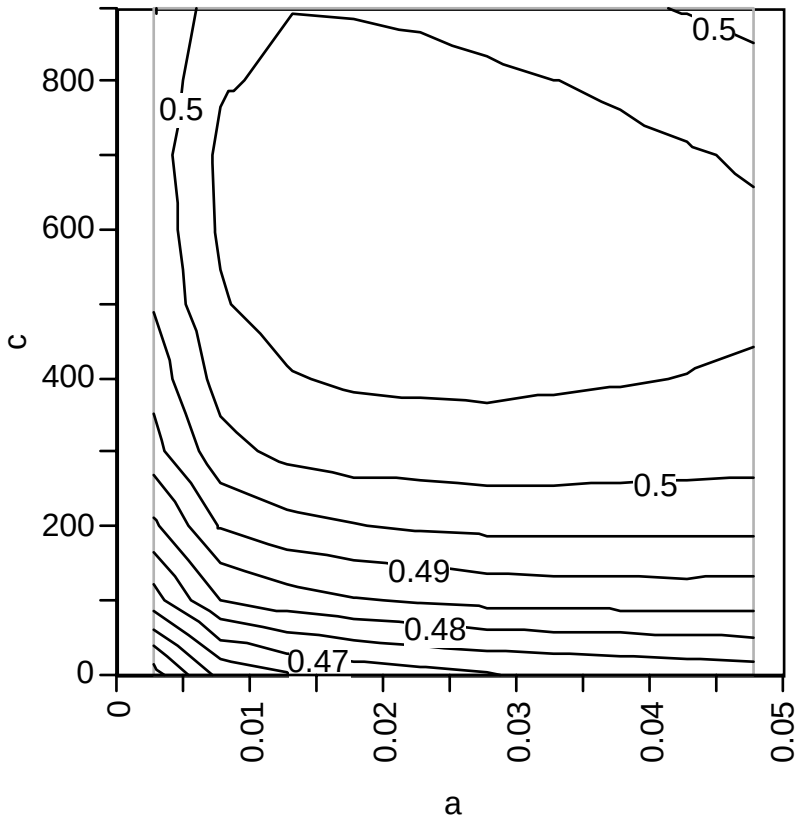

Figure 6.1.7 Contour plot of the annual solar fraction of the modified system as a function of *a* and *c*. The system allows the tank-side pump to be ON only of the collector-side fluid is circulating.

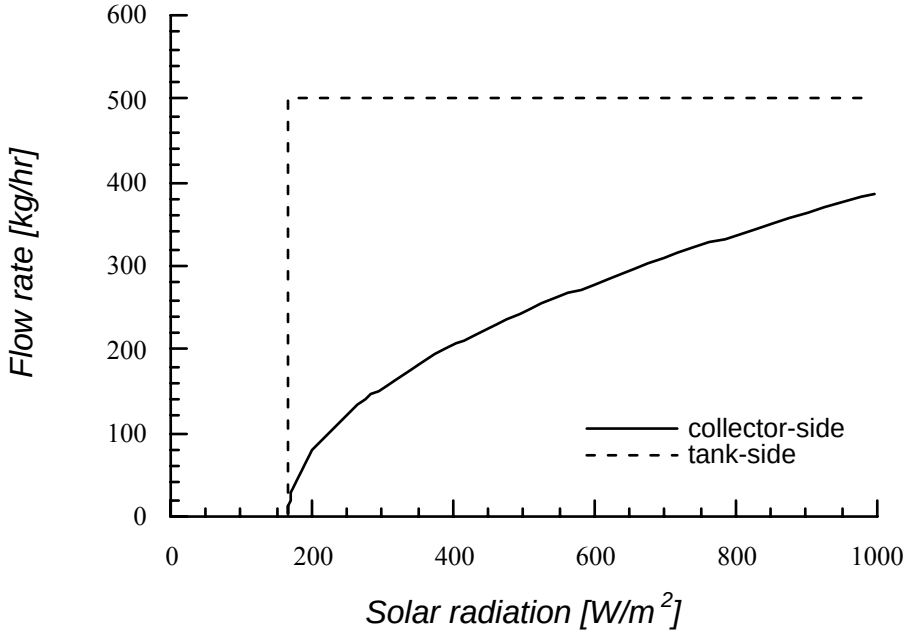

Figure 6.1.8 The optimum collector-side flow rate profile of the modified system and the tank-side flow rate profile.

As another alternative, the AC powered pump of the tank-side fluid could be replaced by a PV pumping system with a flow rate profile identical to the collector-side flow rate. The results of phase one of this control-less system is shown in Figure 6.1.9. The optimum flow rate profile for this system requires the pump to delay starting until a threshold radiation level of 130 W/m^2 is exceeded. The optimum value of the objective function of this control-less system is identical to the optimum value of the base system. Figure 6.1.10 shows the optimum collector-side and tank-side flow rate profile.

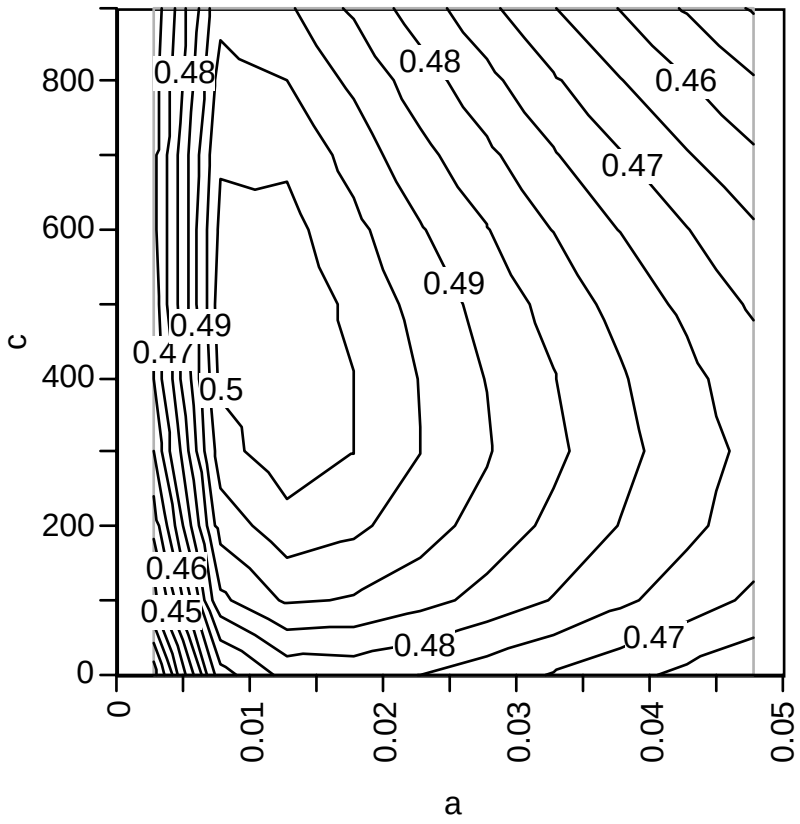

Figure 6.1.9 Contour plot of the annual solar fraction of the modified system as a function of *a* and *c*. The system's collector-side and tank-side fluid is driven by PV pumping system.

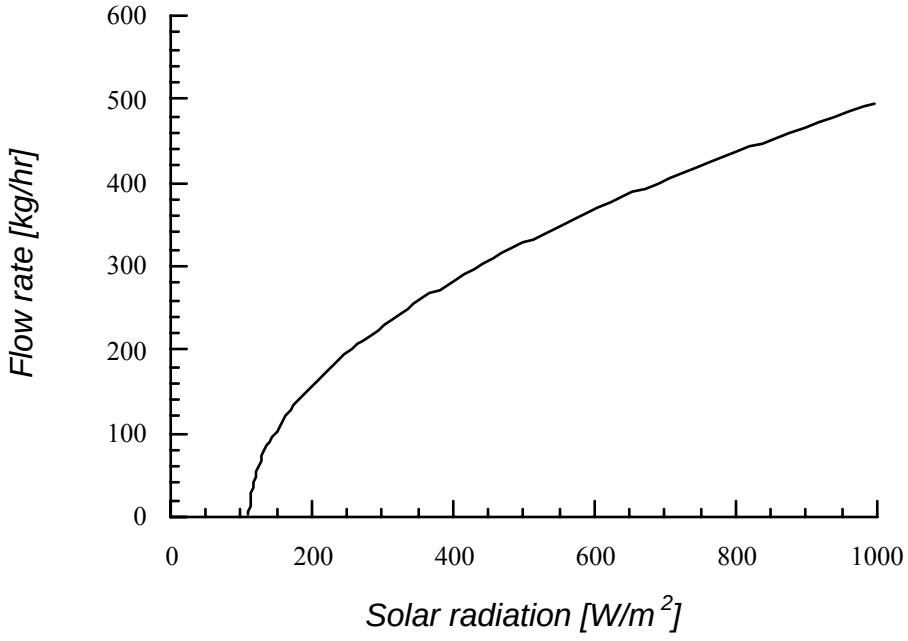

Figure 6.1.10 The optimum collector-side and tank-side flow rate profile of the control-less system. The system's collector-side and tank-side fluid is driven by PV pumping system.

6.1.1.2.1 Effect of the Load Profile on the Optimum Set

The load profile used in the base system was shifted by 10 hours and the optimum computed. The optimum parameter set (a,c) remained identical. Figure 6.1.11 depicts the standard load profile and the resulting contour plots of $\mathcal{F}(a,c)$. Figure 6.1.12 depict the shifted load profile and the resulting contour plots of $\mathcal{F}(a,c)$.

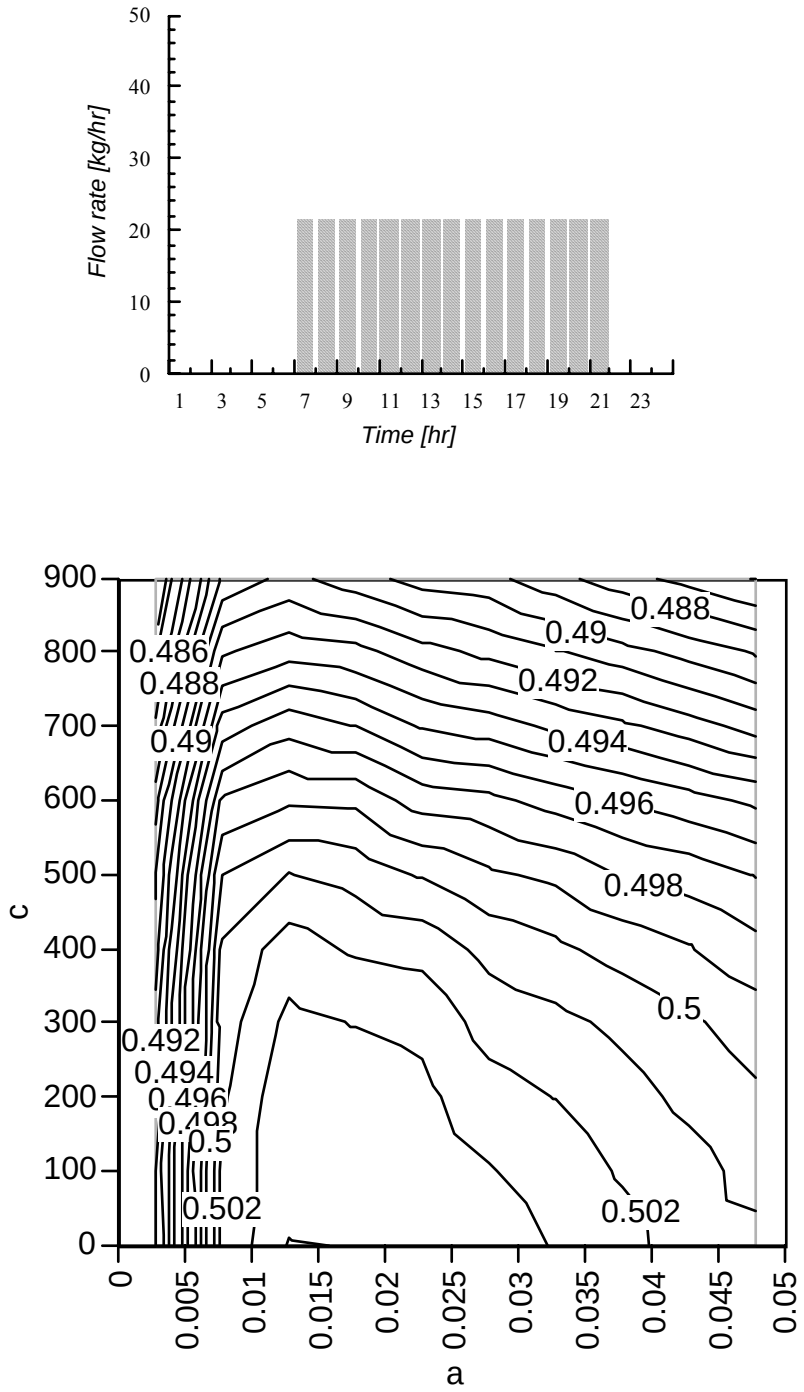

Figure 6.1.11 The standard load profile and the resulting contour plot of the annual solar fraction of the base system as a function of the parameters *a* and *c*.

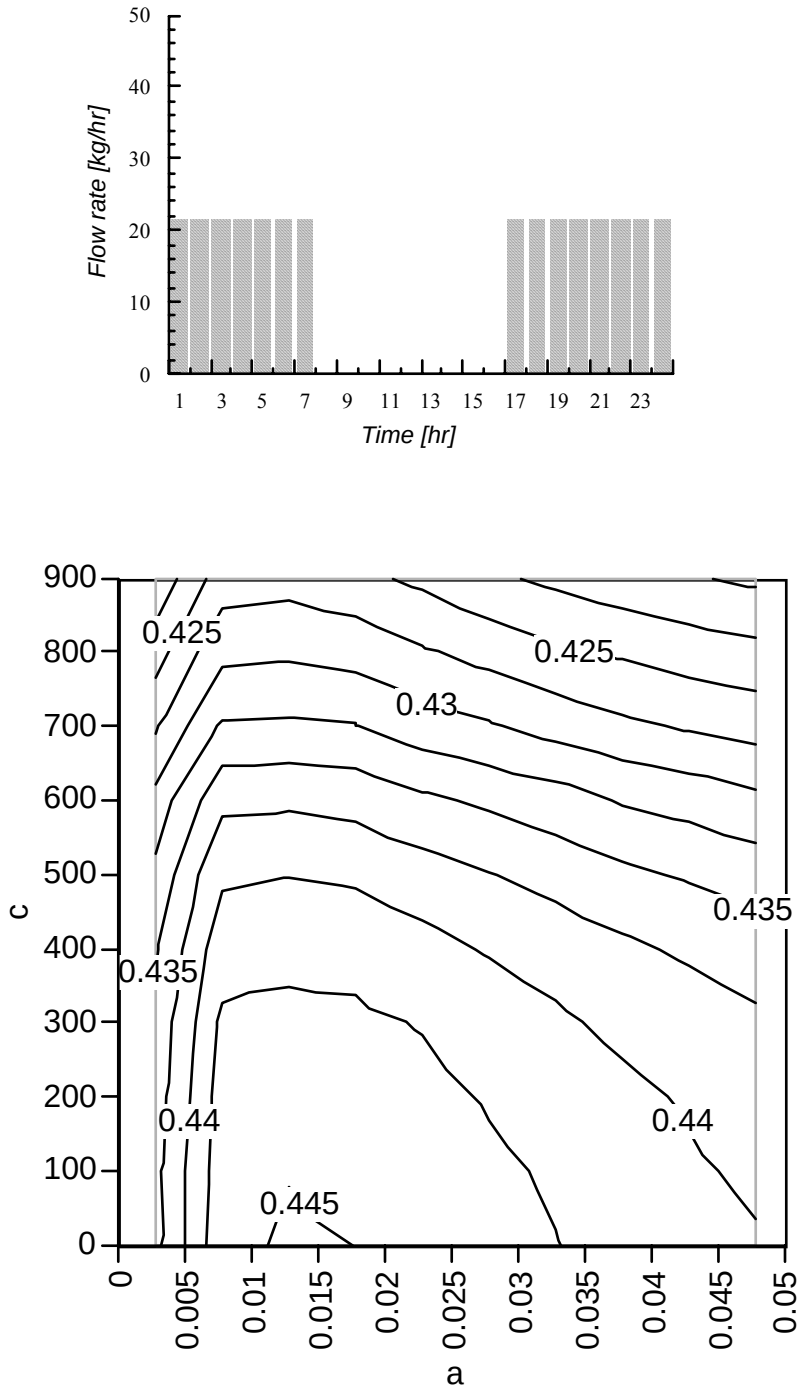

Figure 6.1.12 The shifted load profile and the contour plot of the annual solar fraction of the base system as a function of the parameters *a* and *c*.

6.1.1.2.2 Effect of the System Location on the Optimum Set

A second location (Albuquerque, NM) was studied and the results compared to those of the base system located in Madison, WI. No significant differences were found. The value of $\mathcal{F}$ that would have resulted from the optimum parameter set of the base system was less than 0.01% of the optimum $\mathcal{F}$ in Albuquerque. Figure 6.1.13 depicts the contour plots of $\mathcal{F}$ if the system were located in Albuquerque, NM.

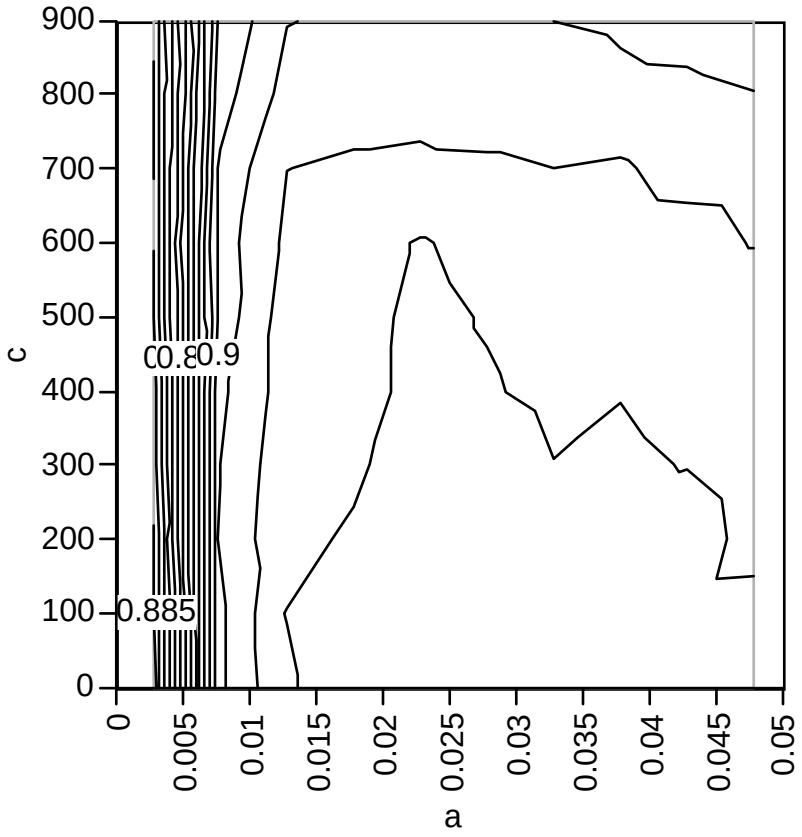

Figure 6.1.13 Contour plot of the annual solar fraction of the system if located in Albuquerque, NM.

6.1.1.2.3 Effect of Heat Exchanger Effectiveness on the Optimum Set

A different heat exchanger, larger than the one used in the base system, was employed to allow for higher values of effectiveness (from 0.6 at a collector flow rate of 600 kg/hr to 0.9 at a collector flow rate of 100 kg/hr). The resulting optimum parameter set was virtually identical to the one of the base system. Figure 6.1.14 shows the contour plots of $\mathcal{F}$.

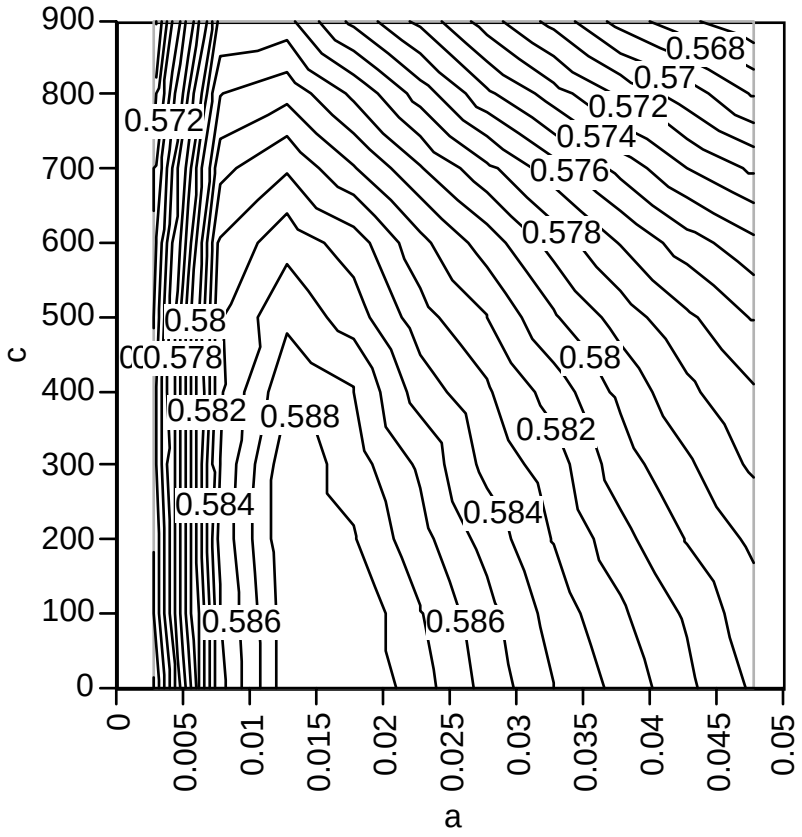

Figure 6.1.14 Contour plot of the annual solar fraction as a function of *a* and *c* for a heat exchanger with higher effectiveness range.

6.1.2 Phase Two6.1.2.1 Base System

The optimum flow rate found in phase one reaches flow rates as high as 500 kg/hr. This dictates the use of a larger base PV cell than the one used for the direct SDHW system. The base PV cell is identical to the PV module tested by FSEC. The base PV cell has a short circuit current of 0.385 Amp, an open circuit voltage of 20.6 Volt, and is capable of delivering a maximum power of 5.68 W.

The reference flow, Q_{ref}, (1.4e-4 m^3/s) was chosen to equal the maximum value reached by the optimum flow profile found in phase one. The value of the reference head, H_{ref}, was consequently determined from the standard SRCC curve. The centrifugal pump has been selected so that the system operating flow rate is within the maximum pump efficiency. The pump exhibits a maximum pump efficiency of 10% . Figure 6.1.15 shows the pump and the piping system characteristic curves.

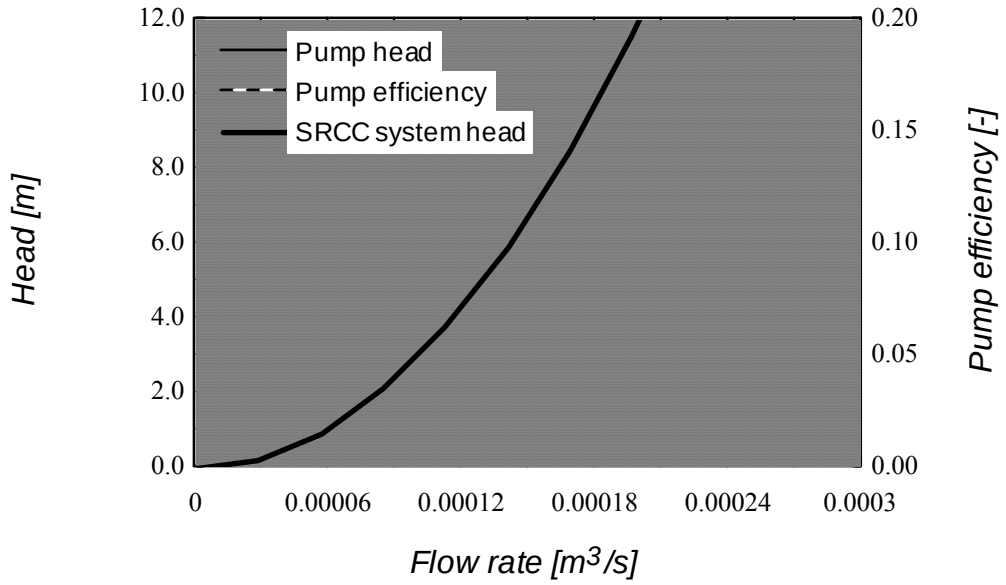

Figure 6.1.15 The characteristic curves of the pump and the piping system employed in phase two.

6.1.2.2 Results

The search for the optimum parameter set $(Type, P, S, C, R)^{opt}$ has been performed using the two-step procedure described for the direct SDHW system. The optimum parameter set was found be

$$(Type, P, S, C, R) = (2, 4, 3, 0.41, 0.01)$$

and the corresponding value of the objective function, ϕ, was 128383.

This means that the number of PV modules in the optimum *indirect* PV-SDHW system, employing a forced convection heat exchanger, equals 12 modules and hence a total of 480 PV cells. In contrast, the number of PV cells required by the optimum *direct* PV-SDHW system was found in chapter 5 to be 2 PV cells only. The reason of this huge increase in the number of PV cells is dictated by the large pumping power required by the optimum indirect PV-SDHW system. At the reference operating condition of a solar radiation of 1000 W/m^2 and a cell temperature of 25 °C, the flow rate of the optimum indirect PV-SDHW system is 490 kg/hr compared to 56 kg/hr for the direct system; and the head of the indirect system is 5.45 m compared to 0.073 m for the direct system. This results in an *indirect* system's pumping power of 655

times the pumping power required by the *direct* system. The input-output energy flow within the optimum indirect PV-SDHW system can be looked at using the same reference operating condition sited above; the energy delivered to the PV cells is 836.5 W, the energy generated from the PV cells is 75.7 W, the output energy from the DC-motor is 71.8 W and the output energy from the pump is 7.2 W.

Figure 6.1.16 depicts the objective function, ϕ, as a function of C and R for $Type = 2$, $P = 4$ and $S = 3$. Figure 6.1.17 compares the optimum flow rate profile found in phase one and the flow rate profile resulting from the optimum PV pumping system found in phase two.

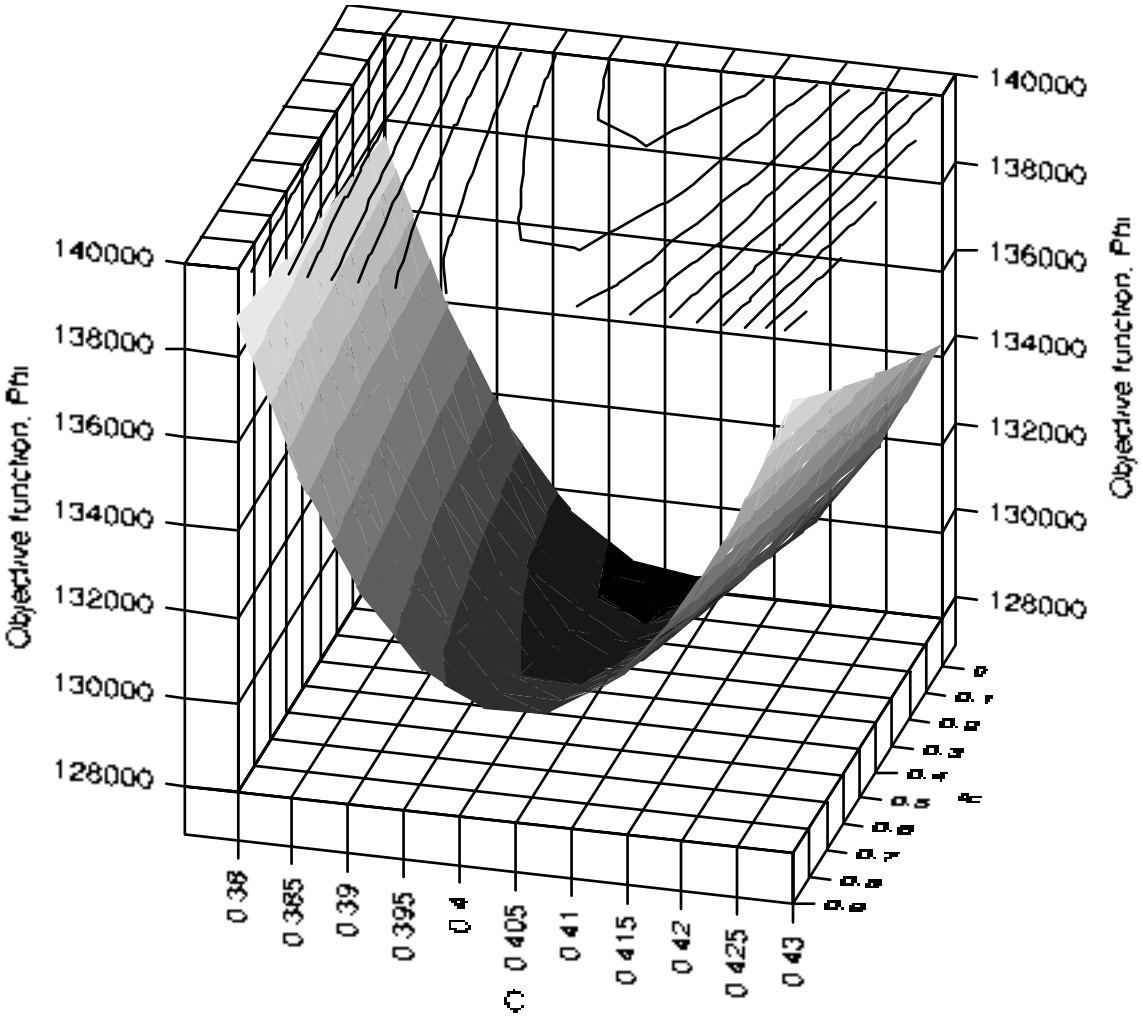

Figure 6.1.16 Graph of the objective function, ϕ, as a function of *C* and *R*. *Type* = 2, *P* = 4 and *S* = 3.ϕ

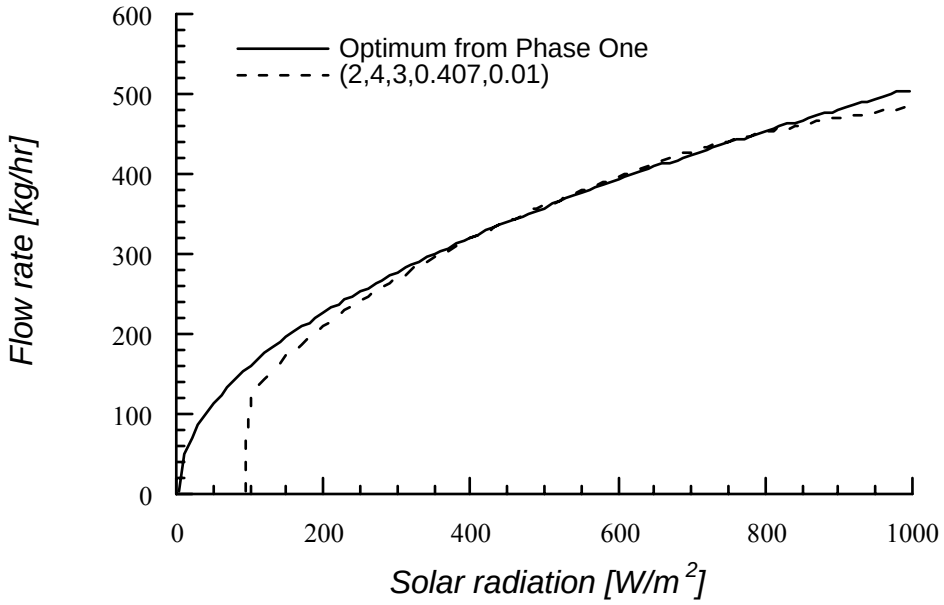

Figure 6.1.17 The optimum flow rate profile found in phase one and the flow rate profile resulting from the optimum PV pumping system found in phase two.

6.2 PV-SDHW with NCHE

6.2.1 Phase One

6.2.1.1 Base System

The difference in the base system with respect to the previous one lies in the type of the heat exchanger used and the connected storage tank. The natural convection heat exchanger is a shell and coil heat exchanger manufactured by Thermo Dynamics, Inc. It consists of four helices of copper tubing with a combined length of 100 feet wound around a core in a four inch diameter cylindrical shell. Detail information about this

component is presented in Appendix C. Figure 6.2.1 illustrates a schematic drawing of the base system used in phase one.

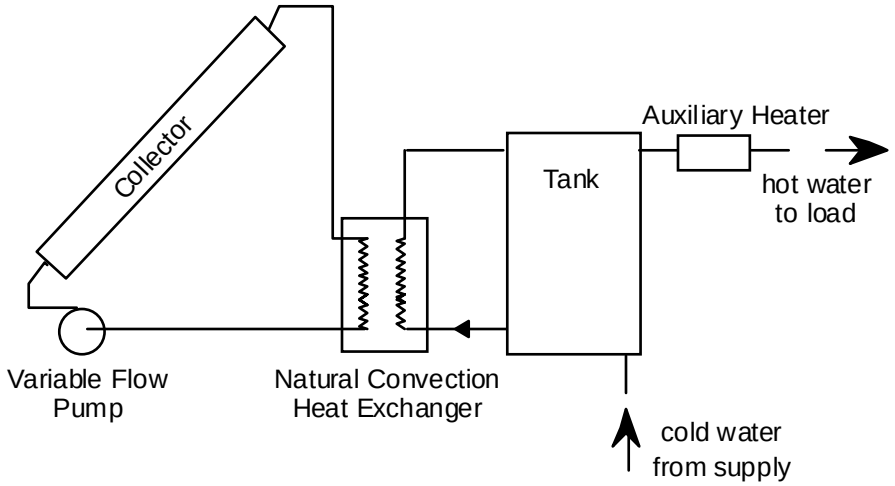

Figure 6.2.1 Schematic drawing of the base system used in phase one.

TRNSYS TYPE 67 was used to simulate the performance of the natural convection heat exchanger. The model requires two sets of data characterizing the pressure drop as a function of the tank flow rate and the heat exchanger effectiveness as a function of the collector flow rate and the tank side inlet temperature. The data set available for the pressure drop as a function of the tank flow rate imposed the use of a slightly different type of tank than the one in the previous section. The tank volume used here is 0.454 m^3, while the one used in the previous section was 0.39 m^3.

6.2.1.2 Results

The optimum flow rate profile was found by the direct evaluation method. The optimum annual solar fraction was found to be 0.635 and the corresponding optimum parameter set was found to be:

$$(a, b, c) = (0.3, 0.0, 0.0)$$

Figure 6.2.2 shows the optimum flow rate profile found in phase one.

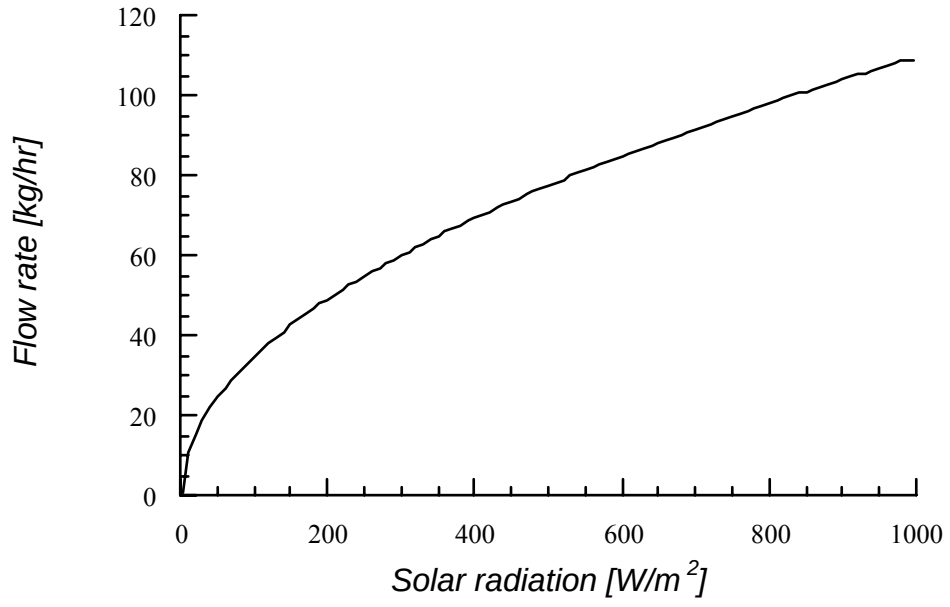

Figure 6.2.2 The optimum flow rate profile found in phase one.

The graph of the objective function, $\mathcal{F}$, shows little variation with respect to the parameters b and c. Figures 6.2.3-5 depict the surface $\mathcal{F}(a,b,c)$ where one of the parameter is fixed in each one of the pictures.

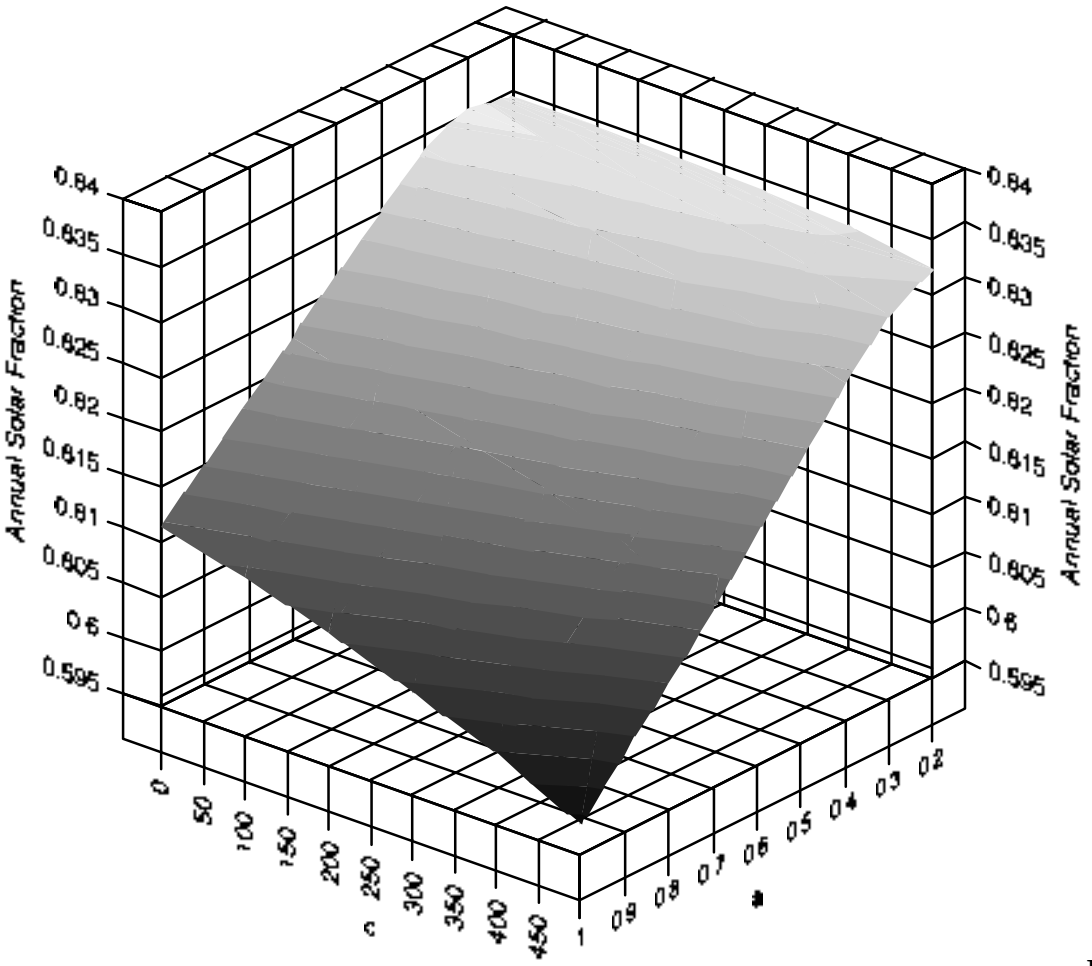

Figure 6.2.3 Graph of the annual solar fraction as a function of a and c, for b equal zero.

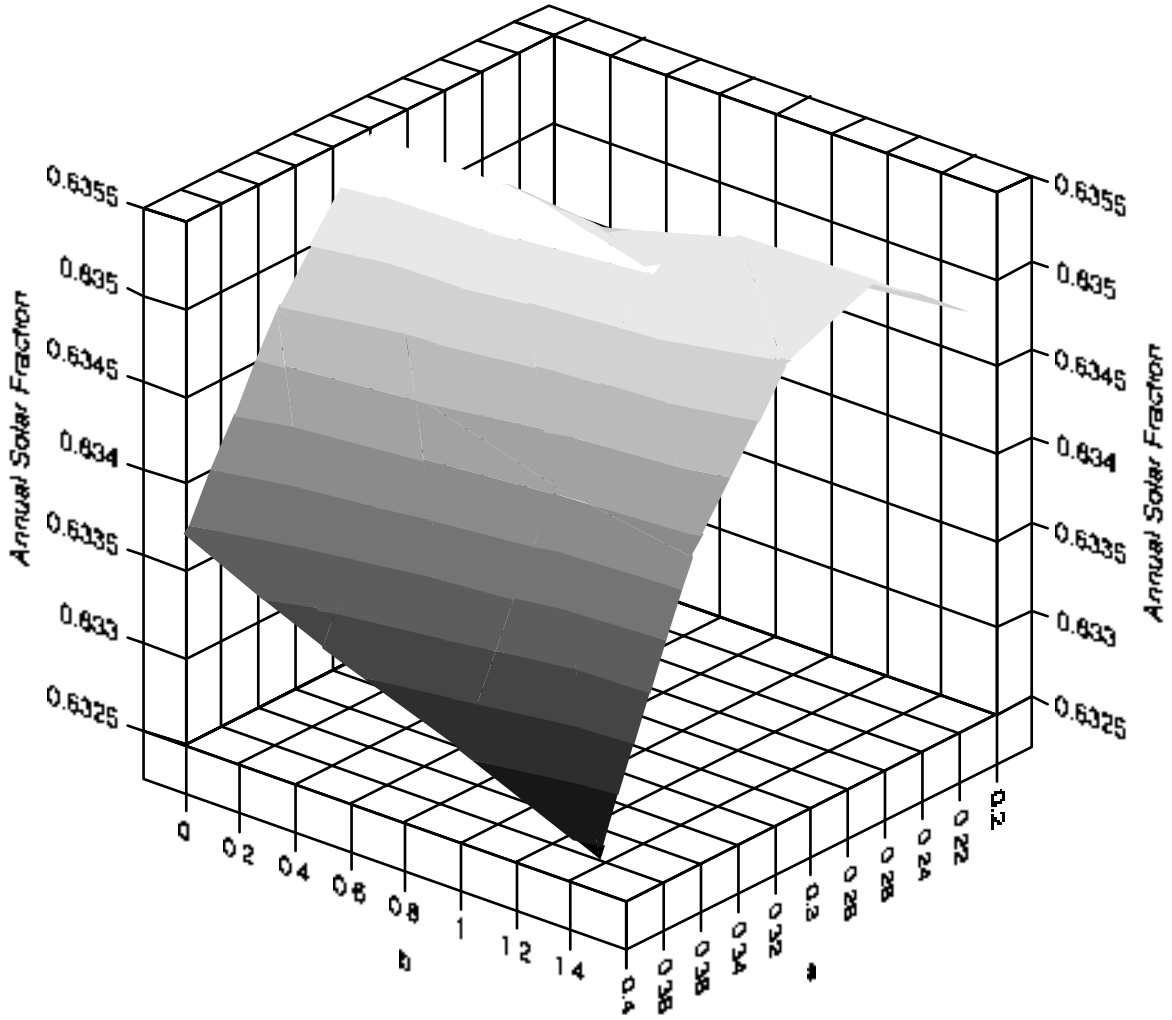

Figure 6.2.4 Graph of the annual solar fraction as a function of *a* and *b*, for *c* equal zero.

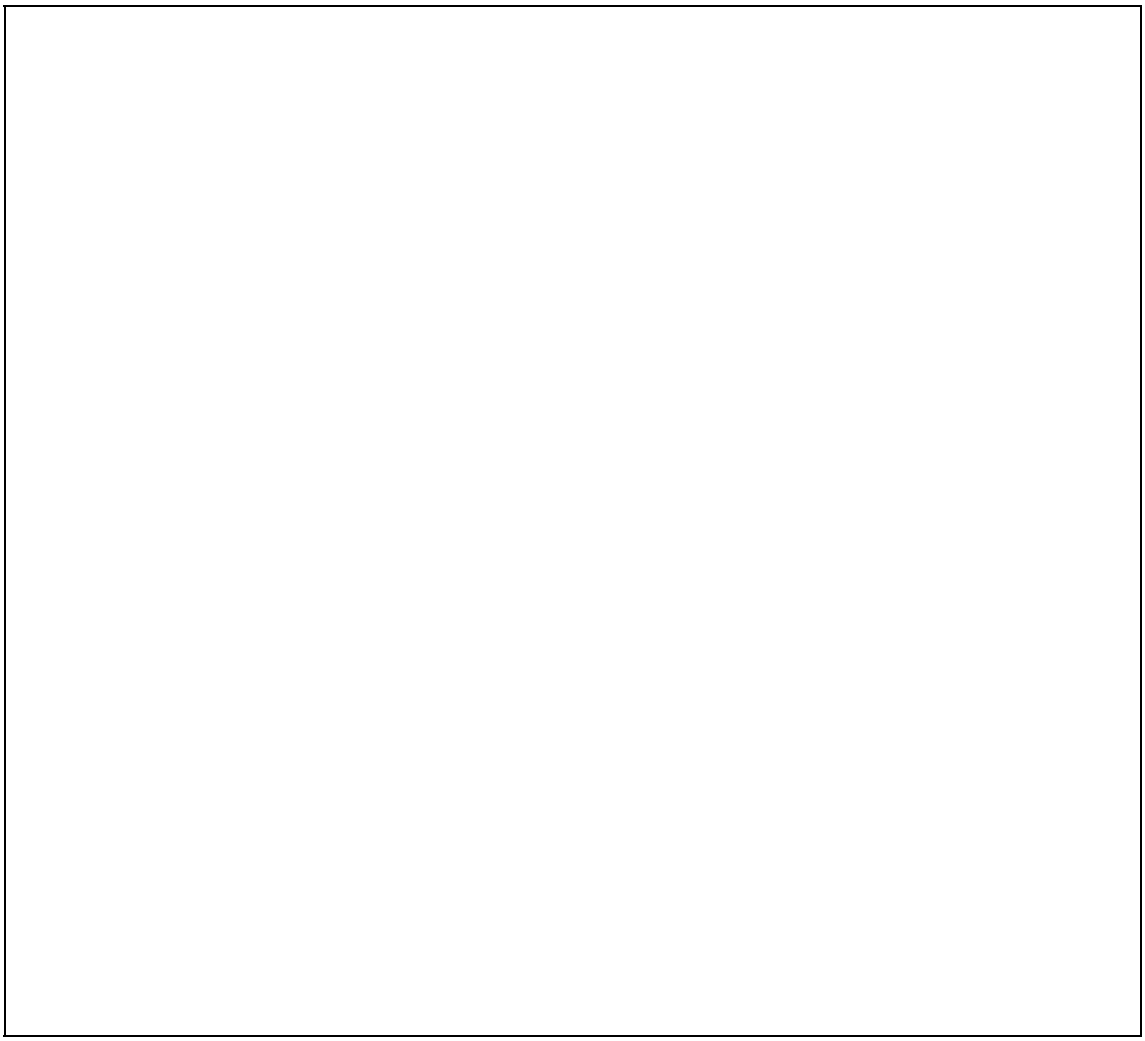

Figure 6.2.5 Graph of the annual solar fraction as a function of *c* and *b*, for *a* equal 0.3.

6.2.2 Phase Two6.2.2.1 Base System

The base PV cell used in this section is identical to the one previously used for the direct SDHW system presented in chapter 5.

The reference flow, Q_{ref}, (2.8e-5 m^3/s) was chosen to equal the maximum value reached by the optimum flow profile found in phase one. The value of the reference head, H_{ref}, was consequently determined from the standard SRCC curve. The centrifugal pump has been selected so that the system operating flow rate is within the maximum pump efficiency. The pump exhibits a maximum pump efficiency of 5%. Figure 6.2.6 shows the pump and the piping system characteristic curves.

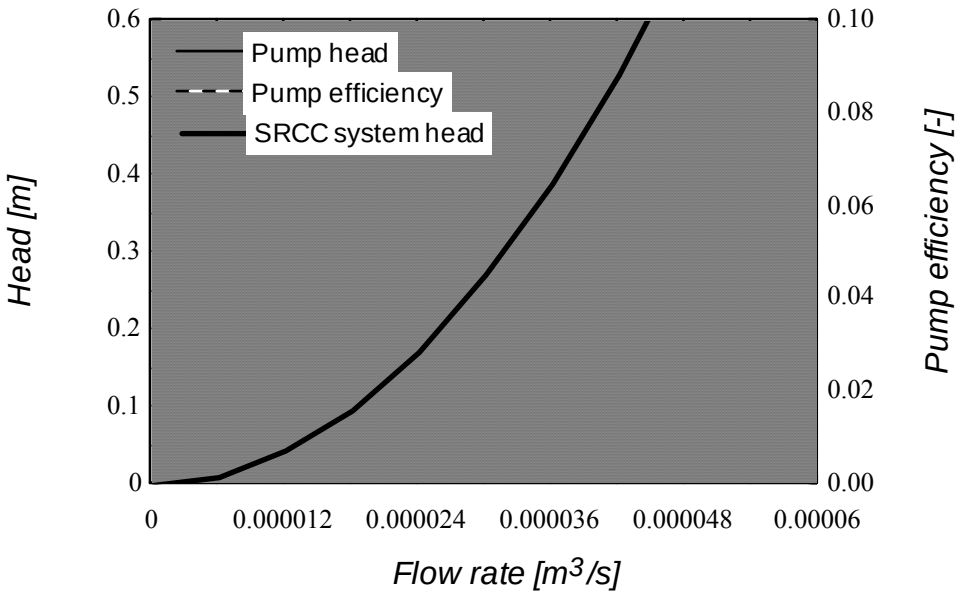

Figure 6.2.6 The characteristic curves of the pump and the piping system employed in phase two.

6.2.2.2 Results

The search for the optimum parameter set $(Type, P, S, C, R)^{opt}$ has been performed using the two-step procedure. The optimum parameter set was found to be

$$(Type, P, S, C, R) = (2, 1, 11, 0.033, 0.3)$$

and the corresponding value of the objective function, ϕ, was 6522. Figure 6.2.7 depicts the objective function, ϕ, as a function of C and R for $Type = 2$, $P = 1$ and $S = 11$.

This optimality result indicates that the optimum indirect PV-SDHW system employing a *natural* convection heat exchanger is superior to the optimum indirect PV-SDHW system employing a *forced* convection heat exchanger. The system employing the natural convection heat exchanger requires a much lesser number of PV cells than the one used for the forced convection (11 versus 480). Not only that, but also is able of achieving a higher annual solar fraction (0.635 versus 0.504). The reduction in the number of PV cells in the natural convection case is due to the lower pumping power required by the pump. At the reference operating condition of 1000 W/m^2 and 25°C, the flow rate of the optimum indirect PV-SDHW system employing a natural convection heat exchanger is 107 kg/hr compared to 490 kg/hr for the forced convection system; and the head of the natural convection system is 0.27 m compared to 5.45 m for the forced convection system. This results in a pumping power of 1.1% of that required by the forced convection system.

Figure 6.2.8 compares the optimum flow rate profile found in phase one and the flow rate profile resulting from the optimum PV pumping system found in phase two.

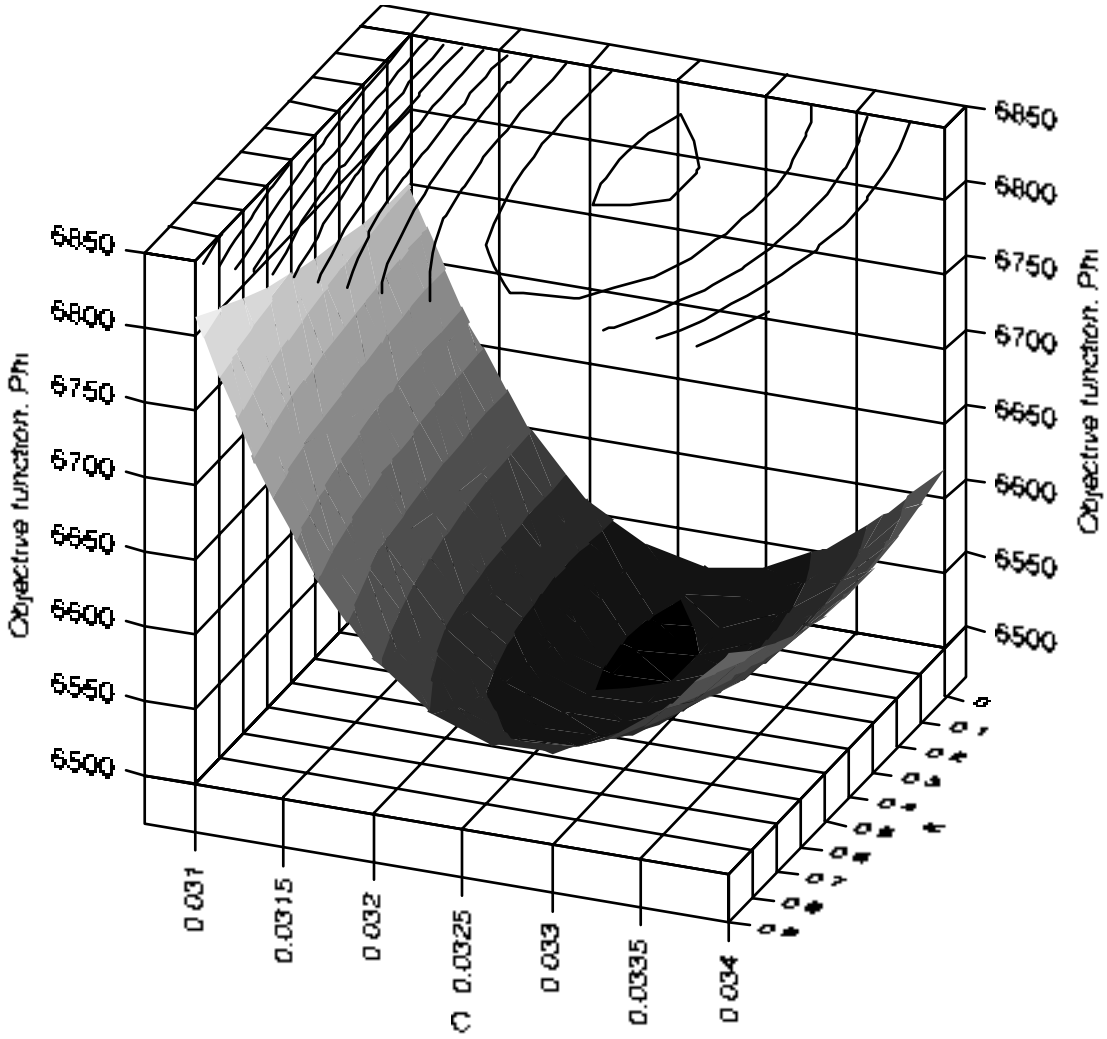

Figure 6.2.7 Graph of the objective function, ϕ, as a function of *C* and *R*. *Type* = 2, *P* = 1 and *S* =11.$^{\phi}$

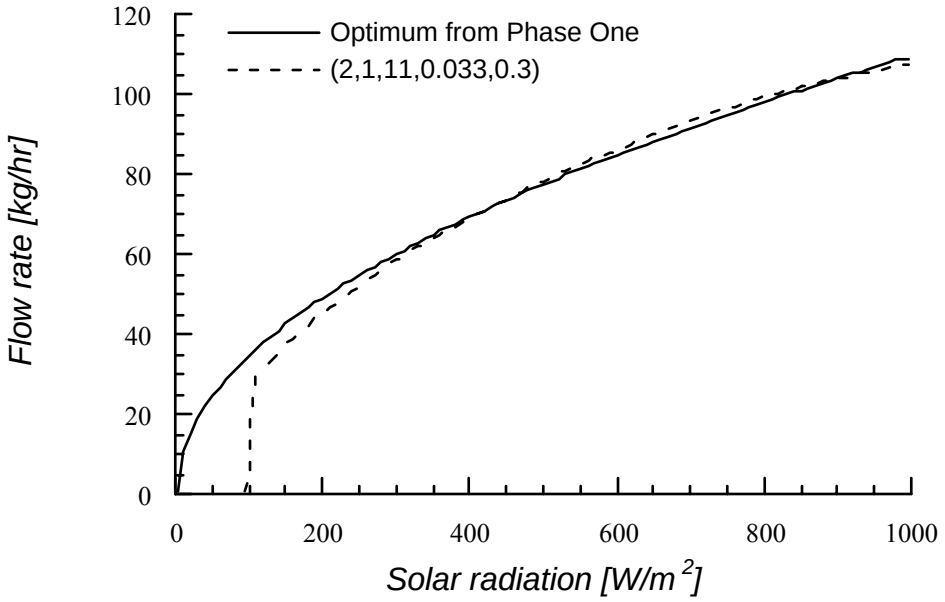

Figure 6.2.8 The optimum flow rate found in phase one and the flow rate resulting from the optimum PV pumping system found in phase two.

Chapter 7 Conclusions and Recommendations

7.1 Conclusions

A search methodology for the optimum configuration of a PV-SDHW system has been presented. The main premise of this methodology is the decoupling of the optimum search process in two phases: the first to find the flow rate profile that maximizes the performance of a given SDHW system, and the second to select the components of the PV pumping system that produce a flow rate profile matching as closely as possible the one found in the first phase. This decoupling considerably eases the process of optimum search. An analysis of actual flow rate profiles of PV pumping systems showed that the optimum search can be restricted to the family of profiles represented by a function dependent upon three parameters only.

The research found that the direct PV-SDHW system can achieve an annual solar fraction of 0.699, whereas the indirect PV-SDHW system achieved a maximum annual solar fraction of 0.504 in the case of the forced convection heat exchanger and a maximum annual solar fraction of 0.635 in the case of the natural convection heat exchanger. In the case of the direct PV-SDHW system the flow rate, at a solar radiation of 1000 W/m^2 and a PV cell temperature of 25 °C, was 56 kg/hr, whereas it reached 107 kg/hr in the case of the indirect PV-SDHW system employing a natural convection heat exchanger and an even higher value of 490 kg/hr in the case of the indirect PV-SDHW system employing a forced convection heat exchanger. In the case of the direct PV-SDHW system, the optimum flow rate profile included a delay in the

motor-pump starting, whereas the optimum in the case of the indirect PV-SDHW system requires the motor-pump to start at very low radiation levels. In all three cases studied, the optimum flow rate profile requires a rapid rate of increase in the flow rate at the starting point. This implies that the optimum flow rate profile can be modeled with only two parameters as follows:

$$Q = \sqrt{\frac{G - c}{a}}$$

Within the direct PV-SDHW family of systems, the aforementioned optimum flow rate profile is superior to SDHW systems operating at various conventional control strategies.

Within the indirect PV-SDHW family of systems, the optimum annual solar fraction in the case of the system employing natural convection heat exchanger was higher than in the case of forced convection. In addition, the system employing natural convection required a much smaller number of PV cells than the forced convection.

The type of DC-motor at which the optimum was attained in every case was that of either the permanent magnet or the separately excited DC-motors, while the series excited DC-motors always ranked last.

For every hour of pump operation, a PV-SDHW system saves a minimum of 3 W-hr over a conventional SDHW system. Counting the thousands of pumps in operation, this constitute an appreciable savings of energy. Moreover, since all these pumps

operate at the same time, including ON-peak utility hours, these savings are the more important from the perspective of the electric utility companies.

7.2 Recommendations

After completing the investigation of selecting an optimum PV-SDHW system, the author would like to make recommendations for experimental investigation aiming towards validating the optimum PV-SDHW systems and experimentally quantifying its gains.

Appendix A Reliability and Practicability of PV Pumping Systems

Among the vast applications of PV systems, small scale water pumping systems driven by PV cells were found to be technically appropriate and economically viable (Dankoff, 1990). The main reason for this success was attributed to the demand profile for water being in harmony with the solar radiation profile.

Furthermore, it was found that PV water pumping systems provide an attractive solution to satisfy various water needs, in term of autonomy, reliability and performance (Carrier and Schiller, 1993). From another prospective, Chowdhury et al. (1993) found that PV powered water pumping in the state of Wyoming, USA, is a cost effective alternative to distribution line extension or other conventional means of water pumping. Customer satisfaction, in terms of functional adequacy and low maintenance requirements of these systems, was found to be high.

Since the first installation of a PV water pumping system in 1978 (Koner et al., 1992a), these systems have gained acceptance and reliability. Dankoff (1991) indicated that over 20,000 photovoltaic pumping systems are working throughout the world; most of them are small systems for remote homes, village and livestock drinking water. In India, Koner et al. (1992a) indicated that the future installation of PV water pumping systems is indeed promising and is expected to replace the existing four to five million diesel powered water pumps, each consuming about 3.5 kW.

Diarra et al. (1989) studied the 10 year performance of four small-scale PV pumping systems in the country of Mali. The study proved the field reliability of the PV water pumping system as the reported failure rate of the four systems was less than 2% during the 10 years of operation.

The field reliability and acceptance of PV pumping systems is highly coupled with the simplicity of its operation. Therefore, components with high failure rates should be avoided (Wijesooriya and Duffy, 1992). PV water pumping systems are normally operated and maintained by non-technical people and therefore, simplicity must be maintained (Roger, 1979).

Appendix B TRNSYS, *a Transient Simulation Program*

TRNSYS is a transient simulation program developed by the Solar Energy Laboratory of the University of Wisconsin-Madison. TRNSYS is a modular, component based simulation program that model each sub-system component at its inputs and outputs using measurable parameters and variables. The TRNSYS library consists of a variety of individual subroutines which model physical components. These component models can be connected to represent a system. Simulations can be run over different time periods and different simulation time steps. The modular structure of TRNSYS gives the program tremendous flexibility, and facilitates the addition to the program of mathematical models not included in the standard TRNSYS library. TRNSYS is well suited to detailed analyses of systems whose behavior is dependent on the passage of time. As a result, numerous SDHW system investigations were done using TRNSYS. Mathematical models of the available components are well documented in the TRNSYS manuals.

Liu *et al.* (1978) performed experimental validation of TRNSYS for SDHW systems. Carlson *et al.* (1991) performed experimental validation of the Solar Rating and Certification Corporation (SRCC) ratings of generic drain back solar water heaters.

Recently, TRNSYS has undergone a major enhancement; a more robust method for solving simultaneous algebraic and differential equations has been implemented. Allowing the solution of backward problems and convergence-promotions are no

more required. It is for the highly-coupled non-linear algebraic equations describing the direct-coupled PV systems that this major enhancement was made.

Appendix C Base Systems Data

Collector:

Parameter	Value
Frontal area, A	6.5 m^2
Working fluid	water
Specific heat, C_{pf}	4.19 kJ/kg °C
Slope,	40.0°
Surface azimuth angle,	0.0°
$F_R(\quad)_n$	0.7
$F_R U_L$	15 kJ/hr m^2 °C
Incident angle modifier linear coefficient, b_0	0.1
Incident angle modifier nonlinear coefficient, b_1	0.0
Collector test flow rate, $\dot{m}$	325 kg/hr

Tank:

Parameter	Value
Volume	0.39 m^3
Overall loss coefficient, U_L	1.44 kJ/hr m^2 °C
Ambient temperature around the tank, T_{env}	21.0 °C
Initial tank temperature, T_i	60.0 °C
Temperature of the replacement fluid, T_L	15.0 °C

Auxiliary heater:

Parameter	Value
Maximum heating rate, $\dot{Q}_{max}$	1e 7 kJ/hr
Set temperature, T_{set}	60.0 °C
Specific heat of fluid, C_{pf}	4.19 kJ/hg °C
Overall heat loss coefficient, *UA*	0.0 kJ/hr °C
Efficiency of auxiliary heater, $_{htr}$	100%

NCHE:

Parameter	Value
Number of nodes for heat exchanger temperature distribution	40
Height of the heat exchanger	0.4064 m
Length of pipe section 2	0.5 m
Length of pipe section 3	0.5 m
Length of pipe section 4	0.5 m
Length of pipe section 5	0.5 m
□Z of pipe section 2	0 m
□Z of pipe section 3	0.064 m
□Z of pipe section 4	0 m
□Z of pipe section 5	0.965 m
□Z of water storage tank	1.4354 m

Diameter of pipe section 2	0.01905 m
Diameter of pipe section 3	0.01905 m
Diameter of pipe section 4	0.01905 m
Diameter of pipe section 5	0.01905 m
Associated minor loss *K* values of pipe section 2	1.5
Associated minor loss *K* values of pipe section 3	1.5
Associated minor loss *K* values of pipe section 4	1.5
Associated minor loss *K* values of pipe section 5	1.5
# of points in modified effectiveness vs. m_w curve for a given glycol flow rate	9
# of points in heat exchanger pressure drop vs. m_w curve	39
% glycol solution	50
# of curves of modified effectiveness vs. m_w (glycol flow rates tested for)	6
Glycol type: 1) propylene glycol solution, 2) ethylene glycol solution	1

PV cell for the direct system and the indirect system employing NCHE:

Parameter	**Value**
Reference solar radiation, G_{ref}	895 W/m^2
Reference cell temperature, $T_{c,ref}$	323 K
Short circuit current at the reference condition, $I_{sc,ref}$	0.385 Amp

Maximum power point current at the reference condition, $I_{mp,ref}$	0.342 Amp
Maximum power point voltage at the reference condition, $V_{mp,ref}$	0.418 Volt
Open circuit voltage at the reference condition, $V_{oc,ref}$	0.515 Volt
Number of PV cells	1
Short circuit current temperature coefficient, μ_{Isc}	0.00251 Amp/K
Open circuit voltage temperature coefficient, μ_{Voc}	-0.001945 Volt/K

PV cell for the indirect system employing FCHE:

Parameter	Value
Reference solar radiation, G_{ref}	895 W/m2
Reference cell temperature, $T_{c,ref}$	323 K
Short circuit current at the reference condition, $I_{sc,ref}$	0.385 Amp
Maximum power point current at the reference condition, $I_{mp,ref}$	0.342 Amp
Maximum power point voltage at the reference condition, $V_{mp,ref}$	16.72 Volt
Open circuit voltage at the reference condition, $V_{oc,ref}$	20.6 Volt
Number of PV cells	40
Short circuit current temperature coefficient, μ_{Isc}	0.00251 Amp/K
Open circuit voltage temperature coefficient, μ_{Voc}	-0.0778 Volt/K

Piping system and pump for the direct system:

Parameter	Value
Static head, H_{stat}	0.0 m
Reference head, H_{ref}	0.051 m
Reference flow, Q_{ref}	1.3e-5 m^3/s
c_1	0.068 m
c_2	-1.00e8 m^5/s^2
e_1	7692.308 s/m^3
e_2	-2.96e8 s^2/m^6
Reference speed, n_{ref}	25 s

Piping system and pump for the indirect system employing FCHE:

Parameter	Value
Static head, H_{stat}	0.0 m
Reference head, H_{ref}	5.915 m
Reference flow, Q_{ref}	1.4e-4 m^3/s
c_1	7.887 m
c_2	-1.01e8 m^5/s^2
e_1	1428.571 s/m^3
e_2	-5.1e6 s^2/m^6
Reference speed, n_{ref}	25 s

Piping system and pump for the direct system employing NCHE:

Parameter	Value
Static head, H_{stat}	0.0
Reference head, H_{ref}	0.272
Reference flow, Q_{ref}	3.0e-5
c_1	0.362 m
c_2	-1.01e8 m^5/s^2
e_1	3333.333 s/m^3
e_2	-5.56e8 s^2/m^6
Reference speed, n_{ref}	25 s

Bibliography

Alghuwainem, S. M., 1992, "Steady-State Performance of DC-Motors Supplied from Photovoltaic Generators with Step-Up Converter," *IEEE Transactions on Energy Conversion*, Vol. 7, No. 2, June.

Allen, P. L., and Ajele, O. J., 1994, "Optimum Configuration of Natural Convection Shell-and-Coil Heat Exchangers with Respect to Thermal Performance", *Proceedings of the ASES Solar 1994 Conference*, San Jose, CA, pp. 292-297.

Anis, W. R. and Metwally, H. M. B., 1994, "Dynamic Performance of a Directly Coupled PV Pumping System," *Solar Energy*, Vol. 53, No. 4, pp. 369-377.

Appelbaum, J., 1986, "Starting and Steady-State Characteristics of DC Motors Powered by Solar Cell Generators," *IEEE Transactions on Energy Conversion*, Vol. EC-1, No. 1, March, pp. 17-25.

Appelbaum, J., 1987, "The Quality of Load Matching of a Direct-Coupling Photovoltaic system," *IEEE Transaction on Energy Conversion*, Vol. EC-2, No. 4.

Appelbaum, J., Chait, A., and Thompson, D., 1991, "Parametrization of Solar Cells and Array," *Proceedings of the ISES Conference*, Denver, Colorado, pp. 283-288.

Avina, J., 1994, "The Modeling of a Natural Convection Heat Exchanger in a Solar Domestic Hot Water System," M.Sc. Thesis, University of Wisconsin, Madison.

Avina, J., Beckman, W. A., and Klein, S. A., 1995, "Simulation of a Natural Convection Heat Exchanger Solar Domestic Hot Water System," *Proceedings of the ASES Solar 95 Conference*, Minneapolis, MN, pp. 299-304.

Balasubramanian, V., 1992, "Important Aspects of Configuring Stand-Alone Solar Photovoltaic Water Pumping Installations to Achieve High Reliability and System Efficiency," *6th International Photovoltaic Science and Engineering Conference*, New Delhi, India, pp. 963-968.

Baur, J. M., 1992, "Simulation of Energy Storage Tanks with Surface Heat Exchangers," M.Sc. Thesis, Mechanical Engineering, University of Wisconsin-Madison.

Beckman, W. A., Thorton, J., Long, S. and Wood, B. D., 1994, "Control Problem in Solar Domestic Hot Water Systems," *Solar Energy*, Vol. 53, No. 3, pp. 233-236.

Bergelt, T. K., Brunger, A. P., and Hollands, K. G., 1993, "Optimum Hydraulic Resistance for Natural Convection SDHW Heat Exchanger Loops," *Energy Efficiency and Solar Energy: Proceedings of the 19th Annual Conference of the Solar Energy Society of Canada*, Quebec City, Quebec, pp. 0-1 to 0-6.

Braunstein, A. and Kornfeld, A., 1981, "Analysis of Solar Powered Electric Water Pumps," *Solar Energy*, Vol. 27, No. 3, pp. 235-240.

Braunstein, A., Bany, J., and Appelbaum, J., 1977, "Determination of Solar Cell Equation Parameters From Empirical Data," *Energy Conversion*, Vol. 17, pp. 1-6.

Brent, R. P., 1973, *Algorithms for Minimization Without Derivatives*, Prentic-Hall, NJ.

Carlson, W. T., Davidson, J. H. and Duff, W. S., 1991, "Comparison of Experimental and TRNSYS SRCC Ratings of a Generic Drain Back Solar Water System," *United State Department of Energy*, DoE Report No. SAN-16306-29.

Carrier, F. and Schiller, E. J.,1993, "Method for Sizing Water Tanks in Solar Water Pumping Systems," *Revue Des Sciences De L'Eau*, Vol. 6, No. 2, pp. 175-193.

Chandra, S. and Litka, A. H., 1979, "Photovoltaic Powered Solar Domestic Hot Water Heater," *Florida Solar Energy Center*, Cape Canaveral, Florida, FSEC publication No. P-126, August.

Chapman, R. N., 1990, "The Synthesis of Solar Radiation Data for Sizing Stand-Alone Photovoltaic Systems," *Conference Record of the 20th IEEE photovoltaic specialist Conference*, pp. 965-970.

Chaurey , A., Sadaphal, P. M. and Tyagi, D., 1992, "Performance evaluation of PV pumping system," *RERIC International Energy Journal*, Vol. 14, No. 2, December, pp. 57-63.

Cheney, W. and Kincaid, D., *Numerical Mathematics and Computing*, Brooks/Cole Publishing Company, Pacific Grove, California, 1985.

Chowdhury, B. H., Ula, S. and Stokes, K., 1993, "Photovoltaic-Powered Water Pumping-Design, and Implementation - Case-Studies in Wyoming," *IEEE Transactions on Energy Conversion*, Vol. 8, No. 4, pp. 646-652.

Cole, R. L. and Bellinger, J. O., 1982, "Natural Stratification in Tanks," Argonne National Laboratory-Illinois, February.

Collares-Pereira, M., Gordon, J. M., and Zarmi, Y., 1984, "Constant Sensible Heat Load Applications; Variable vs. Constant Flow Solar Systems," *Solar Energy*, Vol. 32, No. 1, pp. 135-137.

Corana A., Marchesi, M., Martini, C., and Ridella, S., 1987, "Minimizing Multinodal Function of Continuos Variables with the "Simulated Annealing" Algorithm," *ACM Transaction on Mathematical Software*, Vol. 13, No. 3.

Cromer, C. J., 1983, "Sizing and Matching a Photovoltaic Circulation System with a Solar Domestic Hot water System," *Florida Solar Energy Center*, Cape Canaveral, Florida, Report No. FSEC-PF-29-83.

Cromer, C. J., 1984, "Design of a DC-Pump, Photovoltaic-Powered Circulation System for a Solar Domestic Hot water System," *Proceedings of the ASES Solar 1984 conference*, Anaheim, CA, pp. 233-238.

Cummings, M. S., 1989, "Modeling, Design, and Control of Partial Ice-Storage Air-Conditioning Systems," M.Sc. Thesis, Mechanical Engineering, University of Wisconsin-Madison.

Czarnecki, J. T. and Read, W. R. W., 1978, "Advances in Solar Water Heating for Domestic Use in Australia," *Solar Energy*, Vol. 20, No. 1, pp. 75-80.

Dahl, S. D., and Davidson, J. H., 1996, "Performance and Modeling of Thermal Heat Exchangers for Solar Water Heaters," *Submitted to Transaction of ASME, Journal of Solar Energy Engineering*, June.

Dankoff, W., 1991, "Pump it Up! Using Solar Water Pumping for Reliable Water Supply Beyond the Power Lines," *SunWorld*, Vol. 15, No. 1, pp. 12-15.

Diarra, N'to, Diarra, Mamadou and Traore, Cheickna, 1989, "PV Systems Operation and Maintenance in Mali," *Proceedings of the 9th E. C. Photovoltaic Solar Energy Conference,* Freiburg, Germany, pp. 1080-1083.

Duffie, J. A. and Beckman, W. A., 1991, *Solar Engineering of Thermal Processes*, John Wiley & Sons Inc., New York.

Duffie, J. A., 1993, "Overview of Modeling and Simulation," Appeared in *Active Solar Systems, Edited by L. George*, MIT Press, pp. 3-18.

Dunlop, J. P., 1988, "Analysis and Design Optimization of Photovoltaic Water Pumping Systems," *Proceedings of the IEEE Photovoltaic Specialists Conference*, Las Vegas, Nevada, September 26-30.

Eckstein, J. H., 1990, "Detailed Modeling of Photovoltaic System Components," M.Sc. Thesis, Mechanical Engineering Department, University of Wisconsin, Madison.

Eckstein, J. H., Townsend, T., Beckman, W. A. and Duffie, J. A., 1990, "Photovoltaic Powered Energy Systems," *Proceedings of the ASES Solar 90 Conference*, Austin TX.

Electro-Craft Corporation, 1978, *DC Motors Speed Controls Servo Systems an Engineering Handbook*, 4th Edition, Hopkins, MN.

F-CHART , 1985, *F-CHART User Manual*, *f*-Chart Software, Middleton, WI.

Fam, W. Z. and Balachander, M. K., 1988, "Dynamic Performance of a DC Shunt Motor connected to a Photovoltaic Array," *IEEE Transactions on Energy Conversion*, Vol. 3, No. 3, September.

Fam, W. Z. and Goswami, P., 1992, "Simulation and Testing of a Photovoltaic Solar-Powered Water Pumping Systems," *Energy Sources*, Vol. 14, pp. 265-272.

Fan, J. C. C., 1986, "Theoretical Temperature Dependence of Solar Cell Parameters," *Solar Cell*, Vol. 17, pp. 309-315.

Fanney, A. H. and Klein, S. A., 1988, "Thermal Performance Comparisons for Solar Hot Water Systems Subjected to Various Collector and Heat Exchanger Flow Rate," *Solar Energy*, Vol. 40, No. 1, pp. 1-11.

Flake, B. A., 1994, "Optimal Control of Heating, Ventilating and Air Conditioning Systems," A Preliminary Report Submitted in Partial Fulfillment of the Requirement for the Degree of Doctor of Philosophy at the University of Wisconsin-Madison.

Fraas, A. P., 1989, *Heat Exchanger Design*, 2nd Edition, John Wiley & Sons, Inc. New York.

Fraser, K. F., 1992, "Modeling Natural Convection Heat Exchangers for SDHW Systems," M.Sc. Thesis, University of Waterloo, Canada.

Furbo, S., 1990, "Solar Water Heating Systems Using Low Flow Rates—Experimental Investigations," Thermal Insulation Laboratory, Technical University of Denmark, Report No. 90-13, 1990.

Gansler, R. A., 1993, "Assessment of Generated Meteorological Data for Use in Solar Energy Simulations," M.Sc. Thesis, Mechanical Engineering, University of Wisconsin-Madison.

Goeffe, W., Ferrier, G., and Rogers, J., 1994, "Global Optimization of Statistical Functions with Simulated Annealing," *Journal of Economics*, Vol. 60.

Green, M. A. and Emery, K., 1993, "Solar Cell Efficiency Tables," *Progress in Photovoltaics: Research and Application*, Vol. 1, pp. 25-29.

Green, M. A., 1982, *Solar Cells*, Prentic-Hall, Englewood Cliffs, NJ.

Halle, H., Chenoweth, J. and Wambsganss, M., 1988, "Shell Side Water Pressure Drop Distribution Measurements in an Industrial-Sized Test Heat Exchanger," *Journal of Heat Transfer*, Vol. 110, pp. 60-67.

Hirsch, U. T., 1985, "Control Strategies for Solar Water Heating Systems," M.Sc. Thesis, Chemical Engineering Department, University of Wisconsin-Madison.

Hodge, B., K., 1985, *Analysis and Design of Energy Systems*, Prentic-Hall, Inc., Englewood Cliffs, NJ.

Hollands, K. G. T. and Brunger, A. P., 1992, "Optimum Flow Rates in Solar Water Heating Systems with a Counter Flow Exchanger," *Solar Energy*, Vol. 48, No. 1, pp. 15-19.

Hollands, K. G. T., Richmond, D. R. and Mandlestam, D. R., 1985, "Re-Engineering Domestic Hot Water Systems for Low Flow," *Proceedings of the 9th Biennial Congress of the International Solar Energy Society; INTERSOL 85*, Montreal, Canada, 23-29 June , pp. 544-548.

Hollands, K. G., D'Andrea, L. J. and Morrison, I. D., 1989, "Effect of Random Fluctuations in Ambient Air Temperature on Solar System Performance," *Solar Energy*, Vol. 42, No. 4, pp. 335-338.

Hori, A., Kanematsu, K., Abe, T. and Hamakawa, Y., 1985, "An Optimal Design of Photovoltaic Direct Coupled Water Pumping System," *Conference Record of the 18th IEEE Specialists Conference*, pp. 1626-1631.

Hsiao, Y. R. and Blevins, B. A., 1984, "Direct Coupling of Photovoltaic Power Source to Water Pumping System," *Solar Energy*, Vol. 32, No. 4, pp. 489-498.

Hutchinson, P. A., Darin, E. A. and Vernon Risser, V., 1991, "Synthesis of Worldwide Solar Insolation Data for Photovoltaic System Sizing," *Conference Record of the 21th IEEE Photovoltaic Specialists Conference*.

Imamura, M. S., Helm, P. and Palz, W., 1991, *Photovoltaic System Technology, A European Handbook*, Commission of the European Communities.

Incropera F. P. and De Witt, D. P., 1985, *Introduction to Heat Transfer*, John Wiley & Sons, New York.

Karaki *et al.*, 1985, "A Liquid-Based Flat-Plate Drain-Back Solar Heating and Cooling System for CSU Solar House III June 1984-July 1985 Operations," DoE Report No. SAN-11927-29, November.

Karassik *et al.*, 1976, *Pump Handbook*, McGraw-Hill Book Company, New York.

Khater, F. M. H., 1991, "Losses Consideration of a DC Motor-Photovoltaic Generator System," *Proceedings of the ISES conference*, Denver, Colorado, pp. 519-525.

Kiatsiriroat, T., Nampkakai, P. and Hiranlabh, J., 1993, "Performance Estimation of a PV Water-Pumping Systems Utilizability Function," *International Journal of Energy Research*, Vol. 17, pp. 305-310.

Kilfoyle, D., 1991, "A Numerical Analysis Method for Computer Modeling Photovoltaic I-V Curves," *Proceedings of the ISES conference*, Denver, Colorado, .

Kirkpatrick, S., Gelatt, C. D., and Vecchi, M. P., 1983, "Optimization by Simulated Annealing," *Science*, Vol. 220, pp. 671-680.

Kistler, R. S. and Chenoweth, J. M., 1988, "Heat Exchanger Shellside Pressure Drop: Comparison of Predictions with Experimental Data," *Journal of Heat Transfer*, Vol. 110, pp. 68-76.

Koner, P. K., Joshi, J. C. and Chopra, K. L., 1992a, "Designing Versatility of Photovoltaic Water Pump," *6th International Photovoltaic Science and Engineering Conference*, New Delhi, India, pp. 941-946.

Koner, P. K., Joshi, J. C. and Chopra, K. L., 1992b, "Matching Analysis of Photovoltaic Powered DC Motors and Centrifugal Pumps by Varying Motor Constant," International Journal of Energy Research, Vol. 16, pp. 301-313.

Lavan, Z. and Thompson, J., 1977, "Experimental Study of Thermal Stratified Hot Water Storage Tanks," *Solar Energy*, Vol. 19, pp. 519-524

Liu, S. T., Shih, K. and Wood, B. D., 1978, "Experimental Validation of the Solar Simulation Program TRNSYS for a Solar Domestic Hot Water Heating System," *Proceedings of the DoE Symposium on Systems Simulation and Economic Analysis for Solar Heating and Cooling*, San Diego, June 27-29.

Loxsom, F. and Durongkaveroj, P, 1994, "Estimating the Performance of a Photovoltaic Pumping System," *Solar Energy*, Vol. 52, No. 2, pp. 215-219.

Macomber *et al.*; "Photovoltaic Stand Alone Systems Preliminary Engineering Design Handbook," Report for the National Aeronautics and Space Administration (NASA) Lewis Research Center, NASA CR-165352, 1981.

Merchant, M. C., 1977, "Photovoltaics, the Basics," *Solar Engineering*, November, pp. 30-31.

Mertes, B. P. and Carpenter, S. C., 1985, "Thermal Performance of Photovoltaic Pumped Solar Domestic Hot Water Systems," *Proceeding of the 9th Biennial Congress of the International Solar Energy Society*, Montreal, CANADA, pp. 586-590, June 23-29.

Miller, J. A. and Hittle, D. C., 1993, "Yearly simulation of a PV Pumped, Wrap-Around Heat Exchanger, Solar Domestic Hot Water System," *ASME Solar Engineering, Proceedings of the ASME International Solar Energy Conference*, Washington, D. C., pp. 67-73.

Newton, B. J., 1995, "Modeling of Solar Storage Tanks," M.Sc. Thesis, Mechanical Engineering, University of Wisconsin-Madison.

Novotny, D., 1996, personal communication.

Orbach, A., Rorres, C. and Fischl, R., 1981, "Optimal Control of a Solar Collector Loop Using a Distributed-Lumped Model," *Automatica*, Vol. 17, No. 3, pp. 535-539.

Parent, M. G., Van Der Meer, Th. H., and Hollands, K. G. T., 1990, "Natural Convection Heat Exchangers in Solar Water Heating Systems: Theory and Experiment," *Solar Energy*, Vol. 45, No. 1, pp. 43-52.

Parker, G. J., 1976, "A Forced Circulation System for a Solar Water Heating," *Solar Energy*, Vol. 18, pp. 475-479.

Polman *et al.*, 1986, "A New Method for the Evaluation of Solar Cell Parameters," *Solar Cell*, Vol. 17, pp. 241-251.

Press, W. H, Flannery, B. P., Teukolsky, S. A., and Vetterling, W. T., 1989, *Numerical Recipes; The Art of Scientific Computing (FORTRAN Version)*, Cambridge University Press, Cambridge.

Prido, R., 1977, "Water Pumping System Using Solar Power from Photovoltaic Source," *Proceedings of the 1st E. C. Photovoltaic Solar Energy Conference*, Luxembourg, pp. 1221-1228.

Rabehl, R., 1997, "Parameter Estimation of Heat Exchangers for using Catalogue Data with TRNSYS," M.Sc. Thesis, Mechanical Engineering, University of Wisconsin-Madison.

Rauschenbach, H. S., 1980, *Solar Cell Array Handbook: the Principle and Technology of Photovoltaic Energy Conversion*, Van Nostrand Reinhold, New York.

Roger, J. A. *et al.*, 1977, "Calculations and In Situ Experimental Data on a Water Pumping System Directly Connected to a 1/2 kW Photovoltaic Converter Array," *Proceedings of the 1st E. C. Photovoltaic Solar Energy Conference*, Luxembourg, pp. 1211-1220.

Roger, J. A., 1979, "Theory of the Direct Coupling Between D. C. Motor and Photovoltaic Solar Arrays," *Solar Energy*, Vol. 23, No. 3, pp. 193-198.

SEIR, *Solar Energy Intelligence Report*, 1985, Vol. 11, No. 29, pp. 251, July 22.

Sharma *et al.*, 1993, "Prediction of Solar Array Power Output Based on Limited Measured Data," Solar Energy Materials and Solar Cells, Vol. 29, pp. 67-76.

Sharp, K., 1978, "Thermal Stratification in Liquid Sensible Heat Storage," M.Sc. Thesis in Mechanical Engineering, Colorado State University, Ft. Collins (1978).

Singer, S. and Appelbaum, J., 1993, "Starting Characteristics of Direct Current Motors Powered by Solar Cells," *IEEE Transactions on Energy Conversion*, Vol. 8, No. 1, March.

Slemon, G. R. and Straughen, 1980, *Electric Machines*, Addison-Wesley Publishing Company, Reading, MA.

Streeter, V. L. and Wylie, E. B., 1985, *Fluid Mechanics*, Eighth Edition, McGraw-Hill , Inc., New York

Suehrcke, H., 1988, "The Performance Prediction of Solar Thermal Systems," Ph.D. Thesis, University of Western Australia.

Tabarra, M. and Bowman, N. T., 1985, "The Effect of Load Profiles on Stratified Solar Storage Tanks," *Proceedings of the 9th conference of ISES*, Montreal, Canada, pp. 863-866

Townsend, T. U., 1989, "A Method for Estimating the Long-Term Performance of Direct-Coupled Photovoltaic System," M.Sc. Thesis, Mechanical Engineering, University of Wisconsin-Madison.

TRNSYS, 1996, *A Transient Simulation Program, User's Manual*, Version 14.2, Solar Energy Laboratory, University of Wisconsin-Madison.

Veissid, N., Da Cruz, M, and Andrade, A., 1990, "A Method for the Determination of the Standard Deviations of the Solar Cell I-V Characteristic Parameters," *Solar Cell*, Vol. 28, pp. 351-357.

Weinberg, I., Swartz, C. K., and Hart, R. E., 1987, "Radiation and Temperature Effects in Gallium Arsenide, Indium Phosphade, and Silicon Solar Cells," NASA-TM-89870, .

Whitaker, C. M. *et al.*, 1991, "Effects of Irradiance and Other Factors on PV Temperature Coefficients," *Conference Record of the 21th IEEE Photovoltaic Specialists Conference*, pp. 608-613.

White, F., 1994, *Fluid Mechanics*, Third Edition, McGraw-Hill , Inc., New York.

Wijesooriya, P. D. and Duffy, J. J., 1992, "Stand-Alone PV System Sizing Based on Both Solar and Reliability Uncertainties," *Proceeding of the ASES Solar 1992 Conference*, Cocoa Beach, Florida, pp. 58-62.

Winn, C. B., 1993, "Controls in Active Solar Energy Systems," Appeared in *Active Solar Systems, Edited by L. George*,, MIT Press, pp. 81-150.

Wuestling, M. D., Klein, S. A. and Duffie, J. A., 1985, "Promising Control Alternatives for Solar Water Heating Systems," *Transaction of ASME, Journal of Solar Energy Engineering*, Vol. 107, August, pp. 215-221.